Time-Domain System Identification for Long-EZ Fixed-Wing Aircraft Based on Flight Test Data

Danyang Xu

A Thesis

in

The Department

of

Mechanical, Industrial and Aerospace Engineering

Presented in Partial Fulfillment of the Requirements

for the Degree of Master of Applied Science at

Concordia University

Montreal, Quebec, Canada

January 2019

CONCORDIA UNIVERSITY

School of Graduate Studies

This is to certify that the thesis prepared

By: **Danyang Xu**

Entitled: **Time-Domain System Identification for Long-EZ Fixed-Wing Aircraft Based on Flight Test Data**

and submitted in partial fulfillment of the requirements for the degree of

Master of Applied Science (Mechanical Engineering)

complies with the regulations of the University and meets the accepted standards with respect to originality and quality.

Signed by the final Examining Committee:

_____Chair

Dr. Chevy Chen

_____Examiner

Dr. Wen-Fang Xie

_____External Examiner

Dr. Walter Lucia

_____Thesis Supervisor

Dr. Youmin Zhang

Approved by _____

Dr. Mamoun Medraj, MASc Program Director

Department or Mechanical, Industrial and Aerospace Engineering

_____2019 _____

January 30th, *Dr. Amir Asif, Dean*

Faculty of Engineering and computer Science

ABSTRACT

Time-Domain System Identification for Long-EZ Fixed-Wing Aircraft Based on Flight Test Data

Danyang Xu

System identification using flight test data based on time-domain method is an accurate way of getting a reliable mathematical aircraft model. This thesis provides a system identification procedure on a canard configured fixed-wing aircraft Long-EZ, which is the early and critical stage of providing accurate aircraft models for designing an effective autopilot in the future.

Flight test designed for Long-EZ aircraft has been carried out by International Test Pilot School (ITPS Canada Ltd). The real flight test data recorded from the testbed has been utilized for the identification and verification of a linear transfer function model, a nonlinear neural network model, and a block-oriented model consisting of linear and nonlinear parts. The linear transfer function structure has been determined with aircraft's physical dynamics, and the model parameters have been identified using MATLAB System Identification toolbox. The nonlinearity of the aircraft dynamics has been treated with a Multilayer Perceptron (MLP) neural network structure, which has been developed with a set of Python codes. Flight data has been utilized to train this MLP structure.

The results demonstrate different predicting capabilities of the developed linear, nonlinear,

and combined linear and nonlinear structure, which is also known as the neural network Wiener model. The developed Wiener model in general shows satisfactory predicting capability for the testbed Long-EZ aircraft.

Acknowledgements

I would first give my sincere thanks to my thesis supervisor Dr. Youmin Zhang, who has given me this precious opportunity to be enrolled in the M.ASc. program of Concordia University, and NAVL lab research associate, Dr. Zhixiang Liu, who has given me valuable academic advices throughout my study and thesis work.

Secondly, I'd like to express my gratitude to ITPS Canada Ltd., the president Mr. Giorgio Clementi who has given me a precious internship opportunity while I was completing master's program, where I have gained valuable hands-on experience from aviation industry. I would like to give my special thanks to ITPS supervisor Dr. Andre Celere who have given me valuable training during the internship, and colleagues Mr. João Falcão and Dr. Panos Vitsas who have spent time reading through this thesis and given me valuable suggestions.

Last but not least, I'd like to thank all my family members and friends in China who have encouraged and supported me through my master's study in Canada.

Table of Contents

List of Figures

List of Tables

NOMENCLATURE

List of Symbols

a_x, a_y, a_z	Accelerations along x, y, z body axes, m/s^2
b	Span of the aircraft, m
$\bar{c}$	Mean aerodynamic chord, m
C_L, C_D, C_m	Longitudinal aerodynamic force and moment coefficients
C_Y, C_l, C_n	Lateral directional aerodynamic force and moment coefficients
$C_{L_0}, C_{D_0}, C_{m_0}$	Longitudinal aerodynamic force and moment coefficients at zero sideslip angle
$C_{Y_0}, C_{l_0}, C_{n_0}$	Lateral directional aerodynamic force and moment coefficients at zero sideslip angle
$C_{L_\alpha}, C_{D_\alpha}, C_{m_\alpha}$	Derivatives of longitudinal force and moment coefficients w.r.t angle of attack
$C_{Y_\beta}, C_{l_\beta}, C_{n_\beta}$	Derivatives of lateral directional force and moment coefficients w.r.t sideslip angle
$C_{L_q}, C_{D_q}, C_{m_q}$	Derivatives of longitudinal force and moment coefficients w.r.t pitch rate
$C_{Y_p}, C_{l_p}, C_{n_p}$	Derivatives of lateral directional force and moment coefficients w.r.t roll rate
$C_{Y_r}, C_{l_r}, C_{n_r}$	Derivatives of lateral directional force and moment coefficients w.r.t yaw rate

$C_{L_{\delta_e}}, C_{D_{\delta_e}}, C_{m_{\delta_e}}$	Derivatives of longitudinal force and moment coefficients w.r.t elevator deflection
$C_{Y_{\delta_a}}, C_{l_{\delta_a}}, C_{n_{\delta_a}}$	Derivatives of lateral directional force and moment coefficients w.r.t aileron deflection
$C_{Y_{\delta_a}}, C_{l_{\delta_a}}, C_{n_{\delta_a}}$	Derivatives of lateral directional force and moment coefficients w.r.t rudder deflection
$I_{xx}, I_{yy}, I_{zz}, I_{xz}$	Moment of inertia about x, y, z body axis, and product moment of inertia, $kg\ m^2$
J	Cost function
p, q, r	Roll, pitch and yaw rates respectively, rad/s
S	Wing planform area, m^2
u, v, w	Airspeed components along x, y, z body axis, m/s
V, α, β	Airspeed, m/s, Angle-of-attack, deg, Angle of sideslip, deg
$\delta_a, \delta_e, \delta_r$	Aileron, elevator and rudder deflection angles, deg
ϕ, θ, ψ	Angle of roll, pitch and yaw, deg
Θ	Vector of unknown parameters
ω	Frequency of interest, rad/s

Abbreviations and Acronyms

ANN	Artificial Neural Network
ATO	Approved Training Organization
EASA	European Aviation Safety Agency
FCS	Flight Control System
HITL	Hardware-in-the-Loop
LOES	Low Order Equivalent System
MISO	Multi-Input-Single-Output
MLP	Multilayer Perceptron
OLS	Ordinary Least Squares
OPV	Optionally Piloted Vehicle
POH	Pilot Operation Handbook
RNN	Recurrent Neural Network
RPV	Remotely Piloted Vehicle
SISO	Single-Input-Single-Output
SITL	Software-in-the-Loop
SAS	Stability Augmentation system
UAV	Unmanned Aerial Vehicle

Chapter 1 Introduction

System identification is an old and well-developed discipline that has been broadly utilized in the engineering world. Zadeh [1] has provided a clear definition of system identification:

System identification is the determination, based on observation of input and output, of a system within a specified class of systems to which the system under test is equivalent.

System identification, simulation and control are three general problems in aircraft dynamics and control which are very closely linked to each other [2]. Simulation and control can be carried out on a computer with modern computational technologies. Moreover, more comprehensive data can be gathered to analyze an aircraft's aerodynamic characteristics in wind-tunnel testing. However, system identification has still been intensively utilized to verify theoretical analysis and wind tunnel test results, and furthermore, to obtain more accurate and comprehensive aircraft dynamic models. These models can be more mathematically reliable so that at later stage, aircraft systems such as Stability Augmentation System (SAS) and Flight Control System (FCS), and flight simulators can be designed based on this identified model.

System identification models

There are different ways to classify the identified models. One way is to classify them into parametric models and nonparametric models. Parametric models can be expressed as state space equations, transfer functions, differential equations, etc. They can be linear, nonlinear, continuous or discontinuous, time-invariant or time-variant, deterministic or stochastic. Non-parametric models do not require explicit specification of the system dimension, which can be

expressed as impulse or step responses, frequency responses, correlation functions, spectral densities, etc.

In terms of parametric models, a state space representation in the time-domain is closer to physical reality than any of the frequency-domain transform techniques [3]. Linearized models are often used in the Flight Control System (FCS) design as they replicate aircraft dynamics very well during normal flight (excluding large and rapid maneuver scenarios) and computation load has been greatly reduced for simulation purposes. However, when large and rapid maneuvers are involved, nonlinearity also needs to be considered in the modeling process.

For nonparametric models, frequency response has been commonly used. A frequency response is a data curve identified from the flight-test data that displays the ratio of the response per unit of control input [4]. Fourier transform has been intensively utilized in transforming the time-domain data into frequency domain data, which is often followed by data reduction techniques such as the windowing techniques to get frequency response. The identified results are often presented in Bode plot format, which illustrates the log-magnitude and phase vs log-frequency on a semilog scale. This kind of models are often utilized in rotary-wing aircraft/UAVs system identification [4].

Another way of classifying aircraft models is based on the priori knowledge about the aircraft. These models include White-box models, Black-box models, and Gray-box models. White-box models are often used in the early stage of aircraft system identification as they are close to phenomenological models, which are based on the basic physics principles. These phenomenological models are derived on the Newtonian mechanics. Therefore, the identified parameters often are related to physical interpretations. On the contrary, Black-box models are

close to behavioral models, which provide an alternative way of describing the cause-effect relationship. Neural network is an example of Black-box model that is capable of matching input-output without any specific relevance to the internal behavior of the actual process. Gray-box models are a combination of these two models. A block-oriented approach is a good illustration of the Gray-box modelling. A gray-box model can be represented by a linear block and a nonlinear block. The linear block is similar to a White-box model, and the nonlinear block resembles a Black-box model in its form. Therefore, both linear characteristics corresponding to the Newtonian physics and nonlinear uncertainties in the system have been addressed in the block-oriented Gray-box model.

System Identification Procedure

The proposed system identification procedure in this thesis can break down into a few more detailed steps. Firstly, flight test plan has been designed based on a priori knowledge about the aircraft. Secondly, flight test instrumentations have been installed to the aircraft to record required flight test data. Thirdly, detailed data reduction technique has been carried out. This part includes data compatibility check, model structure determination, model parametrization, and validation. The whole proposed procedure is illustrated in Figure 1.1.

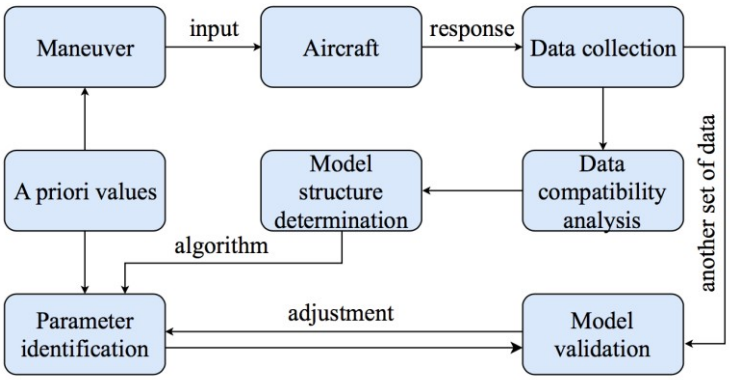

Figure 1.1: Aircraft system identification flow chart

A comprehensive flight test plan is essential to a successful test flight. A flight test plan usually includes test objectives, scope of the test, description of test items, mission description/profile, test schedule, support requirements, flight clearance and operating limitations, instrumentation and data processing, pretest checks, risk analysis, etc. A flight test card can be prepared based on this fight test plan, which is convenient to carry onto the aircraft. The flight test card incorporates all test points to be carried out in sequence in that flight test. Each test point includes detailed descriptions such as test objective, speed and altitude setup and tolerance, aircraft configuration, test maneuvers and procedure, pilot's comments, and data recording section. In this way, both the pilot and engineer will be clear about what to expect during the flight test.

Flight test instrumentations have been chosen and installed to the aircraft to record input-output data of the aircraft flight dynamics. Input variables mainly include control stick inputs: u_{lon} on longitudinal axis and u_{lat} on lateral axis, respectively. Output variables mainly include Euler attitude angles (ϕ, θ, ψ), angular velocities $(p, q, r, \dot{\phi}, \dot{\theta}, \dot{\psi})$, and translational accelerations (a_x, a_y, a_z).

It is assumed that the measured input data is free of measurement noises and process noises. However, measured aircraft response data usually contains measurement noises and system errors. Therefore, data compatibility check is required to decide whether the flight data is satisfactory for analysis and modeling.

Model structure has been determined based on the aircraft dynamics and flight test data available. Model structure determination means a specific form of model needs to be selected based on a priori knowledge about the aircraft and measured values, whether it is parametric or nonparametric, linear or nonlinear. Aircraft models are not unique. A good model should be simple enough to fit in with the measured data and complicated enough to present the aircraft's characteristics with good prediction capabilities.

For parametric models, estimation and optimization algorithms have been defined to parametrize the model. Currently, two most frequently used methods are equation-error method and output-error method. The equation-error method is based on linear regression using ordinary least-squares principle. The output-error method minimizes the sum of weighted square differences between the measured aircraft outputs and model outputs. Iterative nonlinear optimization techniques such as Gauss-Newton (GN) method and Levenberg-Marquard (LM) methods are often used to solve nonlinear equations. For nonparametric models such as neural network structures, learning algorithm such as backpropagation method is often used which requires enough training data to get ideal results.

Finally, the identified model should have satisfactory accuracy and prediction capability. Another set of flight data that has not been used in the identification process has been utilized to validate the models. Model validation methods include residual analysis, autocorrelation

analysis, etc.

1.1 Literature Review

A comprehensive introduction of history and evolution of flight vehicle system identification is given by Hamel and Jategaonkar [5]. At early stage, ordinary and nonlinear least squares method were utilized by Milliken [6] in 1947. With the development of digital computers, Ljung [7] has explicitly explained MATLAB as a system identification tool. In addition, more attention has been paid to flight test and large maneuvers to explore the boundary of the aircraft dynamics. Klein [8] and Klein and Murphy [9] addressed the problem of highly maneuverable modern aircraft system identification. Recent studies [10] [11] [12] have also stressed on rotary-wing and fixed-wing UAVs as testbeds. Liu et al [13] did online parameter identification based on small fixed-wing UAV with recursive techniques which can be applied to real-time onboard data validation. Abdulhamid et al [14] has also studied modeling and identification methods based on UAV platform.

Currently, system identification methods can be classified to three categories: output error method (maximum likelihood method) [15] [16] [17] [18] [19] [20], filter error method [21] [22] [23] [24], and equation error method (least-squares method) [25] [13] [18]. Both time-domain and frequency-domain analyses are applicable to these categories of identification methods. Klein et al [2], Jategaonkar [3], and Tischler et al [4] specially aimed at aircraft system identification. Klein et al [2] provided several explicit examples, such as 1) NASA twin otter yawing moment coefficient estimation using linear regression and output error method with time-domain and frequency-domain data respectively; 2) F-16XL parameter estimation based

on Schroeder sweep forced oscillation data from water tunnel; and 3) Tu-144LL with Low-Order Equivalent System (LOES) model derived from 2-1-1 maneuver. Jategaonkar [3] focused on time-domain system identification. Meanwhile, Tischler et al [4] put the emphasis on the identification of rotorcraft XV-15 with frequency-domain data using CIFER.

With the development of artificial intelligence, modern system identification methods have also greatly evolved towards using neural network to identify nonlinearity in the system [26] [27] [28] [29] [30]. Deboeck and Kohonen [31] described Neural Networks (NNs) as a collection of mathematical techniques that can be used for signal processing, forecasting and clustering and termed it as non-linear, multi-layered, parallel regression techniques [27]. In 1943, McCulloch and Pitts [32] proposed first mathematical model of the neurons and showed how neuron-like networks can be computed. In 1949, the first set of ideas of learning in neural networks was contained in Hebb's book *The Organization of Behaviour* [33]. In 1962, Rosenblatt [34] invented a class of simple neuron-like learning networks called perceptron neural network. In 1969, Minsky and Papert [35] proved that single layer perception has its limitations in learning and presenting abilities which caused researchers to develop symbolic AI methods and systems. In 1974, Werbos [36] presented the Backpropagation (BP) method which has been widely used in NN studies since. From 1977 onwards, Multilayer Perceptron (MLP) has been introduced. Furthermore, Hopfield [37] invented Recursive Neural Network (RNN) with feedback structure which resembles the state space model representations in 1982. In 1988, Radial Basis Function (RBF) neural networks were addressed, which have drawn lots of attention due to its simple network structure and good generalization ability.

Moreover, block-oriented approach is another interesting field being explored. Janczak [26] has explicitly studied block-oriented approach for system identification, and different Wiener models and Hammerstein models with neural network and polynomial as the nonlinear static part have been intensively studied. Wang and Chen [38] have proposed a Hammerstein-wiener recurrent neural network model, where a unique structure of two nonlinear recurrent neural network components with linear state space dynamic model in the middle has been studied.

1.2 Research Motivation

Currently, most studies on aircraft system identification are based on UAV testbeds. However, fixed-wing aircrafts are less studied compared to rotary-wing aircraft, rotary-wing UAVs, and even fixed-wing UAVs as a research testbed due to the following reasons:

Firstly, more rotary-wing UAVs have been researched in the lab environment than fixed-wing UAVs or fixed-wing aircraft in general. Rotary-wing UAVs tests can be conveniently conducted in a lab environment, whereas fixed-wing UAVs and aircrafts flight tests are more susceptible to space requirements, higher flight test instrumentation costs, aircraft availability, pilot availability, weather conditions, etc., which make the fixed-wing testbeds more costly in the long run.

Secondly, test flights for fixed wing aircrafts need to be carried out in higher altitude condition, in which case the gust wind interference is not controllable. On the contrary, UAV (especially rotary-wings) test flights happen at lower altitude or indoor environment with milder test environment and less interference. In this case, some of the flight data for fixed-wing aircraft may not be ideal for analysis due to noises and interferences. Only those data that passes

data compatibility check can be utilized for the modeling, which greatly reduces the data available for modelling and analysis.

Thirdly, most rotary-wing system identification uses frequency sweep as their flight test maneuver and frequency-domain method for data analysis. Frequency sweep is very commonly used in the frequency-domain system identification, which has already been elaborated by Tischler [4]. Commercial software such as CIFER also provides very good reference to verify the identification results in frequency domain. The flight test maneuvers for fixed-wing aircraft/UAVs can be more versatile, and proper flight test instrumentation for the fixed-wing aircraft is required to record the data for analysis.

The Long-EZ aircraft studied in this research is a canard-configured fixed-wing aircraft. ITPS Canada Ltd. intends to modify this aircraft to an Optionally Piloted Vehicle (OPV). As part of the project, a mathematical model of the aircraft is required for software-in-the-loop modeling before carrying out the autonomous flight. Therefore, system identification for mathematical modelling has become the foundation of this project which is essential to the flight tests safety in the future.

1.3 Contributions of This Thesis

The main contributions of this thesis can be summed up as follows:

1. Baseline aircraft model structure of the Long-EZ aircraft has been determined. Stability and control derivatives from this baseline model have been calculated with Roskam's [39] method. Empirical data from a Cessena 172p model (which shares similar size and dynamics with Long-EZ) has been used as reference. This baseline model is essential to

the software-in-the-loop simulations, which will identify potential risks in the flight dynamics of the modified aircraft system in a low-cost and timely manner.

2. Based on the flight test instrumentations available at ITPS, system identification flight test has been planned and carried out to get sufficient data for modeling. Based on this experience, improved flight tests can be planned in the future to improve the baseline model.
3. Linear transfer function model structures have been determined with the physics of the aircraft. Model parameters have been identified on both longitudinal and lateral axes using time-domain method, and have been compared with baseline model and flight data. This linearized transfer function model can be utilized in the future for flight controller design of the Long-EZ aircraft.
4. Nonlinear Artificial Neural Network (ANN) and block-oriented neural network Wiener model structure have been designed. Python codes have been developed and fine-tuned for both structures. The neural networks have been trained with both longitudinal and lateral flight data and compared with the linear model.

All the contributions above have shed some light on the future works that require to be done in the future at ITPS. Various models have been developed for the Long-EZ aircraft, and the model responses have been compared. The linear transfer function and the neural network Wiener model can be used in the future flight controller design for the aircraft. The baseline model parameters can be further improved when air data is available from the testbed, which gives more precise simulation results.

1.4 Thesis Layout

Chapter 1 consists of a system identification introduction, a literature review, and research motivation and main contributions of this research. Chapter 2 introduces detailed aircraft dynamics, which forms the physical basis for modeling the baseline model. Chapter 3 describes the aircraft Long-EZ details as the testbed, the a priori knowledge about the aircraft and detailed flight test plan and results for this study. Chapter 4 introduces the equation error method, and the reason of choosing it out of the three methods for system identification. Moreover, it gives details on how the transfer function model structures have been determined and how the model parameters have been identified. Chapter 5 presents a developed multilayer perceptron neural network, and a block-oriented model consisting of a linear part and a nonlinear part, which is also known as neural network Wiener model, and the comparison among the linear, nonlinear and block-oriented Wiener model. Chapter 6 is the conclusion of this study and an extension to future works.

Chapter 2 Aircraft Dynamics and Modelling

2.1 Aircraft Equations of Motion

When describing aircraft flight dynamics, several different reference frames have been utilized to describe aircraft's coordinate systems. The definitions are summed up as follows.

Inertia axes: Newton's laws apply in an inertia reference frame. Its origin is fixed or moving with a constant velocity.

Earth axes $O_{x_E y_E z_E}$: The origin is at an arbitrary point on the earth surface with positive O_{x_E} axis pointing toward the geographic north, O_{y_E} pointing to the east, and O_{z_E} pointing to the center of the earth. The earth axes are assumed to be inertial axes.

Body axes O_{xyz}: The origin is at the aircraft C.G., with positive O_x axis pointing forward through the nose of the aircraft, O_y pointing out the right wing, O_z pointing downwards. The O_{xz} plane is usually the plane of symmetry of the aircraft.

Stability axes $O_{x_S y_S z_S}$: O_{x_S} is aligned with the direction of the velocity of the aircraft projected to the O_{xz} plane.

Wind axes $O_{x_W y_W z_W}$: Positive O_{x_W} is aligned with the air-relative velocity vector, O_{y_W} axis is out the right side of the aircraft, O_{z_W} axis is through the underside in the O_{xz} plane.

Euler angles are three angles introduced by Leonhard Euler to describe the orientation of a rigid body with respect to a fixed coordinate system. The angular differences between the body axes and earth axes are denoted as Euler angles (ϕ, θ, ψ), which are illustrated in Figure 2.1. Angle of attack (AOA, or α) is the angle between the angle of an aircraft's body and wings relative to its actual flight path. Sideslip angle (β) is the angle between the direction an aircraft

is pointing and the actual flight path. The relationship of body axes, stability axes, wind axes, angle of attack and sideslip angle is presented in Figure 2.2.

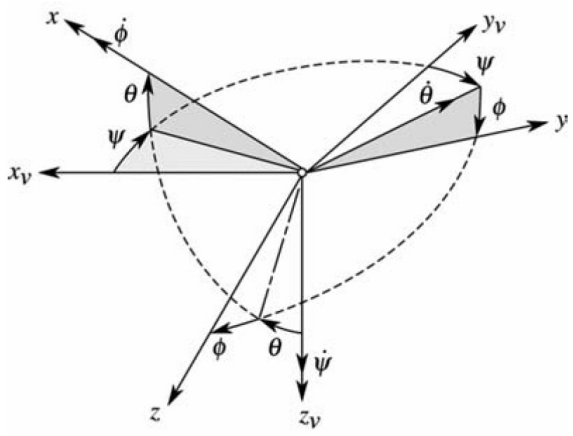

Figure 2.1: Rotation from Earth axes to body axes [2]

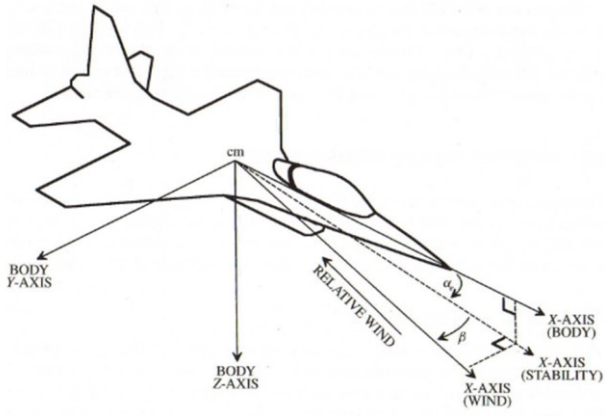

Figure 2.2: Relationship between body, stability and wind axes

The reference frames in this research are right handed and with mutually orthogonal axes. Angular velocities, applied moments, and control surface deflections all follow the right-hand rule. Positive control surface deflections normally have a negative impact on the aerodynamic moment on the aircraft. For example, the positive canard deflection is trailing edge up. Positive aileron deflection is defined as:

$$\delta_a = \frac{1}{2}(\delta_{a_R} - \delta_{a_L}) \tag{2.1}$$

Positive rudder deflection is trailing edge left.

$$\delta_r = \frac{1}{2}(\delta_{r_R} - \delta_{r_L}) \tag{2.2}$$

There are a few assumptions about the aircraft: 1) The aircraft is a rigid body with fixed

mass and mass distribution, aircraft C.G. is at the center of mass. 2) Aircraft is symmetric in the O_{xz} plane. 3) Wind and gust are not taken into consideration. 4) Earth is fixed in inertial space; flight is so close to the earth surface that the surface is considered flat.

The transformation of coordinate system from one to each other is required to simplify the calculation. Relative orientation of body coordinate system to inertial coordinate system is described by three sequential rotations and end up in the following form:

$$T^{BI} = \begin{bmatrix} 1 & 0 & 0 \\ 0 & \cos\phi & \sin\phi \\ 0 & -\sin\phi & \cos\phi \end{bmatrix} \begin{bmatrix} \cos\theta & 0 & -\sin\theta \\ 0 & 1 & 0 \\ \sin\theta & 0 & \cos\theta \end{bmatrix} \begin{bmatrix} \cos\psi & \sin\psi & 0 \\ -\sin\psi & \cos\psi & 0 \\ 0 & 0 & 1 \end{bmatrix}$$

$$= \begin{bmatrix} \cos\theta\cos\psi & \cos\theta\sin\psi & -\sin\theta \\ \sin\phi\sin\theta\cos\psi - \cos\phi\sin\psi & \sin\phi\sin\theta\sin\psi + \cos\phi\cos\psi & \sin\phi\cos\theta \\ \cos\phi\sin\theta\cos\psi + \sin\phi\sin\psi & \cos\phi\sin\theta\sin\psi - \sin\phi\cos\psi & \cos\phi\cos\theta \end{bmatrix} \tag{2.3}$$

where (ϕ, θ, ψ) are the Euler attitude angles between the earth axes and body axes.

From body to stability coordinate system:

$$T^{BS} = \begin{bmatrix} \cos\alpha & 0 & \sin\alpha \\ 0 & 1 & 0 \\ -\sin\alpha & 0 & \cos\alpha \end{bmatrix} \tag{2.4}$$

where α is the angle of attack (AOA).

From stability to wind coordinate system:

$$T^{SW} = \begin{bmatrix} \cos\beta & \sin\beta & 0 \\ -\sin\beta & \cos\beta & 0 \\ 0 & 0 & 1 \end{bmatrix} \tag{2.5}$$

where β is the sideslip angle.

According to Newton's second law, aircraft's translational and rotational motions can be described as:

$$F = \frac{d}{dt}(mV) = m\dot{V} + \omega \times mV \tag{2.6}$$

$$M = \frac{d}{dt}(I\omega) = I\dot{\omega} + \omega \times I\omega \tag{2.7}$$

where F is the applied force, m is the mass, V is the translational velocity, M is the applied moment about the C.G., ω is the angular velocity, and I is the inertia matrix, which break down to three body axes with the following notations:

$$F = \begin{bmatrix} X \\ Y \\ Z \end{bmatrix} \qquad F_A = \bar{q}S \begin{bmatrix} C_X \\ C_Y \\ C_Z \end{bmatrix} \qquad V = \begin{bmatrix} u \\ v \\ w \end{bmatrix} \tag{2.8}$$

$$M = \begin{bmatrix} l \\ m \\ n \end{bmatrix} = \bar{q}S \begin{bmatrix} bC_l \\ \bar{c}C_m \\ \bar{c}C_n \end{bmatrix} \qquad I = \begin{bmatrix} I_x & -I_{xy} & -I_{xz} \\ -I_{yx} & I_y & -I_{yz} \\ -I_{zx} & -I_{zy} & I_z \end{bmatrix} \qquad \omega = \begin{bmatrix} p \\ q \\ r \end{bmatrix} \tag{2.9}$$

Forces acting on an aircraft consist of aerodynamic force F_A, gravity mg and propulsion T. But the gravity is not causing any moments as it is applied thorough the C.G. Forces and moments acting on the aircraft can be further broken down to three body axes [2]. Equations of motion to an aircraft can be represented as follows:

Forces equations in body axis [2]:

$$X = m(\dot{u} + qw - rv) = \bar{q}SC_X - mg\sin\theta + T \tag{2.10}$$

$$Y = m(\dot{v} + ru - pw) = \bar{q}SC_Y + mg\cos\theta\sin\phi \tag{2.11}$$

$$Z = m(\dot{w} + pv - qu) = \bar{q}SC_Z + mg\cos\theta\cos\phi \tag{2.12}$$

Force equations in wind axis:

$$D = \bar{q}SC_D = \bar{q}S(-C_X\cos\alpha + C_Z\sin\alpha) \tag{2.13}$$

$$L = \bar{q}SC_L = \bar{q}S(-C_Z\cos\alpha + C_X\sin\alpha) \tag{2.14}$$

where D and L are drag and lift.

Moment equations [2]:

$$l = \bar{q}SbC_l = I_{xx}\dot{p} + (I_{zz} - I_{yy})qr - I_{xz}(pq + \dot{r}) \tag{2.15}$$

$$m = \bar{q}S\bar{c}C_m + I_p\Omega_p r = I_{yy}\dot{q} + (I_{xx} - I_{zz})pr + I_{xz}(p^2 - r^2) \quad (2.16)$$

$$n = \bar{q}S\bar{c}C_n - I_p\Omega_p q = I_{zz}\dot{r} + \left(I_{yy} - I_{xx}\right)pq + I_{xz}(qr - \dot{p}) \quad (2.17)$$

where I_p is the inertia of rotating mass from aircraft propulsion system, and Ω_p is the angular velocity. The term $I_p\Omega_p$ will be zero when the angular velocity of the mass is constant.

Translational kinematics [2]:

$$\dot{u} = rv - qw + \frac{\bar{q}S}{m}C_X - g\sin\theta + \frac{T}{m} \quad (2.18)$$

$$\dot{v} = pw - ru + \frac{\bar{q}S}{m}C_Y + g\cos\theta\sin\phi \quad (2.19)$$

$$\dot{w} = qu - pv + \frac{\bar{q}S}{m}C_Z + g\cos\theta\cos\phi \quad (2.20)$$

Rotational kinematics [2]:

$$\dot{\phi} = p + tan\,\theta\,(q\,sin\,\phi + r\,cos\,\phi) \quad (2.21)$$

$$\dot{\theta} = q\,cos\,\phi - r\,sin\,\phi \quad (2.22)$$

$$\dot{\psi} = \frac{q\,sin\,\phi + r\,cos\,\phi}{cos\,\theta} \quad (2.23)$$

Or,

$$p = \dot{\phi} - sin\,\theta\,\dot{\psi} \quad (2.24)$$

$$q = cos\,\phi\,\dot{\theta} + sin\,\phi\,cos\,\theta\,\dot{\psi} \quad (2.25)$$

$$r = cos\,\phi\,cos\,\theta\,\dot{\psi} - sin\,\phi\,\dot{\theta} \quad (2.26)$$

2.2 Long-EZ Baseline Model

Stevens et al [40] summed up typical aerodynamic component buildup equations and gave the structure of the aerodynamic model as follows in body axis:

$$C_X = C_{X_0}(\alpha) + C_{X_q}(\alpha)\frac{q\bar{c}}{2V} + C_{X_{\delta_e}}(\alpha)\delta_e \quad (2.27)$$

$$C_Z = C_{Z_0}(\alpha) + C_{Z_q}(\alpha)\frac{q\bar{c}}{2V} + C_{Z_{\delta_e}}(\alpha)\delta_e \quad (2.28)$$

$$C_m = C_{m_0}(\alpha) + C_{m_q}(\alpha)\frac{q\bar{c}}{2V} + C_{m_{\delta_e}}(\alpha)\delta_e \tag{2.29}$$

$$C_Y = C_{Y_0}(\alpha) + C_{Y_\beta}(\alpha)\beta + C_{Y_p}(\alpha)\frac{b}{2V}p + C_{Y_r}(\alpha)\frac{b}{2V}r + C_{Y_{\delta_a}}(\alpha)\delta_a + C_{Y_{\delta_r}}(\alpha)\delta_r \tag{2.30}$$

$$C_l = C_{l_0}(\alpha) + C_{l_\beta}(\alpha)\beta + C_{l_p}(\alpha)\frac{pb}{2V} + C_{l_r}(\alpha)\frac{rb}{2V} + C_{l_{\delta_a}}(\alpha)\delta_a + C_{l_{\delta_r}}(\alpha)\delta_r \tag{2.31}$$

$$C_n = C_{n_0}(\alpha) + C_{n_\beta}(\alpha)\beta + C_{n_p}(\alpha)\frac{pb}{2V} + C_{n_r}(\alpha)\frac{rb}{2V} + C_{n_{\delta_a}}(\alpha)\delta_a + C_{n_{\delta_r}}(\alpha)\delta_r \tag{2.32}$$

Taking the lift coefficient dependence on angle of attack and pitch rate in wind axis as an example, the Taylor series expansion can be written as:

$$C_L = C_{L_0} + \frac{\partial C_L}{\partial \alpha}\Delta\alpha + \frac{\partial C_L}{\partial q}q + \frac{1}{2}\left[\frac{\partial^2 C_L}{\partial \alpha^2}(\Delta\alpha)^2 + 2\frac{\partial^2 C_L}{\partial \alpha \partial q}\Delta\alpha\, q + \frac{\partial^2 C_L}{\partial q^2}q^2\right] + \cdots$$

$$= C_{L_0} + C_{L_\alpha}\Delta\alpha + C_{L_q}\frac{q\bar{c}}{2V_0} + \frac{1}{2}\left[C_{L_{\alpha^2}}(\Delta\alpha)^2 + 2C_{L_{\alpha q}}(\Delta\alpha\,\frac{q\bar{c}}{2V_0}) + C_{L_{q^2}}(\frac{q\bar{c}}{2V_0})^2\right] + \cdots \tag{2.33}$$

For large-amplitude maneuvers and flight at high angle of attack such as spin, flight near stall, polynomial approximation could be inadequate and nonlinear models must be used. Solutions are to add more terms to the model or identify separate models for partitions to the independent variable space, and the latter is easier to solve several smaller subproblems instead of having a very complicated model structure.

Several common tools for non-linear system identification include: polynomials, splines, multi-variable orthogonal model, multipoint method, and Artificial Neural Network (ANN). ANN will be discussed as nonlinear system identification method in later chapters.

For linearization purposes, there are a few assumptions about the equations: firstly, the airspeed does not affect aerodynamic coefficients for subsonic flight. Secondly, $\dot{\alpha}$ contributions to the longitudinal lift and pitch moment coefficients are included in the q terms. Small disturbance theory can be applied to the nonlinear equations of motion. Each variable is assumed to be composed of two parts – a constant component associated with the steady

reference condition, and a perturbation associated with the linear model [2]. Wind axes are used for the force equations and body axes are used for the moment equations. Steady values for each variable are denoted by subscript o, and perturbations are denoted by the prefix Δ. For steady, straight, wings-level symmetric flight with no sideslip at a reference condition, and constant power setting:

$$\beta_0 = p_0 = q_0 = r_0 = \phi_0 = \Delta T = 0$$

To make the Long-EZ aircraft autonomous, the autopilot requires to be tested in a software-in-the-loop simulation environment, where the linearized baseline model simulated in the JSBSim can be represented as [41]:

$$C_a = \theta_0 + \sum_{j=1}^{n-1} \theta_j x_j \tag{2.34}$$

where C_a is the aerodynamic coefficient, θ_0 and θ_j are the parameters to be identified, x_j includes both input and output variables.

Aircraft's longitudinal dynamics can be modeled as:

$$C_L = -C_Z \cos\alpha + C_X \sin\alpha = -\frac{ma_z}{\bar{q}S}\cos\alpha + \frac{(ma_x - T)}{\bar{q}S}\sin\alpha = C_{L_0} + C_{L_\alpha}\Delta\alpha + C_{L_q}\frac{q\bar{c}}{2V} + C_{L_{\delta_e}}\Delta\delta_e \tag{2.35}$$

$$C_D = -C_X \cos\alpha - C_Z \sin\alpha = -\frac{(ma_x - T)}{\bar{q}S}\cos\alpha - \frac{ma_z}{\bar{q}S}\sin\alpha = C_{D_0} + C_{D_\alpha}\Delta\alpha + C_{D_q}\frac{q\bar{c}}{2V} + C_{D_{\delta_e}}\Delta\delta_e \tag{2.36}$$

$$C_m = \frac{1}{\bar{q}S\bar{c}}[I_{yy}\dot{q} + (I_{xx} - I_{zz})pr + I_{xz}(p^2 - r^2)] = C_{m_0} + C_{m_\alpha}\Delta\alpha + C_{m_q}\frac{q\bar{c}}{2V} + C_{m_{\delta_e}}\Delta\delta_e \tag{2.37}$$

where δ_e represents the deflection of canard, which is the only longitudinal control surface of this aircraft.

Lateral dynamics can be represented as:

$$C_Y = \frac{ma_y}{\bar{q}S} = C_{Y_0} + C_{Y_\beta}\beta + C_{Y_p}\frac{b}{2V}p + C_{Y_r}\frac{b}{2V}r + C_{Y_{\delta_a}}\delta_a + C_{Y_{\delta_r}}\delta_r \quad (2.38)$$

$$C_l = \frac{1}{\bar{q}Sb}[I_{xx}\dot{p} + (I_{zz} - I_{yy})qr - I_{xz}(pq + \dot{r})] = C_{l_0} + C_{l_\beta}\beta + C_{l_p}\frac{pb}{2V} + C_{l_r}\frac{rb}{2V} + C_{l_{\delta_a}}\delta_a + C_{l_{\delta_r}}\delta_r \quad (2.39)$$

$$C_n = \frac{1}{\bar{q}Sb}[I_{zz}\dot{r} + (I_{yy} - I_{xx})pq + I_{xz}(qr - \dot{p}) = C_{n_0} + C_{n_\beta}\beta + C_{n_p}\frac{pb}{2V} + C_{n_r}\frac{rb}{2V} + C_{n_{\delta_a}}\delta_a + C_{n_{\delta_r}}\delta_r \quad (2.40)$$

where most of the aerodynamic coefficients have been calculated with Roskam's method [39] and they have been summed up in

Table 2.2. In terms of the other coefficients such as the control derivatives which cannot be calculated with this method, Cessna 172p's values have been taken as reference [42]. Aircraft's moments of inertia have been calculated with OpenVSP [43] software based on Long-EZ's 3D dimensions, which is also validated with two empirical functions. The baseline model has been tested various times in JSBSim.

Table 2.1: Long-EZ aircraft parameters

Parameter	Symbol	Value
Aircraft gross weight	m	650.5
Reference wing span	b	9.9
Reference wing area	S	9.511
Mean aerodynamic chord	$\bar{c}$	1.411
Roll moment of inertia	I_{xx}	487.67
Pitch moment of inertia	I_{yy}	535.58
Yaw moment of inertia	I_{zz}	981.69
Product moment of inertia	I_{xz}	12.75
C.G. location	x_{cg}	2.78

Table 2.2: Long-EZ baseline model parameters

C_{L_0}	0.3632	C_{Y_r}	-0.3022
C_{L_α}	0.1093	$C_{Y_{\delta_r}}$	1.04
C_{L_q}	1.102	C_{l_β}	-0.001965
$C_{L_{\delta_e}}$	0.1074	C_{l_p}	-4.5
C_{D_0}	0.01315	C_{l_r}	0.4399
C_{D_α}	0.0036	$C_{l_{\delta_a}}$	2.4
C_{m_0}	0.6	$C_{l_{\delta_r}}$	0.0349
C_{m_α}	-0.1	C_{n_β}	0.001
C_{m_q}	-3.0	C_{n_p}	-0.098
$C_{m_{\delta_e}}$	1.1	C_{n_r}	0.014
C_{Y_β}	-0.506	$C_{n_{\delta_a}}$	-0.01521
C_{Y_p}	-0.0242	$C_{n_{\delta_r}}$	-0.437

In terms of the baseline model, its derivatives have been calculated with empirical functions largely based on the dimensions of the aircraft which need to be validated with flight data. This part has been presented briefly in Chapter 4. However, with no air data available at this stage, the stability and control derivatives calculated based on aircraft dimensions in the baseline model pertaining to these terms may not be very accurate. The baseline linear model is a good foundation to build upon, which could be improved in the future with air data recordings available for the aircraft Long-EZ.

Linear aircraft models can conform well with the aircraft response at a smooth flight condition. However, when flying at high angle of attack or high-G maneuvers, the linear models may not be sufficient to present aircraft dynamics. Therefore, nonlinear aircraft models are

required to improve the accuracy of predicting aircraft maneuverability. In many practical applications, the aerodynamic models for large amplitudes or rapid excursions from reference flight conditions need to add nonlinear terms. In this thesis, a block-oriented model consisting of linear term and nonlinear term has been studied, which has been explained in Chapter 5.

Chapter 3 Flight Test Design

Flight testing the piloted and unmanned aerial vehicles is an interdisciplinary process that involves many expertise in different branches such as aerospace engineering, electric engineering, and mechanical engineering. Aerospace engineers are normally responsible for the aerodynamics, stability and control of the specific vehicle configuration. Electric engineers are helpful in developing the appropriate instrumentation, evaluating the feedback control loops, and electronics subsystems. Mechanical engineers are specialized in designing mechanical, hydraulic and pneumatic subsystems.

The main purposes of flight testing can be summed up as three-fold: determining the actual characteristics of the machine, providing developmental information, and obtaining research information [44]. The most common way of flight tests classification is associated with the stage of development, such as Developmental Test and Evaluation (DT&E) and Operational Test and Evaluation (OT&E).

The factors that need to be considered in test planning are safety, cost and schedule. Flight testing always comes with risks. However, the risks can be greatly reduced by proper risk management. Moreover, flight test instrumentation is one of the most costly areas. Adequate instrumentation should be installed to the aircraft to collect data. Flight test schedule should be carefully planned to improve efficiency.

Risk management needs to be embedded in the flight plan. All the risks and their probabilities, and mitigation methods have been intensively studied to reduce risks to the minimum level.

The following aspects have been defined for the flight test of Long-EZ: which physical quantities will be measured, how are they going be measured, what the test conditions will be, and how the aircraft is going to be excited. Based on these questions, flight test instrumentations have been specified, flight test condition and aircraft configurations have been determined, and flight maneuvers and inputs have been designed for system identification purpose.

3.1 Aircraft Description

The Long-EZ is a lightweight, home-built experimental class aircraft designed by Rutan Aircraft Factory (RAF), Inc. and features the latest advances in aerodynamics and structure. It's equipped with the Lycoming O-235 (108hp) engine and has an alternator powered electrical system. The canard configuration was designed for improved performance, flying qualities, and safety compared to conventional light plane. Modern airfoils have been used: modified Eppler 1230 airfoil is used for the main wing, and GU25-5(11)8 is used for the canard. The high-lift canard wing has full-span flaps which double as elevator and landing flap [45]. NASA developed winglet system is applied to the aircraft to offset the wingtip vortex and reduce induced drag. It has a reversible type mechanical flight control system with push rods for canard and aileron, and cables for rudders (independent ones). Cockpit adjustable trim is provided for pitch and roll only. Pitch and roll trim tabs are not used. There is a pitch trim lever on the side of the left armrest which is redundant from pitch control, similar to the roll trim mechanism with trim handle located on the right console [45].

Figure 3.1: Aircraft Long-EZ with canard configuration, © ITPS Canada Ltd.

It's cockpit layout is designed to reduce pilot workload with throttle, mixture, carb heat, pitch trim and landing controls on the left side console and a side stick controller on the right console [45]. The inboard portion of wing strakes can be utilized as storage area, which alleviates the situation of a compact cockpit. According to the owner of this aircraft, the empty weight of the aircraft is around 927lb, and the max gross takeoff weight is 1325lb, and can reach 1425lb under certain conditions. The fuel system consists of two individually selected wing tanks, each with 26-gallon capacity.

3.2 Optimal Input Design

Aircraft dynamics can be excited by applying control pulse, step, multistep, or harmonic inputs (Figure 3.2). Flight test maneuvers for system identification purpose include short period maneuver, phugoid maneuver, pushover-pull-up, level turn, thrust variation, bank-to-bank roll, Dutch roll maneuver, and steady heading steady sideslip [3].

Short period maneuvers can be excited with doublet, 2-1-1 and 3-2-1-1 inputs. The natural frequency of the aircraft f_n determines the input duration Δt which has been explained below. The phugoid mode will be excited with speed variation around trim point and trust variation. Level turn maneuver starts at a wings level flight by smoothly banking the aircraft to 30, 45, 60 deg bank at a rate of 10 deg/s, holding the bank attitude for 5 seconds, and then rolling to the opposite direction, holding for 5 seconds, and then return to wings-level again, resulting an S-type flight path. Longer-duration doublet throttle input can be performed to determine the dynamic effects due to thrust variation on the longitudinal motion. Bank-to-bank roll and Dutch roll maneuvers are necessary to get lateral-directional derivatives. Bank-to-bank is performed by starting from a level flight, applying a sharp aileron input, holding till at least 30-deg bank and followed by rapid bank input to the opposite side, and then returning to wings-level conditions. This test will be repeated with increasing bank angles 30, 45 and 60. The Dutch roll mode of the basic aircraft is usually lightly damped and will be excited with rudder doublet inputs. Steady Heading Steady Sideslip (SHSS) provides information on the directional stability, lateral-directional control and cross coupling effects. SHSS is started from a horizontal level flight by applying pedal input and opposite aileron to maintain constant heading for about 10-15 s. The same procedure will be repeated in the other direction of side slipping.

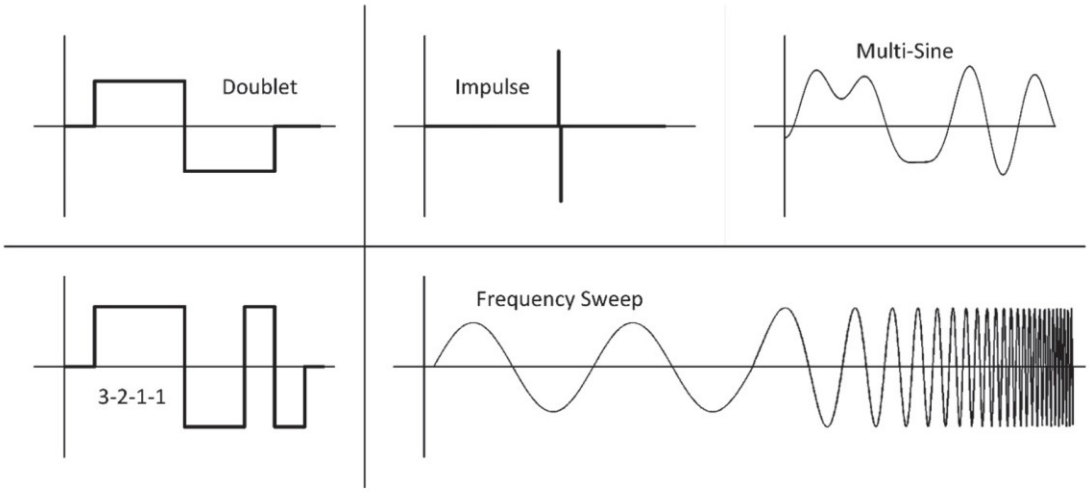

Figure 3.2: Schematics of typical inputs [46]

Apart from choosing appropriate maneuver inputs, a variety of different flight test conditions (altitude and speed) are required to form a test matrix. An example has been shown in Figure 3.3.

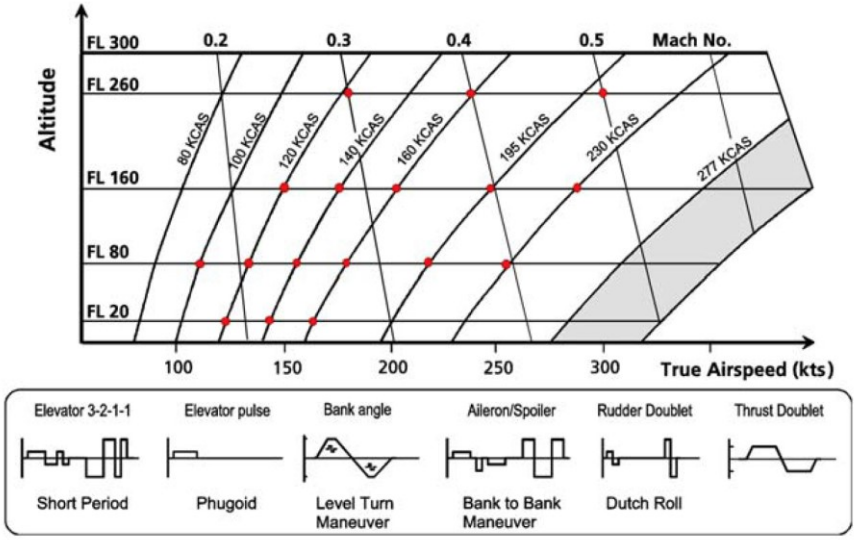

Figure 3.3: Typical flight-test program for system identification [3]

At current stage, there is no system available to record the air data for Long-EZ aircraft, therefore, it is not feasible to get complete stability and control derivatives at this stage to validate the baseline model in Chapter 2. However, frequency sweep and 3-2-1-1 input have

been designed for parameter identification test flight with a range of different test conditions. Only two maneuvers have been chosen considering the flight endurance. The flight test data will still be a valuable source to validate the baseline model.

Frequency sweep

Frequency sweep is a series of sinusoidal inputs in one axis with gradually increased frequency to excite the aircraft's primary oscillation mode. It has been planned in this system identification flight for pilot to get a feeling of the aircraft Long-EZ's natural frequency, which will be utilized as a basis to design the short-period test maneuver inputs. A typical example of frequency input has been presented in Figure 3.4.

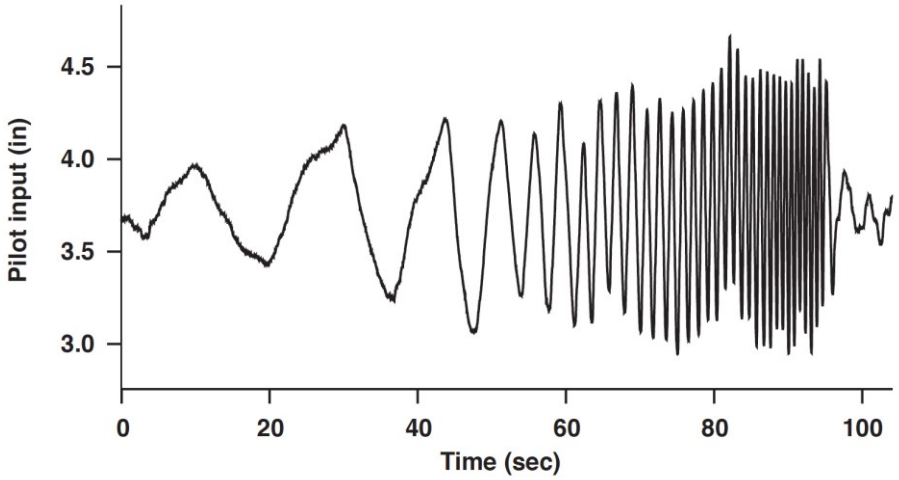

Figure 3.4: Typical frequency sweep input [4]

The frequency sweep maneuver has many advantages in system identification. The excitation spectral content has a very uniform distribution across the desired frequency range. Therefore, the frequency-sweep input delivers accurate and reliable identification results without the requirement of a priori knowledge about the aircraft. A good frequency sweep maneuver usually starts and ends at a trimmed condition. The response time-history is roughly

symmetrical, with deviations in input and output generally symmetrical around a trimmed point. However, frequency sweeps are more time-consuming compared with optimal inputs such as the 3-2-1-1 input.

3-2-1-1 input

3-2-1-1 is a series of alternating inputs with widths in the ratio 3-2-1-1. The time step Δt is chosen so that the natural frequency of the mode being excited lies in the center or in the upper third of the input spectrum:

$$\Delta t_{3211} \approx \frac{1}{4f_n} \tag{3.12}$$

or:

$$\Delta t_{3211} \approx \frac{1}{3f_n} \tag{3.13}$$

3-2-1-1 inputs are easy to implement in flight as long as there is a preliminary knowledge of the aircraft's natural frequency. 3-2-1-1 can be repeated, with one starting by pulling the aircraft and the second time by pushing the stick.

The minor aspects of 3-2-1-1 inputs are: firstly, it is asymmetric about the trimmed condition. There are four steps in one direction and three steps in the other direction. Secondly, the first input has larger duration, which leads to deviation from trimmed point before the following steps. However, these effects can be minimized by modifying the amplitudes of the 3-2-1-1 inputs. Another method is to repeat the 3-2-1-1 but start from the opposite direction. Another variation of 3-2-1-1 is the 1-1-2-3 which has the same power spectrum but starts with the higher frequency which prevents the vehicle from going too far away from the trimmed condition. A typical 3-2-1-1 input and response has been presented in Figure 3.5.

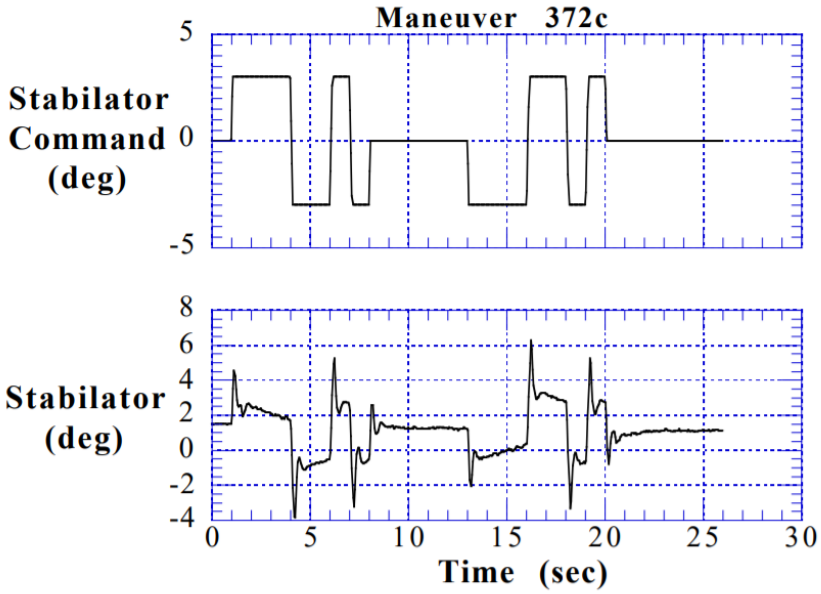

Figure 3.5: Typical 3-2-1-1 input and response [47]

Different test conditions have been chosen for the Long-EZ parameter identification flight. According to flight test plan, maneuvers speeds have been set at 120kts, 115kts, 110kts, 105kts and minimum trim speed, and maneuver altitudes have been set at 8000ft and 5000ft respectively. Each maneuver starts at a trimmed condition with clean configuration. Frequency sweeps on longitudinal and lateral axes have been carried out and followed by three times of 3-2-1-1 inputs for each test point. The flight test conditions have been listed in Table 3.1.

Table 3.1: Test conditions of Long-EZ parameter identification flight

Test Point	Maneuvers	V_{trim} (KIAS)	Altitude (ft)
1	Frequency sweep and 3-2-1-1 on longitudinal axis	116	8000
2	Frequency sweep and 3-2-1-1 on	116	8000

	lateral axis		
3	Frequency sweep and 3-2-1-1 on longitudinal axis	110	8000
4	Frequency sweep and 3-2-1-1 on lateral axis	110	8000
5	Frequency sweep and 3-2-1-1 on longitudinal axis	105	8000
6	Frequency sweep and 3-2-1-1 on lateral axis	105	8000
7	Frequency sweep and 3-2-1-1 on longitudinal axis	Minimum trim speed	8000
8	Frequency sweep and 3-2-1-1 on lateral axis	Minimum trim speed	8000
9	Frequency sweep and 3-2-1-1 on longitudinal axis	120	5000
10	Frequency sweep and 3-2-1-1 on lateral axis	120	5000

3.3 Flight Test Instrumentation

The accuracy of measured data has a direct impact on the result of parameter identification. The following variables need to be measured to build aircraft models: control surface deflections, linear and angular rates and accelerations, attitude angles, air data are required to

get stability and control derivatives of the aircraft.

Accurate air-relative velocity data include angle of attack (α), sideslip angle (β), and airspeed (V), which are the most difficult to obtain. These quantities are easily influenced by the local flows about the aircraft. At current stage, this kind of sensor is not available to the aircraft Long-EZ. Therefore, air data is not available at current stage.

Aircraft angular velocity components are usually measured using rate gyros attached to the aircraft and aligned with body axes. In theory, the location of these sensors can be anywhere on the aircraft because angular rates are the same at any point of a rigid body.

Translational accelerometers should be located near aircraft's C.G. and aligned with the body axes. The main negative aspect of these sensors is that their frequency response is very excellent so that they also pick up structural responses and engine vibrations, which makes the signals quite noisy.

Rotational acceleration. This kind of sensors are not common, but they are useful of providing additional information content to the data for output-error modeling. This data can be extracted from numerical differentiation of rate gyros information.

Euler angles are usually measured using integrating gyros or magnetometers. Euler angles are less important in aircraft system identification because the aerodynamic forces and moments do not depend on aircraft orientation relative to earth axes. However, they are useful in data compatibility analysis.

Sensors that measure control surface deflections and pilot control deflections are typically some type of potentiometer, which produce a voltage proportional to rotational or linear motion. These sensors are reliable and have low noise level.

Due to the availability of the current flight test instrumentation at ITPS, the flight test instrumentations being used in this project include SBG sensor and Graphtec with string pods, which have been installed in the backseat area near the C.G. of the aircraft.

SBG sensor (Figure 3.6) includes a MEMS-based Inertial Measurement Unit (IMU) integrating three gyroscopes, three accelerometers, and three magnetometers. It runs an enhanced Extended Kalman Filter (EKF) which fuses inertial data with Global Navigation Satellite System (GNSS), Odometer, and Differential GPS (DGPS) information for excellent orientation and navigation data in the most challenging environments. It records aircraft response such as Euler attitude angles (ϕ, θ, Ψ), translational accelerations (a_x, a_y, a_z) and $(\dot{u},\ \dot{v},\ \dot{w})$, body-axis angular velocities (p, q, r) and $(\dot{\phi},\ \dot{\theta},\ \dot{\Psi})$.

String pods have been used to measure control inputs u_{lon} and u_{lat}, which have been recorded real-time by Graphtec (Figure 3.7). The variables being measured during the flight test have been summed up in Figure 3.8.

Figure 3.6: SBG, © SBG-systems

Figure 3.7: Graphtec, © Graphtec corp.

Figure 3.8: Input and output measurements for Long-EZ test flight

Ideally, all the measured signals should be sampled at the same constant rate for convenience purpose. But it is also acceptable for the measured quantities to be sampled at different sampling rates due to instrumentation limitations. In this case, the high sampling rate data need to be reduced to match the low sampling rate data so that all data is converted to the same sampling rate before analysis. A good rule of thumb for selecting the sampling rate f_s is

$$f_s = 25 f_{max} \tag{3.14}$$

For many aircraft, the frequencies of the rigid-body dynamic modes are below 2Hz, which puts the ideal sampling rate f_s at 50Hz. In our case, the SBG has 50Hz sampling rate, but the Graphtec only has 20Hz. Therefore, the data from SBG and Graphtec must be reduced to the same sampling rate for data analysis, which has been introduced later.

3.4 Flight Test Results

The flight data of test point one and test point two has been presented from

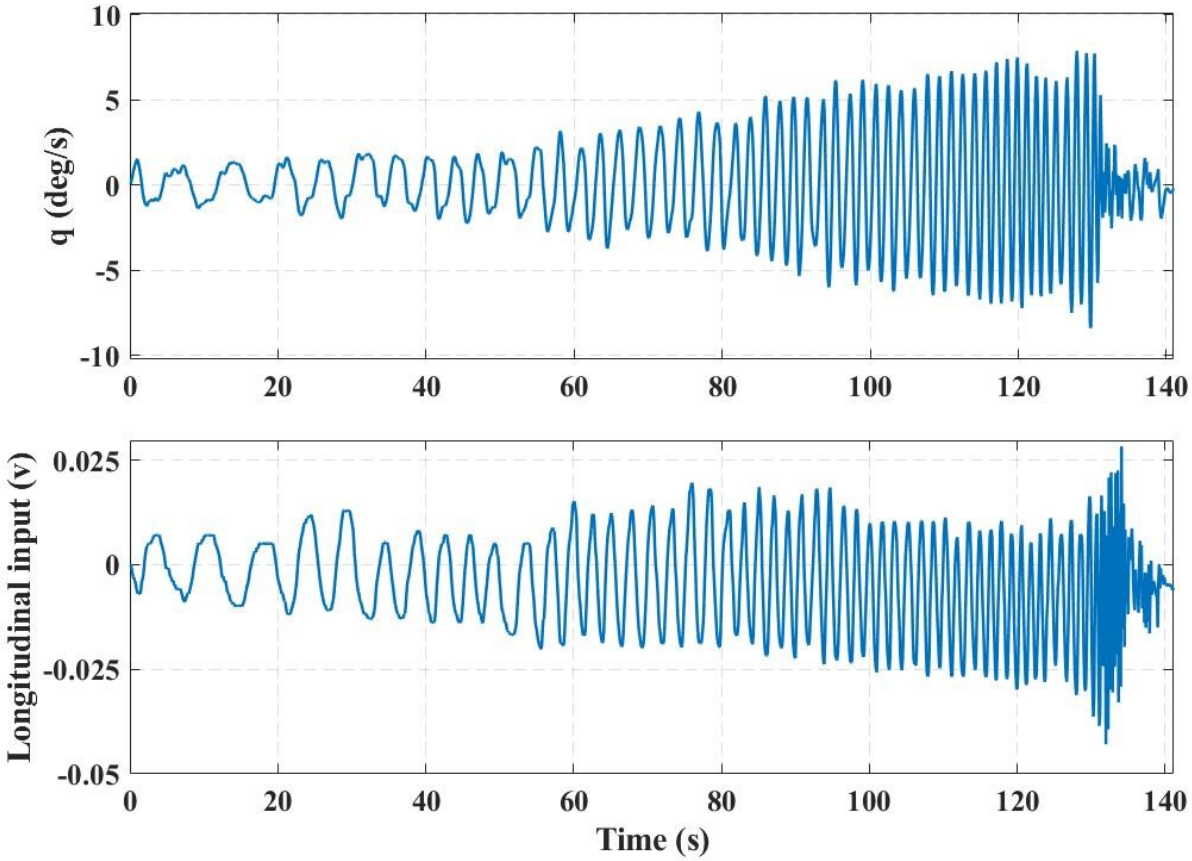

Figure *3.9* to Figure 3.12. Aircraft test altitude was at 8000 feet (ft) and airspeed was at 116 knots (kts), and flight maneuvers were frequency sweep and 3-2-1-1 input on longitudinal and lateral axes respectively. The longitudinal frequency sweep has a total length of 2 mins with broad frequency from low to high (0.9 - 5 rad/s) covered by pilot. The lateral frequency sweep has a total length of 100 seconds also with broad frequency ranged covered (0.6 - 5.6 rad/s). Figure 3.10 shows a spike in the input signal around 303 s, which is a noise in the voltage signal that should be filtered out.

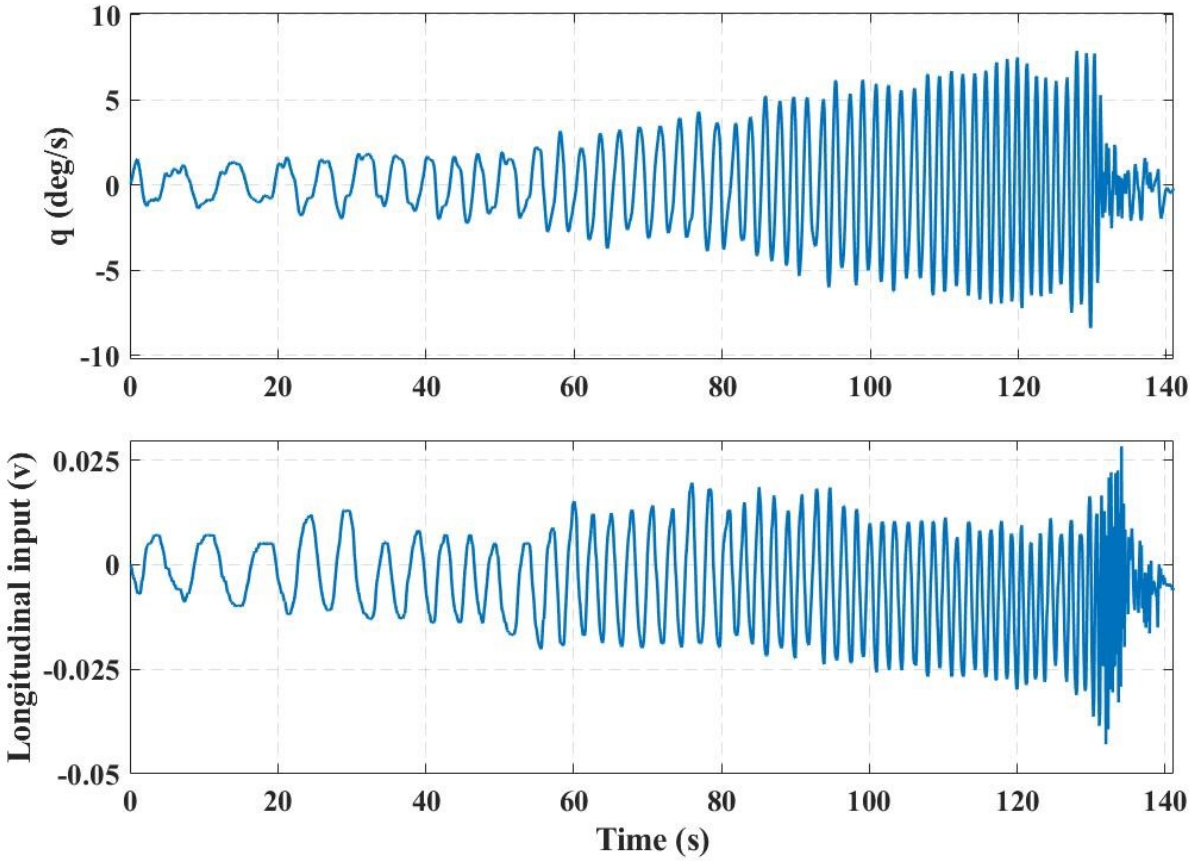

Figure 3.9: Longitudinal frequency sweep input and pitch rate response, test point one

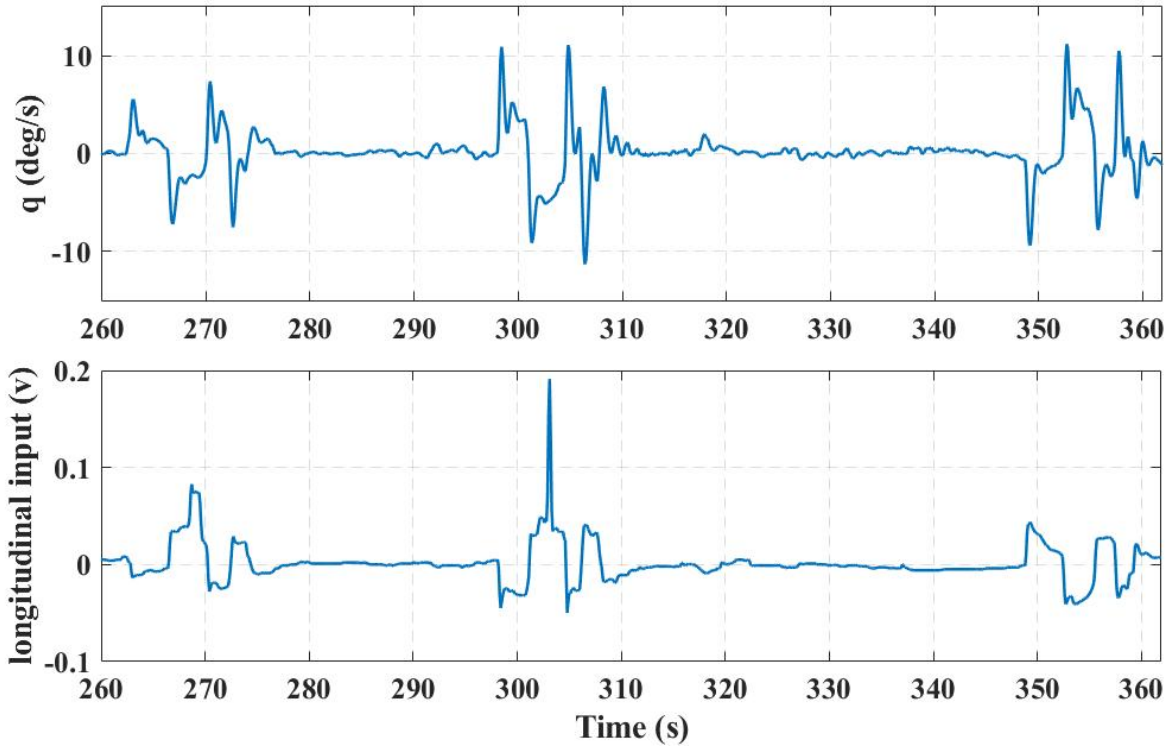

Figure 3.10: Longitudinal 3-2-1-1 input and pitch rate response, test point one

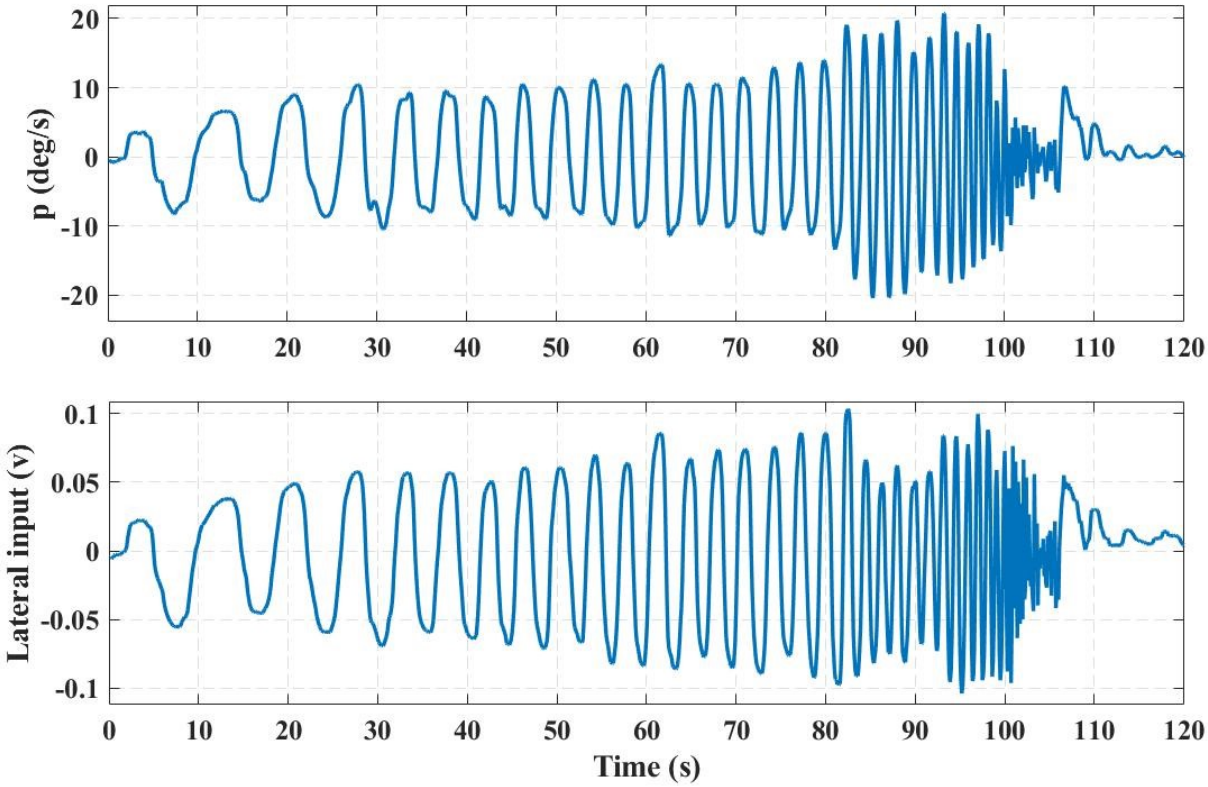

Figure 3.11: Lateral frequency sweep input and pitch rate response, test point two

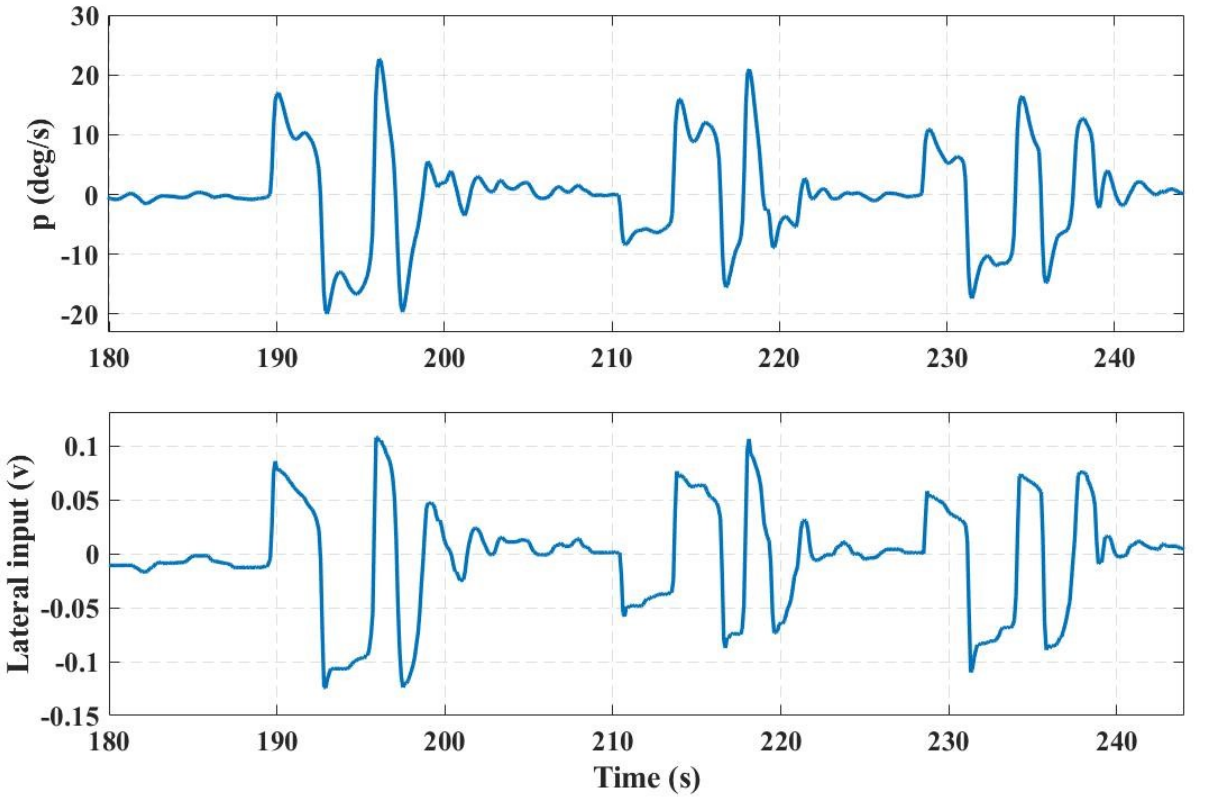

Figure 3.12: Lateral 3-2-1-1 input and pitch rate response, test point two

3.5 Data Compatibility Check

Data compatibility check between measured accelerations, rates, and positions associated with the translational and rotational motion about the C.G. is required before further data analysis, to ensure the reliability of the produced model. The kinematic relationship among the measured quantities has been used to check that the measurements are mutually consistent.

Translational kinematics and rotational kinematics have been introduced in the second chapter from equation (2.24) and (2.25), and they are presented below again for convenience:

$$p = \dot{\phi} - sin\,\theta\,\dot{\psi}$$

$$q = cos\,\phi\,\dot{\theta} + sin\,\phi\,cos\,\theta\,\dot{\psi}$$

A list of typical instrumentation errors that can affect the quality of recorded flight data have been presented in Table 3.2.

Table 3.2: Typical instrumentation errors

Sensor	Variable	Bias error	Scale factor error
Translational accelerometer	$a_x,\ a_y,\ a_z$	X	--
Rate gyro	$p,\ q,\ r$	X	--
Airflow angle vane	$\alpha,\ \beta$	X	X
Dynamic pressure sensor	V	X	X
Integrating gyro	$\phi,\ \theta,\ \psi$	X	X

The data from four frequency sweep test points has been used to present the compatibility check results on both longitudinal and lateral axes, which have been presented in Figure 3.13. As showed in Figure 3.13, lateral data compatibility checks for test point 1 (longitudinal) and

test point 2 (lateral) are in general satisfactory. However, there is a lack of coherence between $2.02 - 2.04 \times 10^4$ sample section on the longitudinal frequency sweep. Possible reasons could be: 1) aircraft is experiencing gust wind interference, 2) there is sensor error during that period of time, 3) some dynamic mode of the aircraft has been excited, and 4) there is some periodical noise on the aircraft.

The data in general has good coherence. Since this longitudinal test point is the only data available at this stage, they will be utilized in this thesis for system identification in Chapter 4 and Chapter 5. In the later stage where more data is available, more consistent data can be used to get a better model.

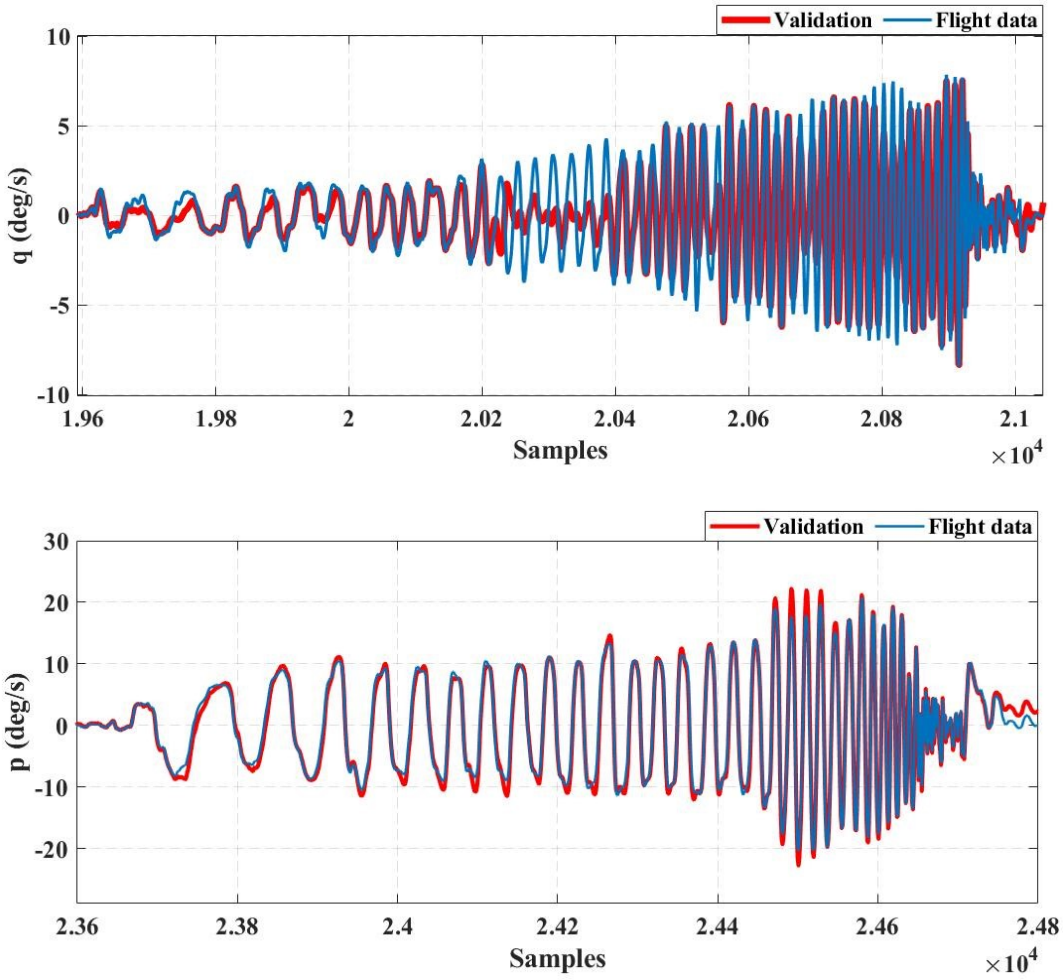

Figure 3.13: Data compatibility check in longitudinal and lateral axes

Chapter 4 Equation Error Method

4.1 Introduction

The system identification methods can be classified into three categories: output error method, filter error method, and equation error method.

Output error method assumes that process noises are negligible, and measurements are corrupted by measurement noises only, which is the most widely applied time-domain method to estimate aircraft parameters from flight data [2].

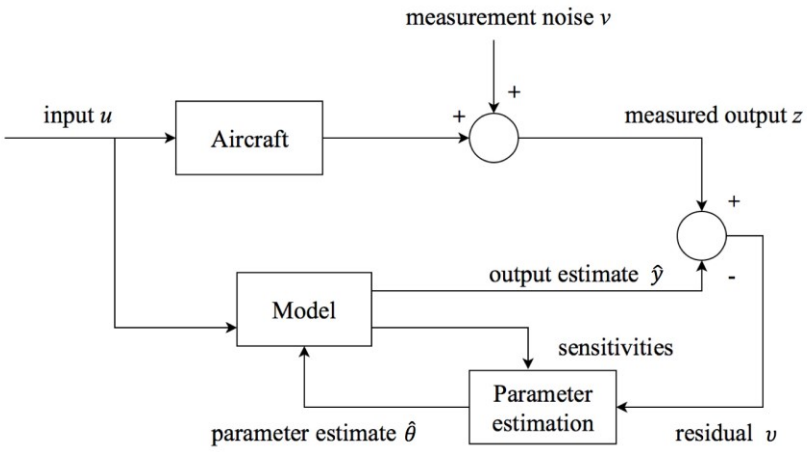

Figure 4.1: Block diagram for output-error parameter estimation [2]

Filter error method accounts for both process and measurement noises. The maximum likelihood estimator includes a Kalman filter updating the states and filtering out noises. When there is turbulence, the output error method won't yield very satisfactory results. Besides, they generally lead to a faster convergence rate as they are less sensitive to stochastic disturbances. The filter error method can be applied to aircraft system identification because the aircraft data has been taken at a certain sampling rate, which are a series of discrete numbers.

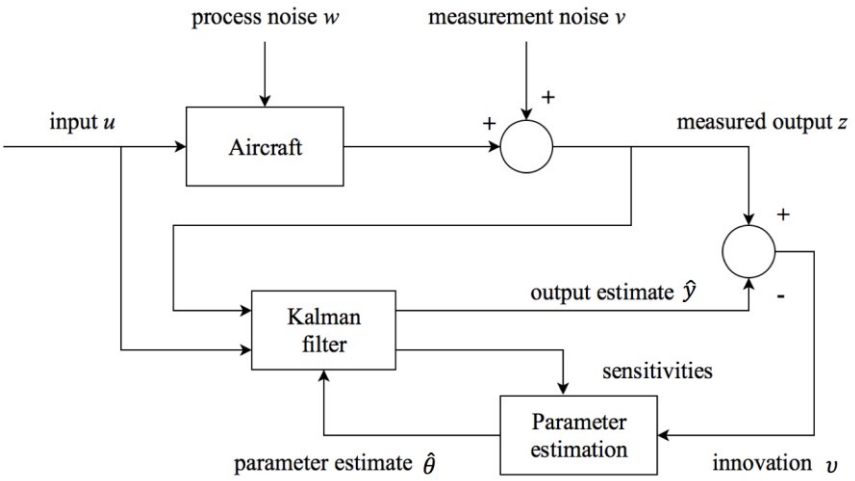

Figure 4.2: Block diagram of filter-error parameter estimation [2]

Least-squares estimation is one of the oldest estimation theories with broad engineering applications. The Least-Squares (LS) technique, also known as regression analysis, belongs to the equation-error methods as they minimize a cost function defined directly from input-output equation. Classical Ordinary Least-Squares (OLS) method assumes that independent variables are error free and noise free, and dependent variables are corrupted by uniformly distributed noise, it is based on Fisher model [3].

The basic principle of least-squares method is to minimize the sum of squares of the errors between the measurements and model response. The estimates can be obtained by applying matrix algebra in a one-shot computational procedure, which has great advantages in its mathematical simplicity. Nonlinear models can also be solved with the same principle but with iterative procedures.

There are significant advantages of using linear regression methods for modeling aircraft aerodynamics based on flight data. The whole modeling of the aircraft can break down into a series of small equations that can deal with one problem at a time. Linear regression estimation

is relatively simple, and the linear model can be used to test unstable aircraft that must be tested with an automatic feedback control system. Moreover, it is simpler to analyze large-amplitude maneuvers through a series of linear models, to judge individual parameters through stepwise regression, and to apply to unstable aircraft.

Besides, linear regression model parameters are usually stability and control derivatives that multiply aircraft states or controls to form the baseline model of Long-EZ as presented in Chapter 2.

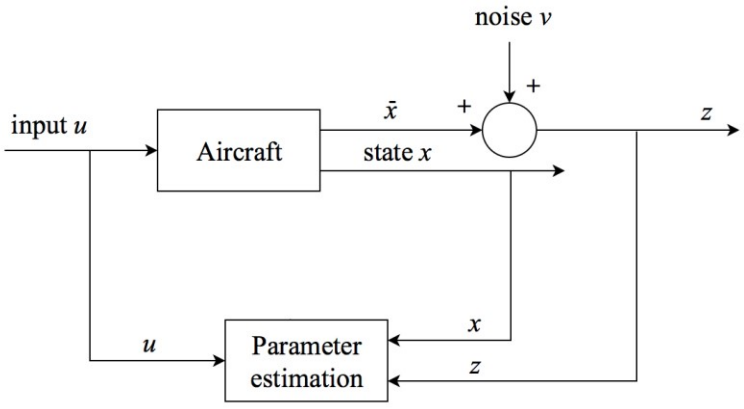

Figure 4.3: Block diagram for equation-error parameter estimation [2]

Depending on the residuals are linear or non-linear, the least-squares can be divided to two categories: ordinary least-squares and nonlinear least-squares. The linear least-squares technique has its mathematical simplicity. Estimates can be obtained by applying matrix algebra in a one-shot computational procedure [3]. However, nonlinear least-squares problems can be solved only iteratively.

The linear equations of measurements can be presented as follows [2]:

$$z = X\theta + v \tag{4.1}$$

where z is $N \times 1$ vector of measurements, θ is a vector of unknown constant parameters,

and v is a random vector of measurement noises. X is a matrix of vectors of ones and regressors.

There are three different models for the uncertainties in the parameters and measurements: Bayesian model, Fisher model, and least-squares model. Probability density is involved in the first two models. For least-squares models, no uncertainty models for θ and v are used, but v is assumed to be zero mean and uncorrelated, and with constant variance [2].

$$E(v) = 0 \qquad E(vv^T) = \sigma^2 I \tag{4.2}$$

The cost function of ordinary least-squares estimator can be represented as [2]:

$$J(\theta) = \frac{1}{2}(z - X\theta)^T(z - X\theta) \tag{4.3}$$

For the entire measured data $z(i), i = 1, 2, \dots, N,$ the ordinary least-squares estimator is obtained by minimizing the cost function [2]:

$$J(\theta) = \frac{1}{2}\sum_{i=1}^{N}[z(i) - X(i)\theta]^2 \tag{4.4}$$

The estimated parameter $\hat{\theta}$ can be obtained by minimizing the cost function [2]:

$$\frac{\partial J}{\partial \theta} = -X^T z + X^T X\hat{\theta} = 0 \tag{4.5}$$

therefore,

$$\hat{\theta} = (X^T X)^{-1} X^T z \tag{4.6}$$

Define the matrix $\mathcal{D}$ as [2]:

$$\mathcal{D} \equiv (X^T X)^{-1} = \left[d_{jk}\right] \quad j, k = 1, 2, \dots, n_p \tag{4.7}$$

The variance of the jth estimated parameter in the parameter vector $\hat{\theta}$ is the jth diagonal element of the covariance matrix [2]:

$$\mathrm{Var}\left(\hat{\theta}_j\right) = \sigma^2 d_{jj} \equiv s^2\left(\hat{\theta}_j\right) \;\; j = 1, 2, \dots, n_p \tag{4.8}$$

And the covariance between two estimated parameters $\hat{\theta}_j$ and $\hat{\theta}_k$ is [2]:

$$\mathrm{Cov}(\hat{\theta}_j, \hat{\theta}_k) = \sigma^2 d_{jk} \quad j,k = 1,2,\dots,n_p \tag{4.9}$$

The correlation coefficient can be represented as [2]:

$$r_{jk} \equiv \frac{d_{jk}}{\sqrt{d_{jj}d_{jk}}} = \frac{\mathrm{Cov}(\hat{\theta}_j, \hat{\theta}_k)}{\sqrt{\mathrm{Var}(\hat{\theta}_j)\mathrm{Var}(\hat{\theta}_k)}} \quad j,k = 1,2,\dots,n_p$$

$$-1 \le r_{jk} \ll 1 \quad j,k = 1,2,\dots,n_p \tag{4.10}$$

The residual $v(i)$ is defined as the difference between measured output $z(i)$ and the estimated output $\hat{y}(i)$ [2]:

$$v(i) = z(i) - \hat{y}(i) = z(i) - X(i)\hat{\theta} \qquad i = 1,2,\dots,N \tag{4.11}$$

or, in the vector form:

$$v = [I - X(X^T X)^{-1} X^T]z \tag{4.12}$$

The whiteness of the residual can be checked with the autocorrelation function of the residuals [2]:

$$\hat{\mathcal{R}}_{vv}(k) = \frac{1}{N}\sum_{i=1}^{N-k} v(i)v(i+k) \qquad k = 0,1,2,\dots,N-1 \tag{4.13}$$

When the residuals are completely uncorrelated, $\hat{\mathcal{R}}_{vv}(k) = 0, k \neq 0$. However, in practice, the $\hat{\mathcal{R}}_{vv}(k)$ values are never exactly zero even with an adequate model, instead, it will vary slightly around zero.

The non-linear least-squares model was formulated as [2]:

$$z = h(\theta) + v \tag{4.14}$$

or

$$z(i) = f[x(i), \theta] + v(i) \qquad i = 1,2,\dots,N \tag{4.15}$$

The least-squares estimator can be obtained by minimizing the sum of squared errors [2]:

$$J(\theta) = \frac{1}{2}\sum_{i=1}^{N}\{z(i) - f[x(i), \theta]\}^2 \tag{4.16}$$

The minimum of the preceding cost function is found by satisfying the normal equations [2]:

$$\frac{\partial J}{\partial \theta}|_{\theta=\hat{\theta}} = -\sum_{i=1}^{N}\{z(i) - f[x(i), \hat{\theta}]\}\frac{\partial f[x(i),\theta]}{\partial \theta}|_{\theta=\hat{\theta}} = 0 \tag{4.17}$$

where $\partial J/\partial \theta$ is a row vector containing the partial derivatives of the nonlinear scalar function $J(\theta)$ with respect to the elements of θ, and $\partial f[x(i),\theta]/\partial \theta$ is a row vector of output sensitivities to change in the model parameters. It is a set of nonlinear algebraic equations. This means that $\hat{\theta}$ cannot be obtained by simplex algebra. Instead, an iterative nonlinear optimization technique must be used.

Gauss-Newton method

The Gauss-Newton method of nonlinear optimization belongs to a class of second-order algorithms and is one of the most widely applied methods in flight vehicle system identification in the time-domain [3]. It is a modified method based on the Newton method, which is also known as the Newton-Raphson method.

Minimizing the likelihood function with respect to unknown parameters is given by [3]:

$$\frac{\partial J(\Theta)}{\partial \Theta} = 0 \tag{4.18}$$

The Taylor-series expansion of the $\partial J(\Theta)/\partial \Theta$ about the ith value is given by [3]:

$$\left(\frac{\partial J}{\partial \Theta}\right)_{i+1} \approx \left(\frac{\partial J}{\partial \Theta}\right)_i + \left(\frac{\partial^2 J}{\partial \Theta^2}\right)_i \Delta\Theta \tag{4.19}$$

where $\Delta\Theta = \Theta_{i+1} - \Theta_i$ is the parameter change and $(\partial^2 J/\partial \Theta^2)_i$ is the second gradient of the cost function with respect to Θ at the ith iteration. The term $\Delta\Theta$ can be solved by equating the right-hand side of (4.19) to zero [3]:

$$\Delta\Theta = -\left[\left(\frac{\partial^2 J}{\partial \Theta^2}\right)_i\right]^{-1}\left(\frac{\partial J}{\partial \Theta}\right)_i \tag{4.20}$$

The preceding change in Θ on the $(i+1)$ th iteration makes local $(\partial J/\partial \Theta)_{i+1}$

approximately zero [3]. Therefore, starting from an initial guess value of Θ_0, $\Theta_{i+1} = \Theta_i + \Delta\Theta$ provides an iterative solution to find the minimum of a function, which is known as the Newton-Raphson method [48].

In the case of flight data, the residual covariance matrix can be determined with [3]:

$$R = \frac{1}{N}\sum_{k=1}^{N}[z(t_k) - y(t_k)][z(t_k) - y(t_k)]^T \tag{4.21}$$

with the cost function being in the form of [3]:

$$J(\Theta) = \frac{1}{2}\sum_{k=1}^{N}[z(t_k) - y(t_k)]^T R^{-1}[z(t_k) - y(t_k)] \tag{4.22}$$

the partial differentiation of Eq. (4.23) gives [3]:

$$\frac{\partial J}{\partial \Theta} = -\sum_{k=1}^{N}\left[\frac{\partial y(t_k)}{\partial \Theta}\right]^T R^{-1}[z(t_k) - y(t_k)] \tag{4.23}$$

the partial differentiation of Eq. (4.23) with respect to Θ gives [3]:

$$\frac{\partial^2 J}{\partial \Theta^2} = \sum_{k=1}^{N}\left[\frac{\partial y(t_k)}{\partial \Theta}\right]^T R^{-1}\left[\frac{\partial y(t_k)}{\partial \Theta}\right] - \sum_{k=1}^{N}\left[\frac{\partial y(t_k)}{\partial \Theta}\right]^T R^{-1}[z(t_k) - y(t_k)] \tag{4.24}$$

The residual term $[z(t_k) - y(t_k)]$ tends to cancel out when summed over a sufficient period of time, because the noise is assumed to be zero mean and independent [3]. Therefore, the above equation can be simplified as [49]:

$$\frac{\partial^2 J}{\partial \Theta^2} \approx \sum_{k=1}^{N}\left[\frac{\partial y(t_k)}{\partial \Theta}\right]^T R^{-1}\left[\frac{\partial y(t_k)}{\partial \Theta}\right] \tag{4.25}$$

The advantage of this simplification is that it greatly reduces the computational burden but keeps the rapid, quadratic convergence.

The quasi-linearization [50] method, which is a first-order approximation, can be expressed as:

$$y(\Theta) = y(\Theta_0 + \Delta\Theta) \approx y(\Theta_0) + \frac{\partial y}{\partial \Theta}\Delta\Theta \tag{4.26}$$

When applied with Eq. (4.24), Gauss-Newton and quasi-linearization methods lead to a

system of linear equations, the former equation turns into [3]:

$$\sum_{k=1}^{N}\left[\frac{\partial y(t_k)}{\partial \Theta}\right]^T R^{-1}\left[\frac{\partial y(t_k)}{\partial \Theta}\right]\Delta\Theta = \sum_{k=1}^{N}\left[\frac{\partial y(t_k)}{\partial \Theta}\right]^T R^{-1}[z(t_k)-y(t_k)] \tag{4.27}$$

which can be represented as [3]:

$$\Theta_{i+1} = \Theta_i + \Delta\Theta, \text{ and } \mathcal{F}\Delta\Theta = -\mathcal{G} \tag{4.28}$$

where i is the iteration index, and $\mathcal{F}$ and $\mathcal{G}$ are given by [3]:

$$\mathcal{F} = \sum_{k=1}^{N}\left[\frac{\partial y(t_k)}{\partial \Theta}\right]^T R^{-1}\left[\frac{\partial y(t_k)}{\partial \Theta}\right] \tag{4.29}$$

$$\mathcal{G} = -\sum_{k=1}^{N}\left[\frac{\partial y(t_k)}{\partial \Theta}\right]^T R^{-1}[z(t_k)-y(t_k)] \tag{4.30}$$

$\mathcal{F}$ is the information matrix and $\mathcal{G}$ is the gradient vector, and $\Delta\Theta$ is the parameter change vector. Therefore, the measurement noise covariance matrix R can be firstly computed using Eq. (4.22), and then the Gauss-Newton method can be used to update the parameters by using Eqs. (4.29-4.31), which can be solved by any standard algorithm from linear algebra.

4.2 Transfer Function Model Identification

According to the principle of parsimony [51]:

Given two models fitted to the same data with nearly equal residual variances, choose the model with the fewest parameters.

The transfer function models are a very useful intermediate result in the overall flight-mechanics because they contain the least possible number of parameters that will characterize the system response [4]. With this principle in mind, the transfer functions have been streamlined to have least parameters but still gives satisfactory results.

4.2.1 Longitudinal model

As for longitudinal axis, there are a few assumptions being made about model structure. Firstly, the denominator of the transfer function consists of a pair of conjugate roots representing short period mode $[\zeta_{sp}, \omega_{sp}]$ and another pair of conjugate roots representing phugoid mode $[\zeta_{ph}, \omega_{ph}]$. The flight control linkage system from pilot's stick input to the control surface deflection is represented by $1/(\tau_1 s + 1)$, where τ_1 is an unknown time constant. Secondly, the numerator consists of two zeros represented by $-1/T_{\theta_1}$ and $-1/T_{\theta_2}$. Thirdly, constant thrust has been maintained within the same test point, and the aircraft state does not deviate too much from its trimmed position. Therefore, the pitch rate transfer function full model can be represented as a fifth-order system:

$$\frac{q}{u_{lon}} = \frac{K(s+1/T_{\theta_1})(s+1/T_{\theta_2})}{(s^2+2\zeta_{sp}\omega_{sp}s+\omega_{sp}^2)(s^2+2\zeta_{ph}\omega_{ph}s+\omega_{ph}^2)(\tau_1 s+1)} \tag{4.31}$$

In order to minimize the unknown parameters to be identified with MATLAB but still remain good model quality, the model order has been reduced from fifth order to third order with the phugoid component being eliminated from the model. Moreover, the flight maneuvers have been mainly focused on exciting the short-period dynamics. The phugoid mode has not been excited with proper maneuvers. Therefore, a simplified third-order system that mainly represents the system's short period dynamics has been generated below.

$$\frac{q}{u_{lon}} = \frac{K(s+1/T_{\theta_1})(s+1/T_{\theta_2})}{(s^2+2\zeta_{sp}\omega_{sp}s+\omega_{sp}^2)(\tau_1 s+1)} \tag{4.32}$$

Parameter identification and model validation are integral parts of system identification. The various aspects of model validation can be broadly classified into three subcategories: 1) statistical properties of the estimates, 2) residual analysis, 3) model predictive quality, which

provide clues into the effectiveness of model parameters. These subcategories can further break down to following criteria: 1) Standard deviations of the parameter estimates, 2) Correlation coefficients among the estimates, 3) Goodness of fit, 4) Statistical analysis of residuals, 5) Model deficiencies in terms of residual control inputs, 6) Plausibility of estimates, and 7) Model predictive capability.

Longitudinal transfer function model parameters have been identified using MATLAB's system identification toolbox. Gauss-Newton method has been chosen as the iteration method. The identified longitudinal model response has been compared with flight data. Lower frequency sweep input-response from 0 to 70 sec, higher frequency sweep input-response from 70 sec to 130 sec, 3-2-1-1 input-response, and model residuals have been presented respectively from Figure 4.4 to Figure 4.7, and the model parameters have been summed up in Table 4.1.

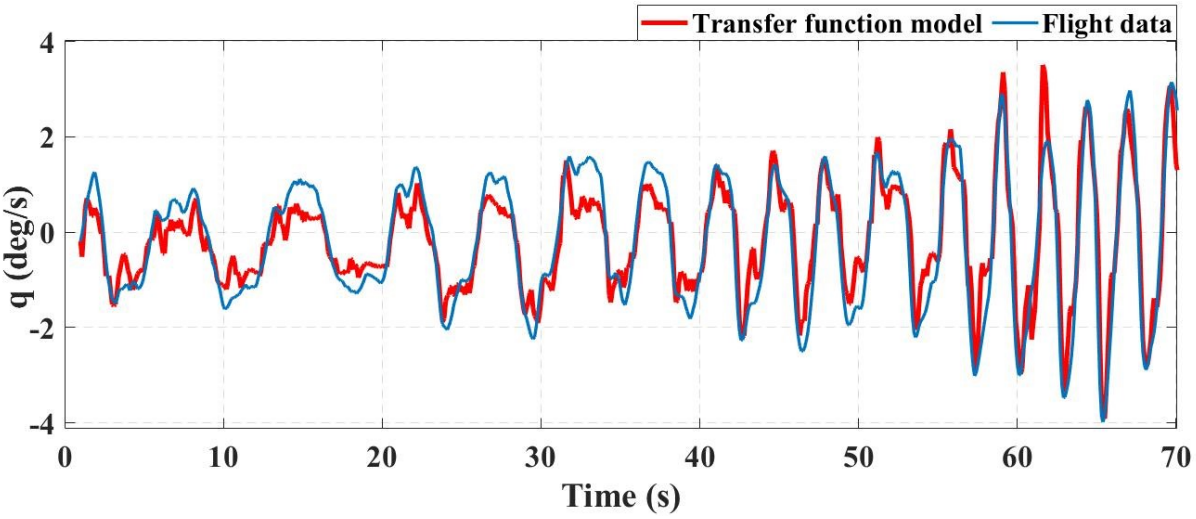

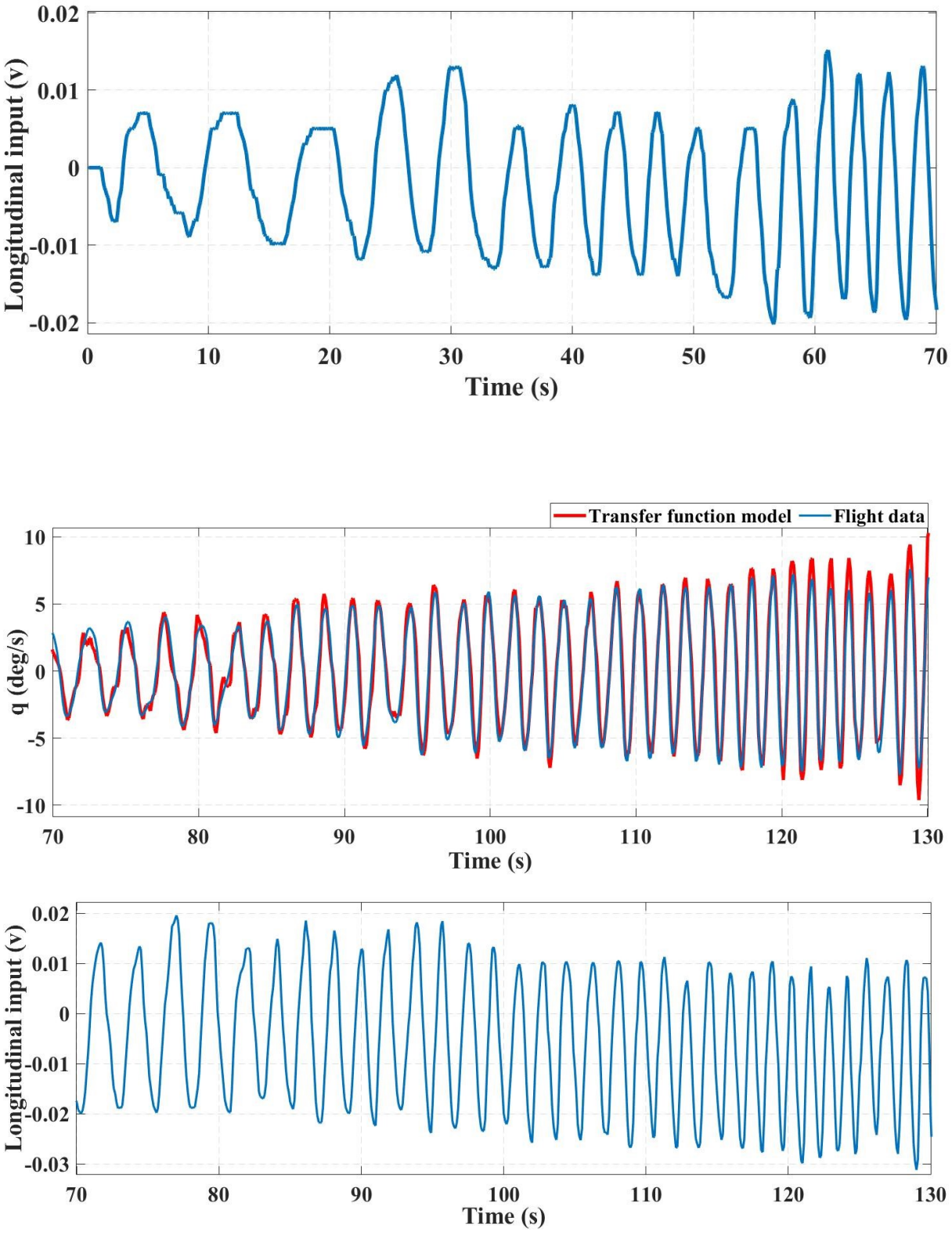

Figure 4.4: Identified longitudinal transfer function model output compared to flight data, frequency sweep

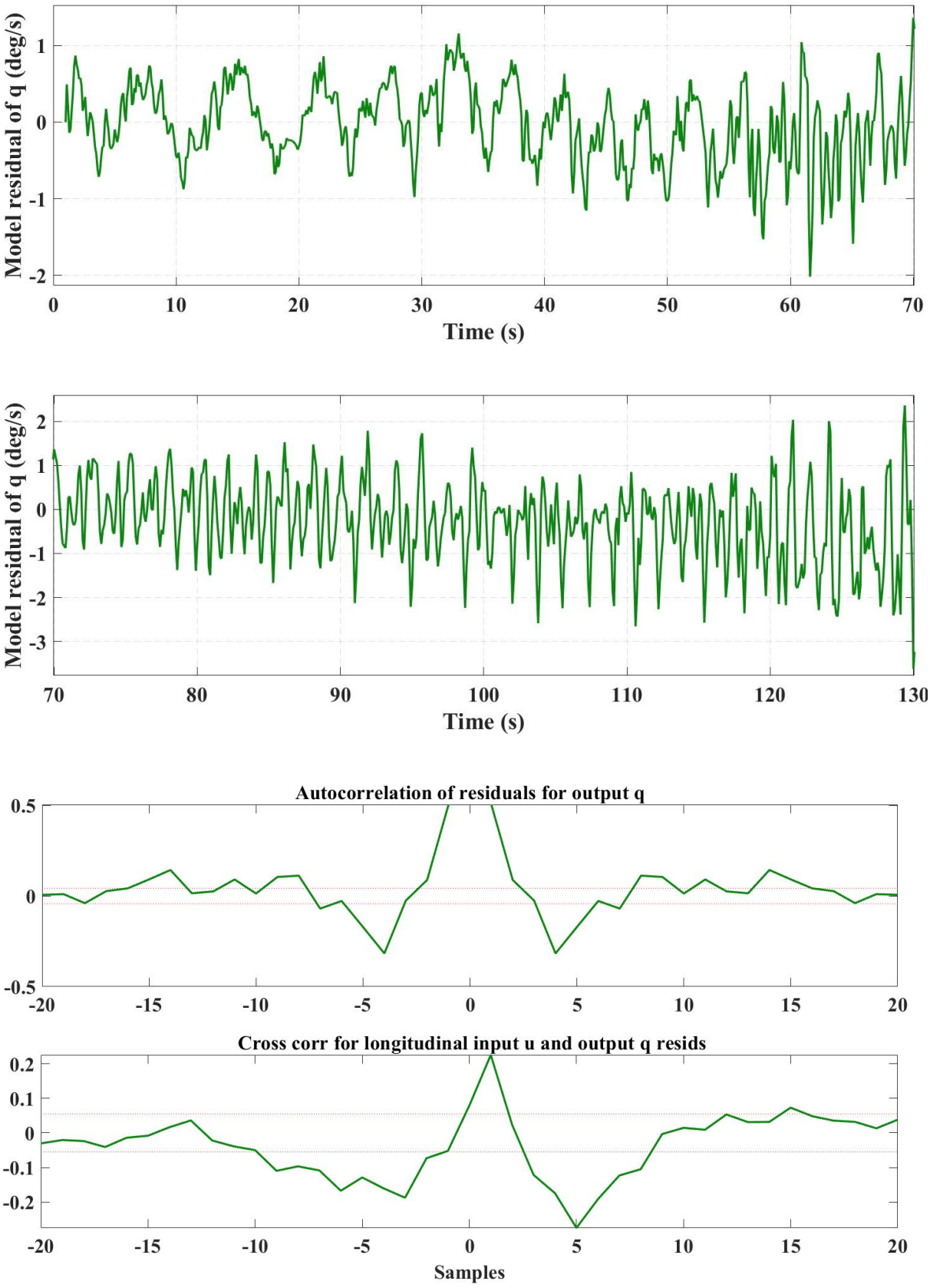

Figure 4.5: Identified longitudinal transfer function model residuals, frequency sweep

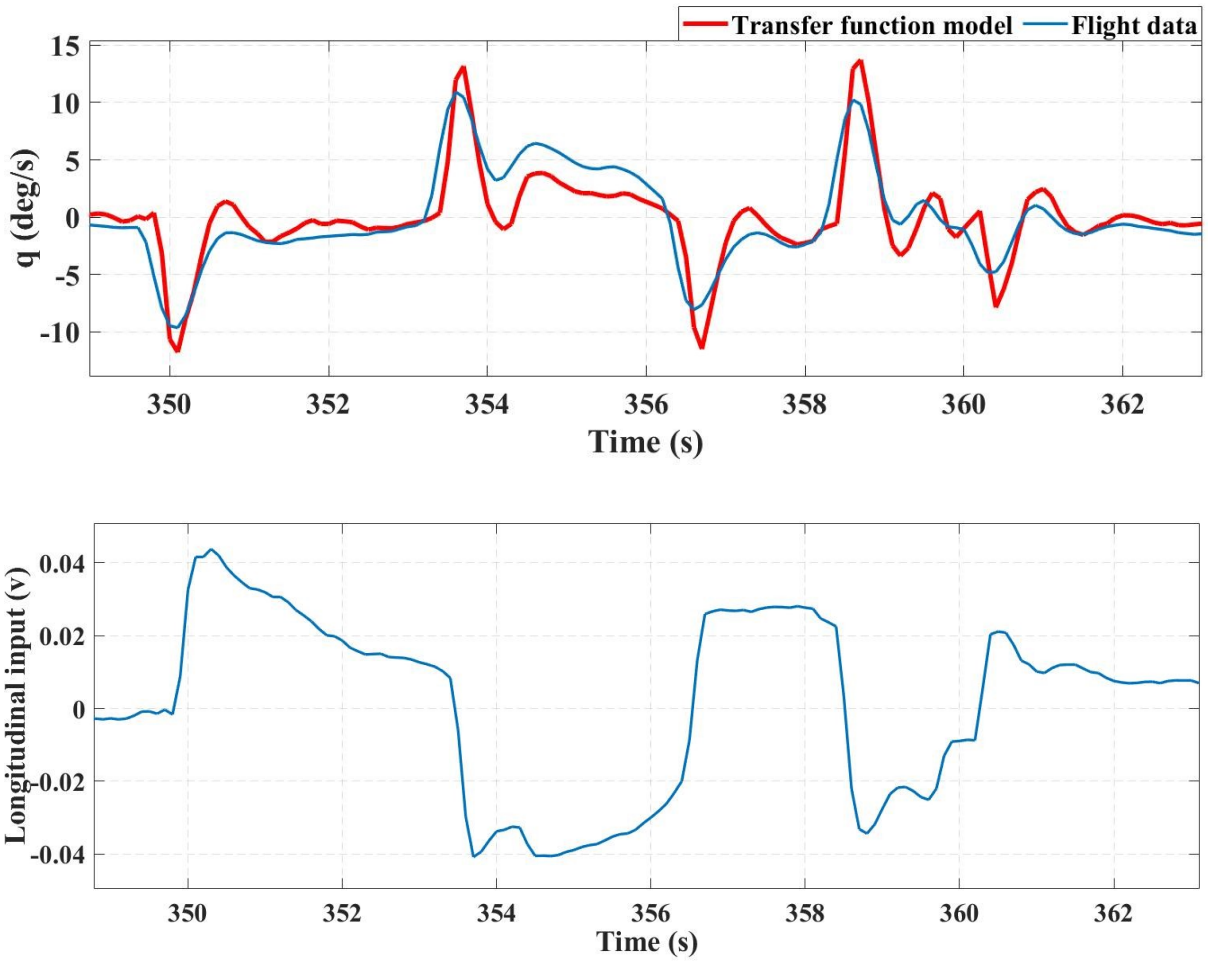

Figure 4.6: Identified longitudinal transfer function model output compared to flight data, 3-2-1-1 input

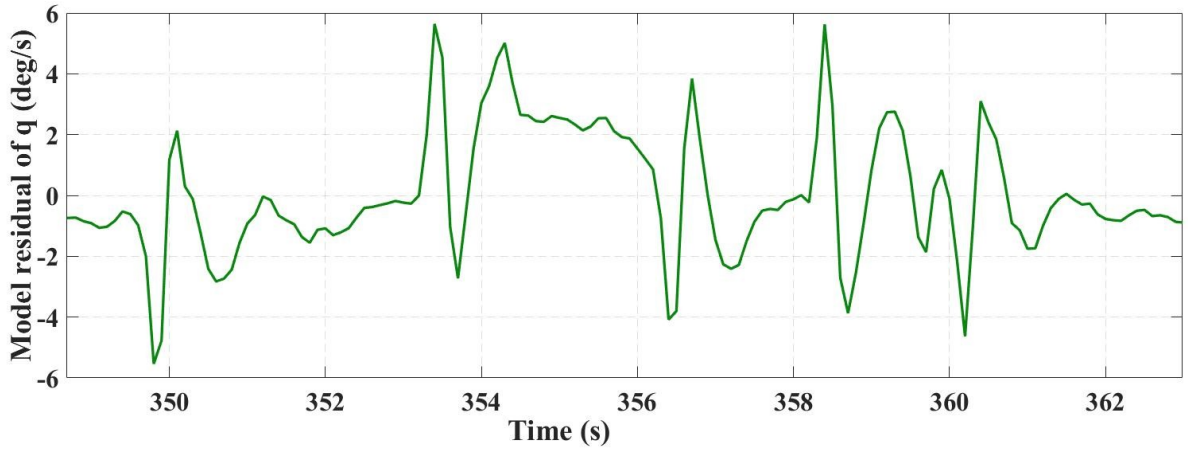

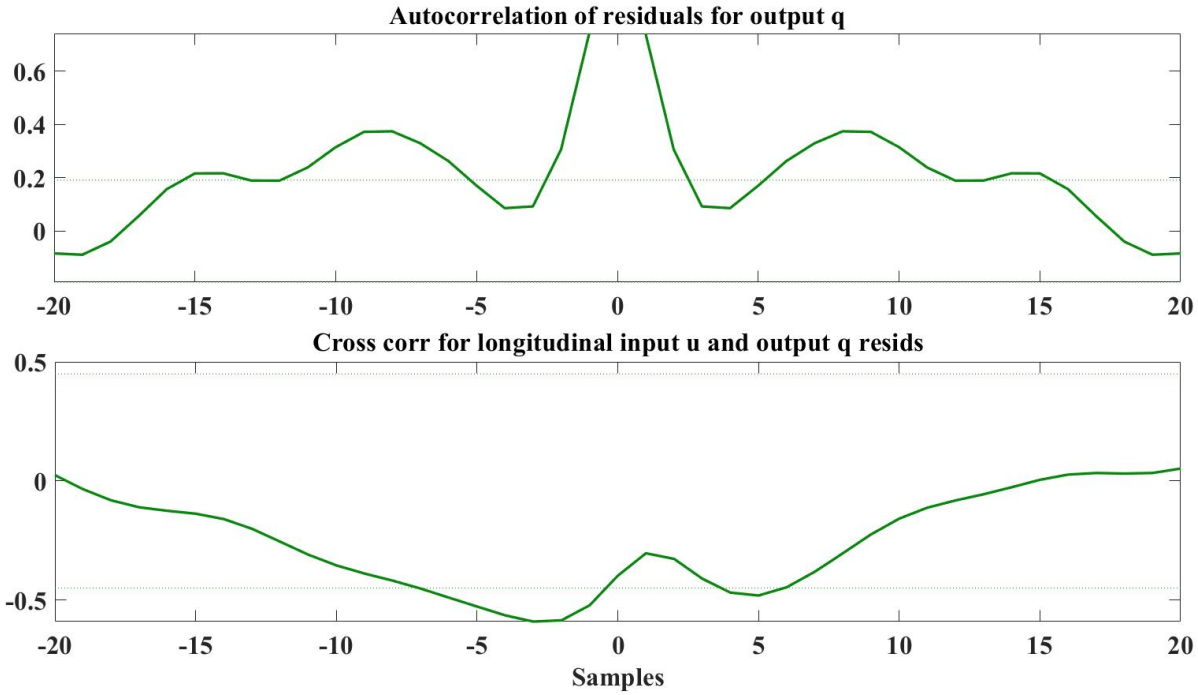

Figure 4.7: Identified longitudinal transfer function model residuals, 3-2-1-1 input

Table 4.1: Identified transfer function parameters in longitudinal axis

K	-24900
T_{θ_1}	0.837
T_{θ_2}	0.247
ζ_{sp}	0.463
ω_{sp}	4.91 rad/s
τ_1	0.0138

The identified longitudinal model has been presented below:

$$\frac{q}{u_{lon}} = \frac{-24900\,s^2 - 130500\,s - 120400}{s^3 + 76.8\,s^2 + 352.7\,s + 1743}$$

4.2.2 Lateral model

As for lateral axis, a complete transfer function model structure includes roll mode, spiral model and Dutch roll mode. The flight control system from pilot's stick input to the control surface deflection is represented by $1/(\tau_2 s + 1)$, τ_2 is an unknown time constant.

$$\frac{p}{u_{lat}} = \frac{L_{\delta_a}(s^2+2\zeta_\phi\omega_\phi s+\omega_\phi^2)}{(s+1/T_r)(s+1/T_s)(s^2+2\zeta_{dr}\omega_{dr}s+\omega_{dr}^2)(\tau_2 s+1)} \tag{4.33}$$

where T_r is roll mode time constant and the inverse of the roll damping stability derivative $(1/T_r = -L_p)$, T_s is spiral mode time constant, L_{δ_a} is the aileron roll-control sensitivity, $[\zeta_\phi, \omega_\phi]$ are complex zeros that determines the appearance of the Dutch-roll model in the roll response. $[\zeta_{dr}, \omega_{dr}]$ is the Dutch-roll complex mode [4].

In order to reduce the parameters to be estimated, the model order has been reduced from fifth to third order with the roll mode and spiral mode being eliminated from the transfer function structure. The reduced order transfer function in lateral axis in terms of the stick input u and the roll rate p can be simplified as follows:

$$\frac{p}{u_{lat}} = \frac{L_{\delta_a}(s^2+2\zeta_\phi\omega_\phi s+\omega_\phi^2)}{(s^2+2\zeta_{dr}\omega_{dr}s+\omega_{dr}^2)(\tau_2 s+1)} \tag{4.34}$$

Longitudinal transfer function model parameters have been identified using MATLAB's system identification toolbox. Gauss-Newton method has been chosen as the iteration method. The identified lateral model has also been compared with flight data. Lower frequency sweep input-response from 0 to 75 sec, higher frequency sweep input-response from 75 sec to 100 sec, 3-2-1-1 input-response, and model residuals have been presented respectively from Figure 4.8 to Figure 4.11, and the identified parameters have been summed up in Table 4.2.

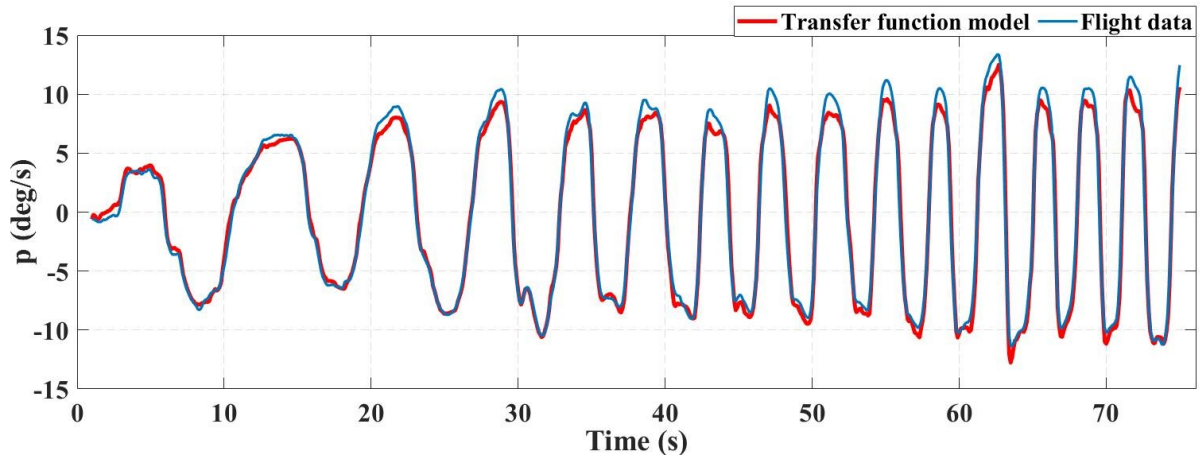
Transfer function model
Flight data
p (deg/s)
Time (s)

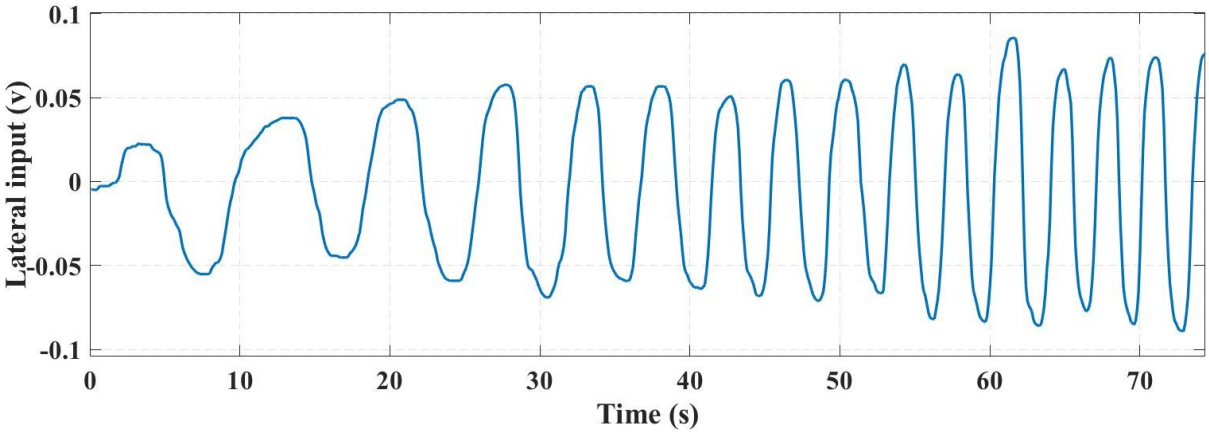
Lateral input (v)
Time (s)

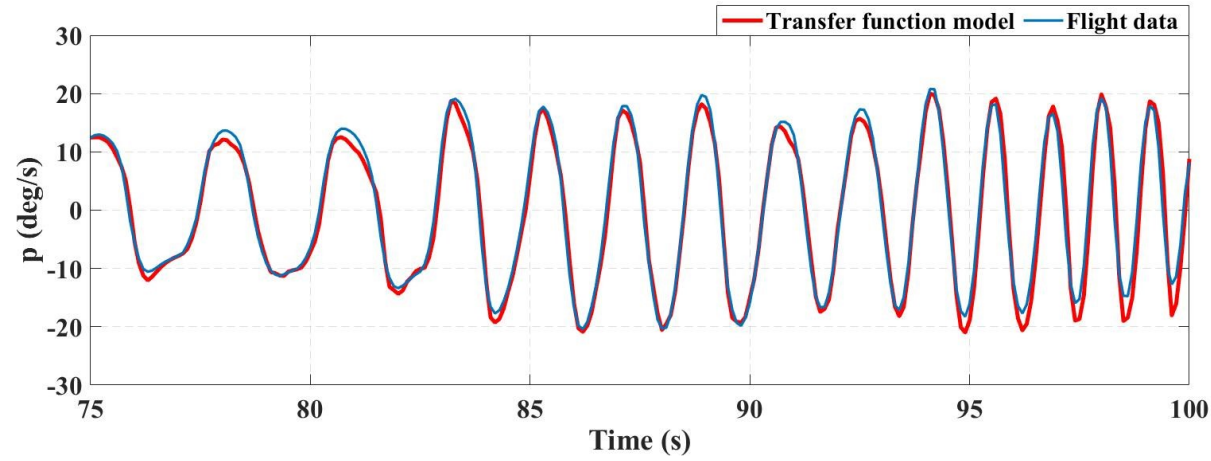
Transfer function model
Flight data
p (deg/s)
Time (s)

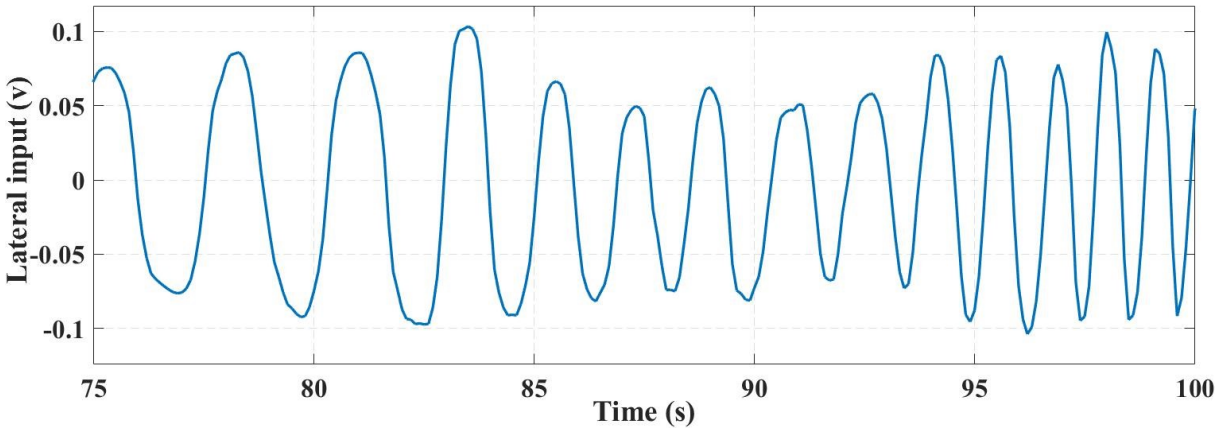

Figure 4.8: Identified lateral transfer function model output compared to flight data, frequency sweep

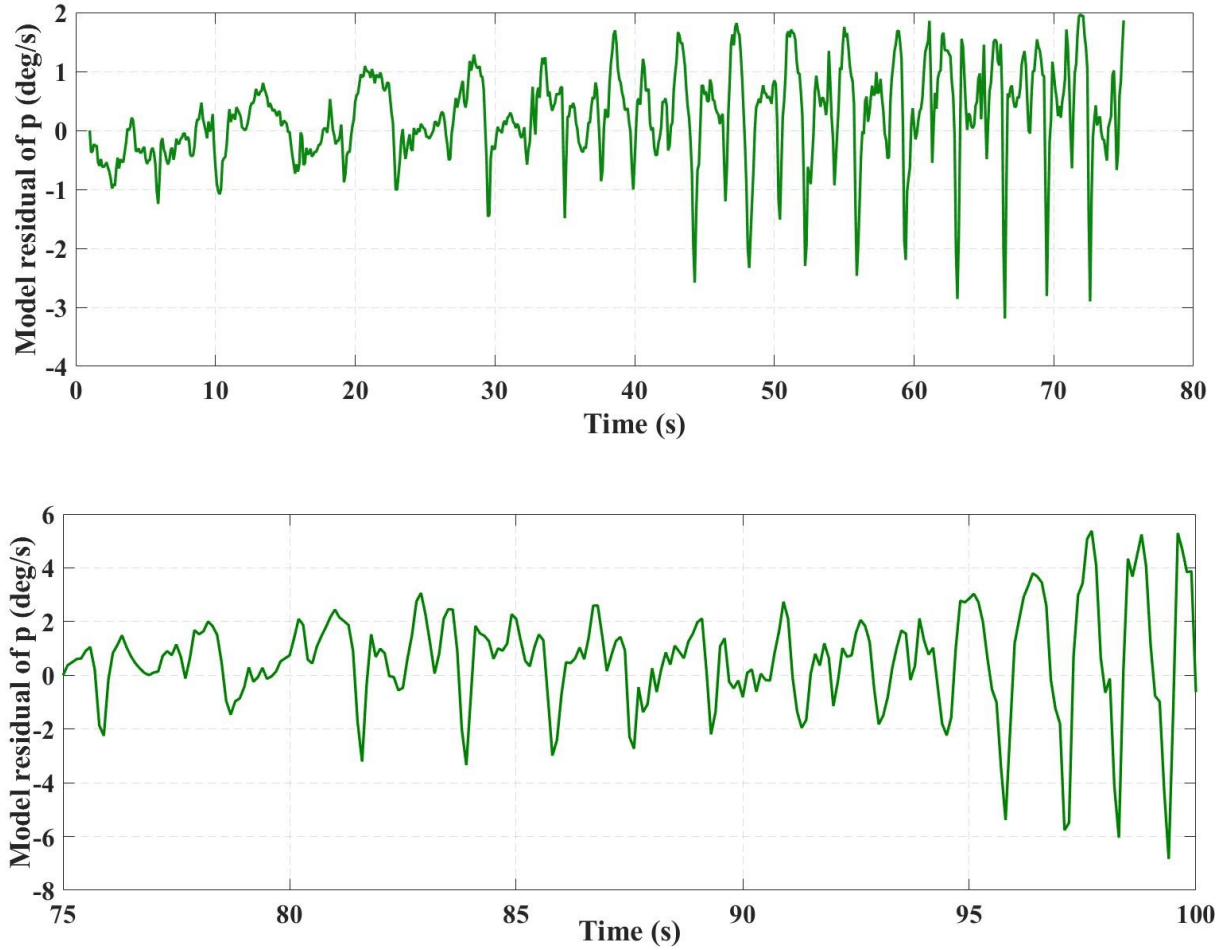

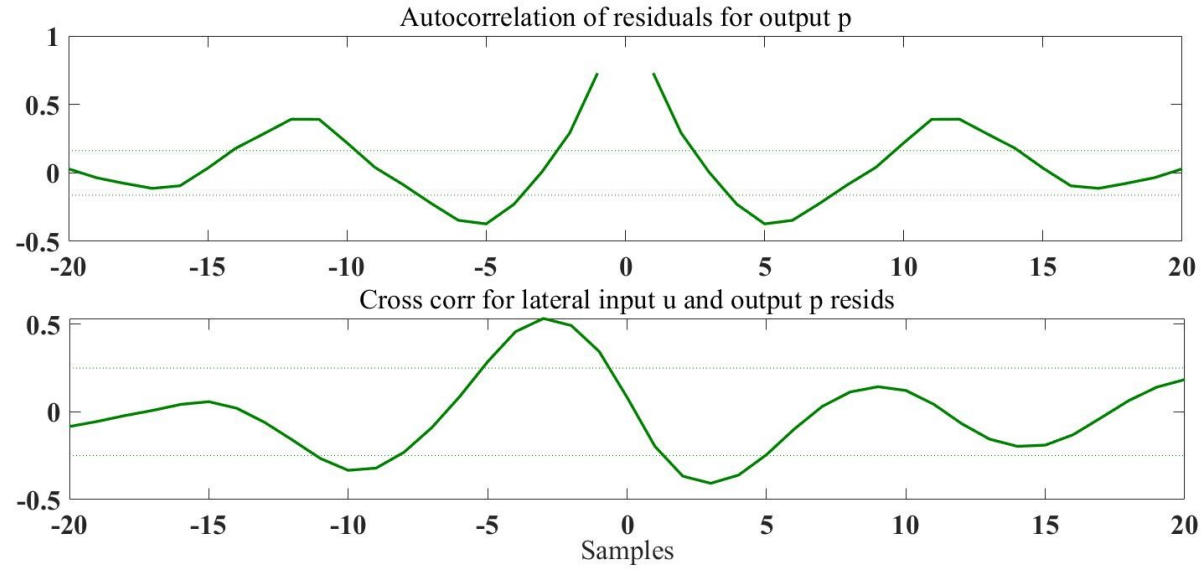

Figure 4.9: Identified lateral transfer function model residuals, frequency sweep

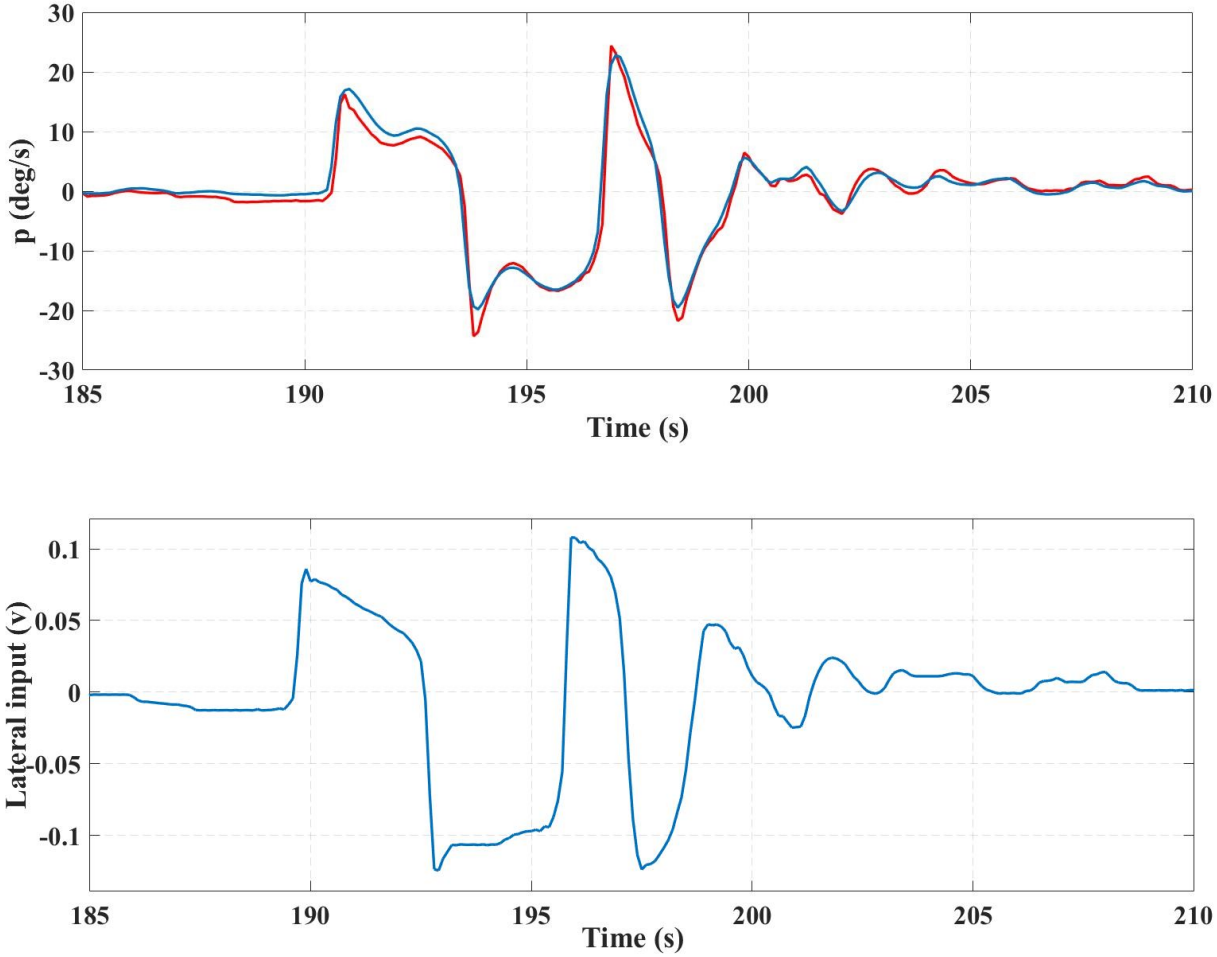

Figure 4.10: Identified lateral transfer function model output compared to flight data, 3-2-1-1 input

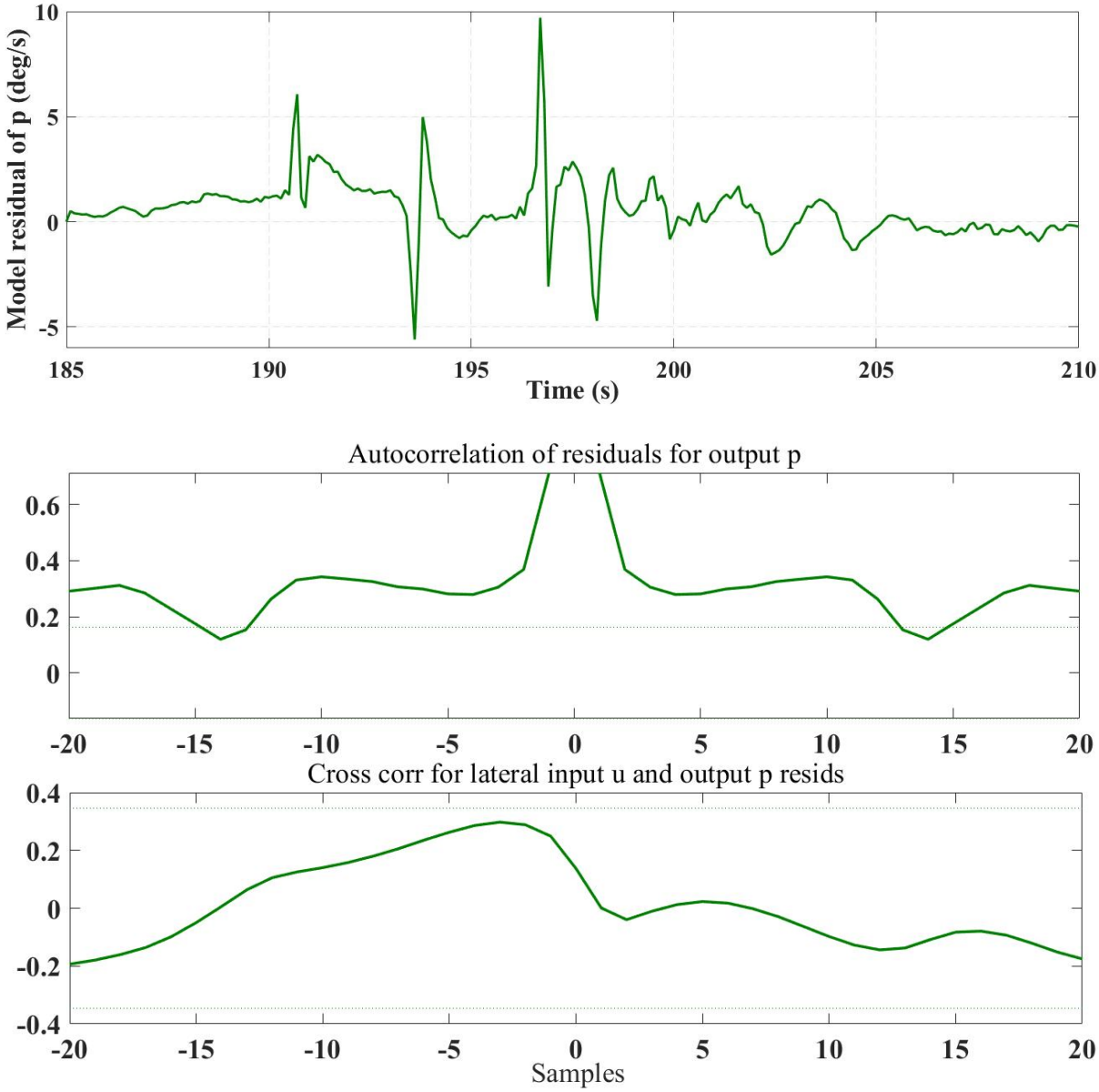

Figure 4.11: Identified lateral transfer function model residuals, 3-2-1-1 input

Table 4.2: Identified transfer function parameters in lateral axis

L_{δ_a}	66360
ζ_{ϕ}	0.206
ω_{ϕ}	2.762
ζ_{dr}	0.159

ω_{dr}	3.08 rad/s
τ_2	0.00281

The identified transfer function has been presented below:

$$\frac{p}{u_{lat}} = \frac{66360\,s^2 + 75400\,s + 506200}{s^3 + 356.8\,s^2 + 358.4\,s + 3375}$$

The baseline model for longitudinal axis generated in Chapter 2 has been compared with flight data and transfer function model in Figure 4.12. From this graph, it is concluded that the longitudinal baseline model still needs to be improved in terms of amplitude prediction. However, the baseline model phase matches well with flight data.

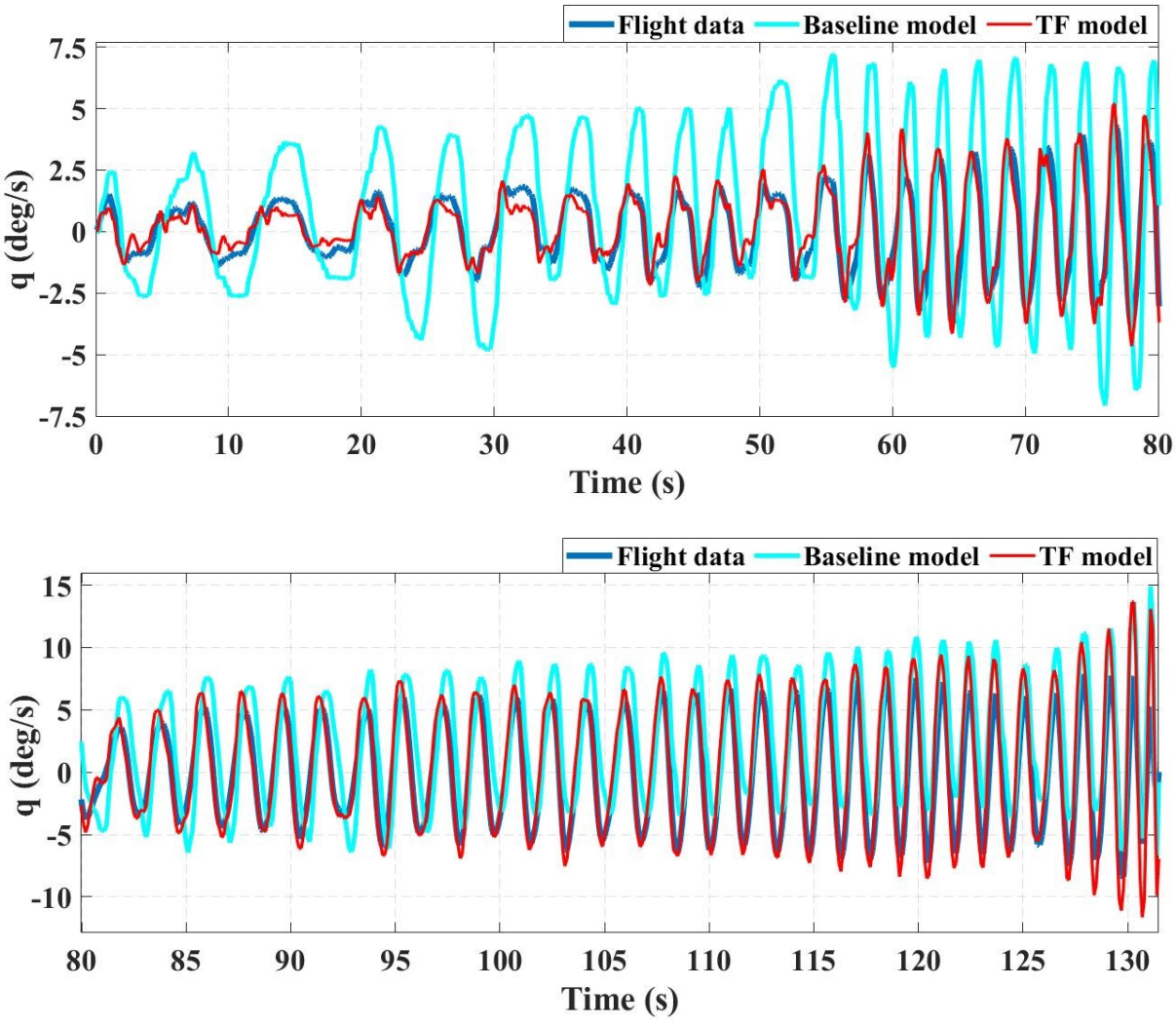

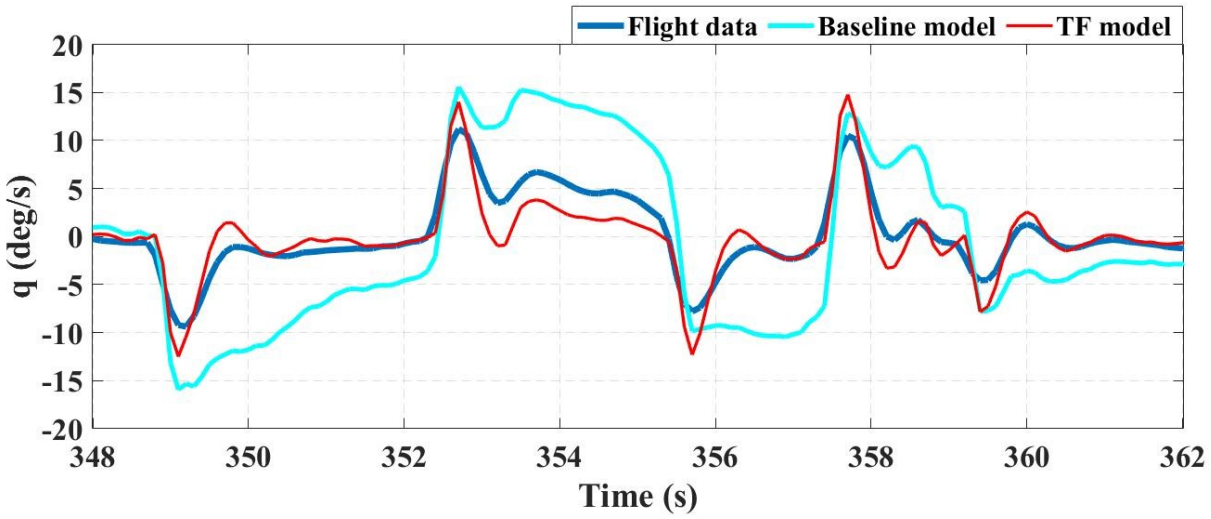

Figure 4.12: Long-EZ baseline model compared with flight data and identified transfer function model in longitudinal axis

4.3 Analysis and Discussion

One metric to quantify the accuracy of the model prediction $\hat{y}(i)$ to the flight data $z(i)$ is to use the coefficient of determination R^2, which is related to the total sum of squares SS_T, the regression sum of squares SS_R, and the residual sum of squares SS_E. They are defined as follows [2]:

$$SS_T = SS_R + SS_E \tag{4.35}$$

$$R^2 = \frac{SS_R}{SS_T} = 1 - \frac{SS_E}{SS_T} \tag{4.36}$$

where

$$SS_T \equiv \sum_{i=1}^{N}[z(i) - \bar{z}]^2 = z^T z - N\bar{z}^2 \tag{4.37}$$

$$\bar{z} = \frac{1}{N}\sum_{i=1}^{N} z(i) \tag{4.38}$$

$$SS_R \equiv \sum_{i=1}^{N}[\hat{y}(i) - \bar{z}]^2 \tag{4.39}$$

$$SS_E \equiv \sum_{i=1}^{N}[z(i) - \hat{y}(i)]^2 = \left(z - X\hat{\theta}\right)^T\left(z - X\hat{\theta}\right) \tag{4.40}$$

$$= z^T z - \hat{\theta}^T X^T z$$

Value of R^2 varies from 0 to 1, where 1 represents a perfect fit to the data.

Root Mean Square Error (RMSE) is another measure of accuracy. A value of 0 indicates perfect fit to the data. Therefore, a lower RMSE value is better than a higher one. Both the R^2 and RMSE values of the identified transfer function models have been presented in Table 4.3, which shows that the accuracy of identified transfer function models for both pitch and roll dynamics is satisfactory in general.

However, the baseline model accuracy still needs improvement compared to the transfer function model. As has been discussed in Chapter 2, the baseline model has been calculated based on the empirical functions and aircraft dimensions, which needs to be further improved when the air data recording system is available for the aircraft Long-EZ.

Table 4.3: RMSE and R^2 of transfer function model and baseline model

	RMSE	R^2
Longitudinal TF	1.0048	0.7322
Lateral TF	1.8395	0.9354
Baseline longitudinal	2.9763	0.6301

Figure 4.4 to Figure 4.11 show that longitudinal model residual is between $\pm 1\ \mathrm{deg/s}$ for most of the low to middle frequencies (below 4.71 $\mathrm{rad/s}$), and model residual increases to $\pm 2\ \mathrm{deg/s}$ when the frequency increases above 4.71 $\mathrm{rad/s}$, which is very close to the natural frequency of Long-EZ's short period mode ($\omega_{sp} = 4.91\ \mathrm{rad/s}$).

Lateral model residual is within $\pm 1\ \mathrm{deg/s}$ in the low frequency (below $3.14\ \mathrm{rad/s}$), and within $\pm 2\ \mathrm{deg/s}$ in the middle frequency range when frequency increases to around

3.14 rad/s, this result matches the identified Dutch roll mode frequency, $\omega_{dr} = 3.08$ rad/s. The lateral model accuracy decreases when the aircraft's Dutch roll mode has been excited.

The autocorrelation function of the residuals is presented in Eq. (4.14). When the residuals are completely uncorrelated, $\hat{\mathcal{R}}_{vv}(k)$ values will vary slightly around zero, as is demonstrated from Figure 4.4 to Figure 4.11.

Figure 4.12 shows the Long-EZ baseline model validated with flight data and compared with the identified transfer function model. The baseline model has good predictability in middle to high frequency range (above 3.14 rad/s) in terms of its amplitude. However, the model tends to generate higher value during low frequency, which is obvious in the 3-2-1-1 input response. Moreover, the phase delay in the baseline model also needs to be addressed in the future.

The results for the longitudinal and lateral transfer functions have been presented in the following equations:

$$\frac{q}{u_{lon}} = \frac{-24900\,s^2 - 130500\,s - 120400}{s^3 + 76.8\,s^2 + 352.7\,s + 1743}$$

$$\frac{p}{u_{lat}} = \frac{66360\,s^2 + 75400\,s + 506200}{s^3 + 356.8\,s^2 + 358.4\,s + 3375}$$

The parametric system identification gives a Newtonian physics meaning to the identified model. From the figures, it is concluded that the identified transfer function models have good predictability of the aircraft dynamics, especially in the low to middle frequency range. The short period mode and Dutch roll mode have been identified with the longitudinal and lateral transfer functions respectively, which are valuable references for future flight test design.

Chapter 5 Artificial Neural Network

5.1 Introduction

Artificial neural Network (ANN) is a network of small processing units or nodes jointed to each other by weighted connections. Artificial neural networks are usually defined by type of neuron (nodes), connectionist architecture, learning algorithm, and recall algorithm. The input and output nodes (neurons or processing elements) are at large fixed. However, the nodes in the hidden layer may vary in numbers and structure. The processing elements in the hidden layer consist of sigmoidal functions, which provide approximation capabilities to the ANN. The output layer elements can be linear or nonlinear. Three commonly used networks in system identification are: Feedforward Neural Network (FNN), Recurrent Neural Network (RNN), and Radial Basis Function (RBF) neural network.

FNN normally consists of an input layer, one or two hidden layers, and an output layer. FNN processes information in only one direction, which makes it the simplest of the neural networks. FNNs are the most powerful and most popular neural networks for nonlinear regression [27]. Multilayer feedforward neural network, also referred to as Multilayer Perceptron (MLP), is the most widely known and used neural network [28]. MLP is a feedforward neural network with one or more hidden layers of nonlinear elements, but one hidden layer is the most common choice in practice [26]. MLP has many advantages such as high approximation accuracy, lower numbers of nodes and weights, wide variety of functions, and does not suffer from oscillatory interpolation and extrapolation. However, it also has some drawbacks such as the use of local optimization methods to update the weights, and risk of

getting trapped in a shallow local minimum [26].

For a single neural network, the algorithm of single neural network can be described as:

$$Net_i = \sum_j w_{ij} x_j + s_i - \theta_i \tag{5.1}$$

$$u_i = f(Net_i) \tag{5.2}$$

$$y_i = g(u_i) = h(Net_i) \tag{5.3}$$

where $g(u_i) = u_i,\ y_i = f(Net_i)$.

The single neural network structure has been illustrated in Figure 5.1.

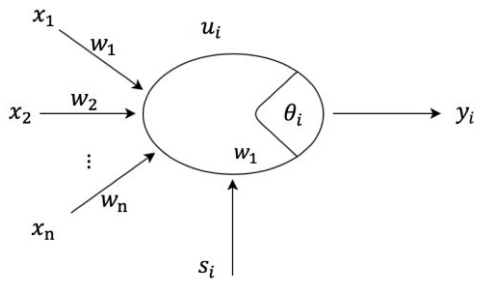

Figure 5.1: Single neural network model

Common activation functions $f(Net_i)$ include: threshold value, linear function, and nonlinear function, which have been presented in the figures below.

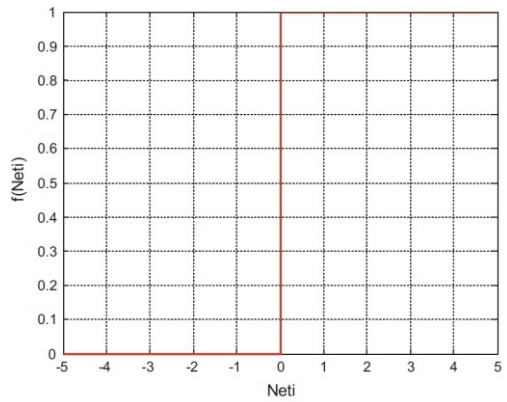

Figure 5.2: Threshold function

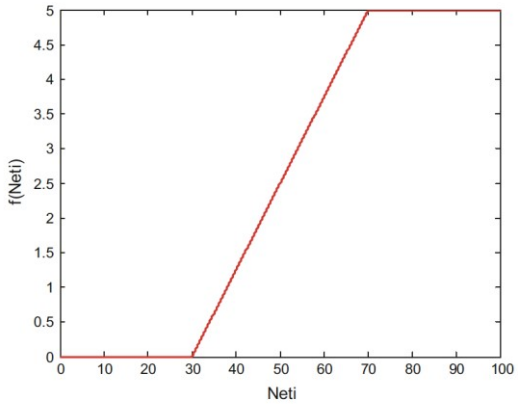

Figure 5.3: Linear function

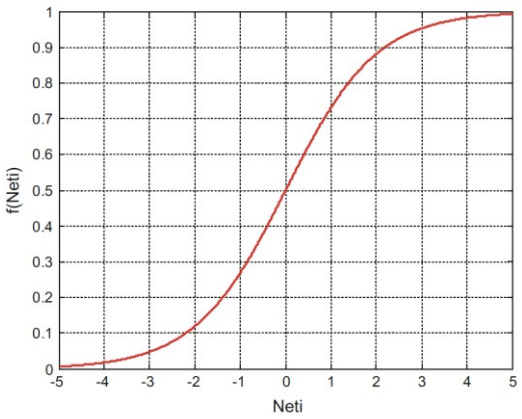

Figure 5.4: Nonlinear function

A feed-forward neural network is shown in Figure 5.5, the input of hidden layer is:

$$x_j = \sum_i w_{ij} x_i \tag{5.7}$$

where w_{ij} is the jth weight of the ith neuron.

Output of hidden layer is:

$$x'_j = f(x_j) = \frac{1}{1+e^{-x_j}} \tag{5.8}$$

Output of output layer is:

$$y_o(k) = \sum_j w_{jo} x'_j \tag{5.9}$$

The approximation error is:

$$e(k) = y(k) - y_n(k) \tag{5.10}$$

The error index function is designed as:

$$E = \frac{1}{2} e(k)^2 \tag{5.11}$$

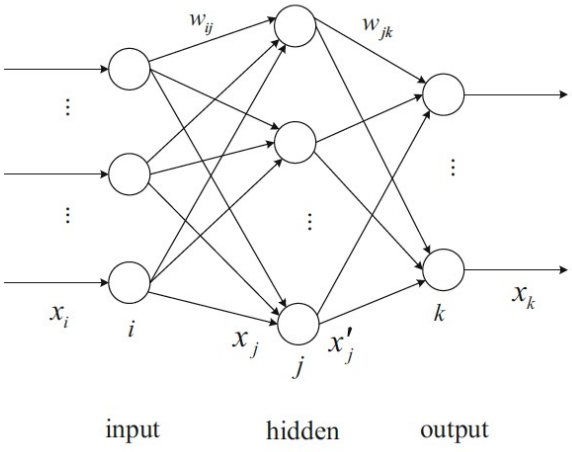

Figure 5.5: MLP structure

Learning algorithms

The most common technique used for training MLP is the nonlinear optimization of neural network weights. The cost function J, which is the sum of squared errors between the system output and the neural network output, can be minimized by using gradient-based learning methods.

Backpropagation (BP) learning algorithm was developed by Werbos in 1974, which is an iterative procedure that allows to adjust the weights in a hidden layer. The backpropagation learning algorithm uses the backpropagation algorithm as a technique for computing the gradient of the MLP w.r.t. its weights [29]. BP learning algorithm operates based on a linear approximation of the cost function, which may cause very slow convergence problems [52]. Higher order approximations of the cost function should be used to achieve a significantly higher convergence rate. Examples of such techniques include Levenberg-Marquard method, quasi-Newton methods [29], conjugate gradient methods, and the Recursive Least-Squares (RLS) learning algorithms [53].

According to the steepest gradient descent method, the learning of weight value w_{ki} is

$$\Delta w_{jo} = -\eta \frac{\partial E}{\partial w_{jo}} = \eta \cdot e(k) \cdot \frac{\partial y_o}{\partial w_{jo}} = \eta \cdot e(k) \cdot x'_j \tag{5.12}$$

The weight value at time $k+1$ is

$$w_{jo}(k+1) = w_{jo}(k) + \Delta w_{jo} \tag{5.13}$$

The learning of weight value w_{ij} is

$$\Delta w_{ij} = -\eta \frac{\partial E}{\partial w_{ij}} = \eta \cdot e(k) \cdot \frac{\partial y_o}{\partial w_{ij}} \tag{5.14}$$

where $\frac{\partial y_o}{\partial w_{ij}} = \frac{\partial y_o}{\partial x'_j} \cdot \frac{\partial x'_j}{\partial x_j} \cdot \frac{\partial x_j}{\partial w_{ij}} = w_{jo} \cdot \frac{\partial x'_j}{\partial x_j} \cdot x_i = w_{jo} \cdot x'_j(1 - x'_j) \cdot x_i$

The weight value at time $k+1$ is

$$w_{ij}(k+1) = w_{ij}(k) + \Delta w_{ij} \tag{5.15}$$

The algorithm of weight value is

$$w_{jo}(k+1) = w_{jo}(k) + \Delta w_{jo} + \alpha(w_{jo}(k) - w_{jo}(k-1)) \tag{5.16}$$

$$w_{ij}(t+1) = w_{ij}(t) + \Delta w_{ij} + \alpha(w_{ij}(t) - w_{ij}(t-1)) \tag{5.17}$$

where $\eta \in [0,1]$ is the learning rate, $\alpha \in [0,1]$ is the momentum factor.

By using BP neural network approximation, Jacobian value can be calculated as:

$$\frac{\partial y(k)}{\partial u(k)} \approx \frac{\partial y_o(k)}{\partial u(k)} = \frac{\partial y_o(k)}{\partial x'_j} \times \frac{\partial x'_j}{\partial x_j} \times \frac{\partial x_j}{\partial x(1)} = \sum_j w_{jo} x'_j(1 - x'_j) w_{1j} \tag{5.18}$$

Model structure optimization

It is well known that the mathematical model should be as complex as necessary and as simple as possible. The same principle applies to MLP models. The MLP models should not be too complex otherwise they would learn noise. However, they should not be too simple because they would not be able to capture the process behavior [29]. For one-layer MLP, the architecture optimizing means to choose the number of hidden layer nodes and eliminate insignificant weights [29].

The overall model error is composed of bias error and variance error. With growing model complexity, the bias error decreases and variance error increases. A bias/error tradeoff needs to be found to optimize the model architecture.

Network growing and network pruning are two methods to optimize neural networks. Network growing is to add new nodes or layers to a small size network till the structure meets requirement. On the contrary, the pruning method assumes that there is redundant information stored in the fully connected MLP. Therefore, some selected weights will be weakened or eliminated from a large structure to simplify the network.

5.2 MLP Neural Network Model Identification

MLP neural network structure has been realized by a set of python codes developed for the system identification purpose. Keras has been utilized to realize the MLP structure. Keras is a high-level neural networks Application Programming Interface (API), written in Python and capable of running on top of TensorFlow, Cognitive Toolkit (CNTK), or Theano [54]. Keras models can be classified to two categories: sequential model and functional API model. The sequential model is a linear stack of layers, which is a convenient way of realizing the MLP structure. The functional API can define complex models such as multi-output models, MIMO models, directed acyclic graphs, or models with shared layers.

The multilayer perceptron neural network model has been chosen and programmed with Python. The MLP structure has been developed with network growing and network pruning techniques. When the numbers of hidden layer and nodes of each hidden layer are small, the training result is not optimized. On the other hand, when too many hidden layers and nodes

have been added to the network, the result does not improve significantly. Therefore, appropriate numbers of hidden layers and nodes need to be set in the network. After numerous times of fine tuning the layers and nodes numbers, the MLP neural network structure has been optimized to give the best output which is closest to the flight data. The MLP structure has been presented in Figure 5.6.

Hyperbolic tangent activation function has been chosen as the activation function of hidden layers, linear function has been chosen as the output layer activation function. RMSProp has been chosen as optimization method, mean square error method has been chosen to deal with the loss. Learning rate, batch size, and epoch number have been set at 0.0001, 5 and 100 respectively.

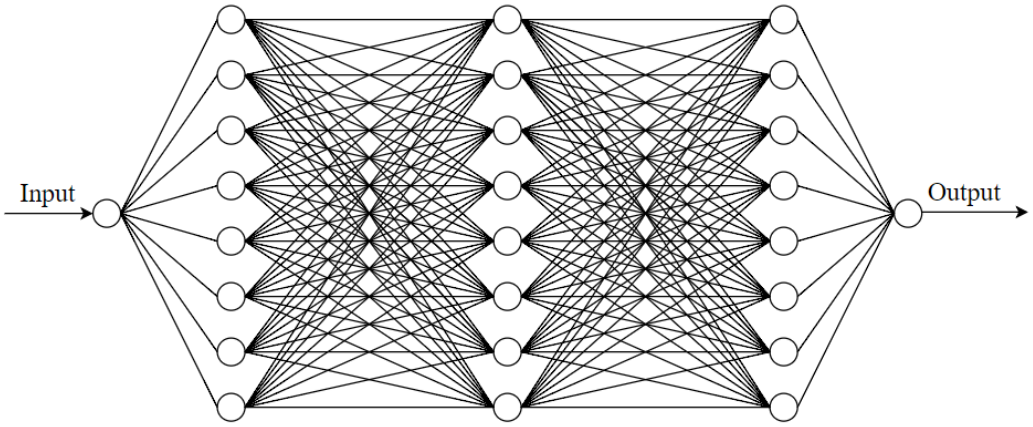

Figure 5.6: MLP neural network structure for system identification

5.2.1 Longitudinal model

The longitudinal MLP neural network in Figure 5.6 has been trained and compared with flight data, model output has been presented in Figure 5.7 and Figure 5.8. It shows that the model matches flight data well at lower frequency, where the model residual is within 1 deg/s.

However, with increased input frequency, the aircraft's response in pitch rate increases more significantly, but the model output does not match the increased magnitude of aircraft response. One way to improve the MLP model output accuracy is to increase input variables including speed of the aircraft, frequency of the input, etc.

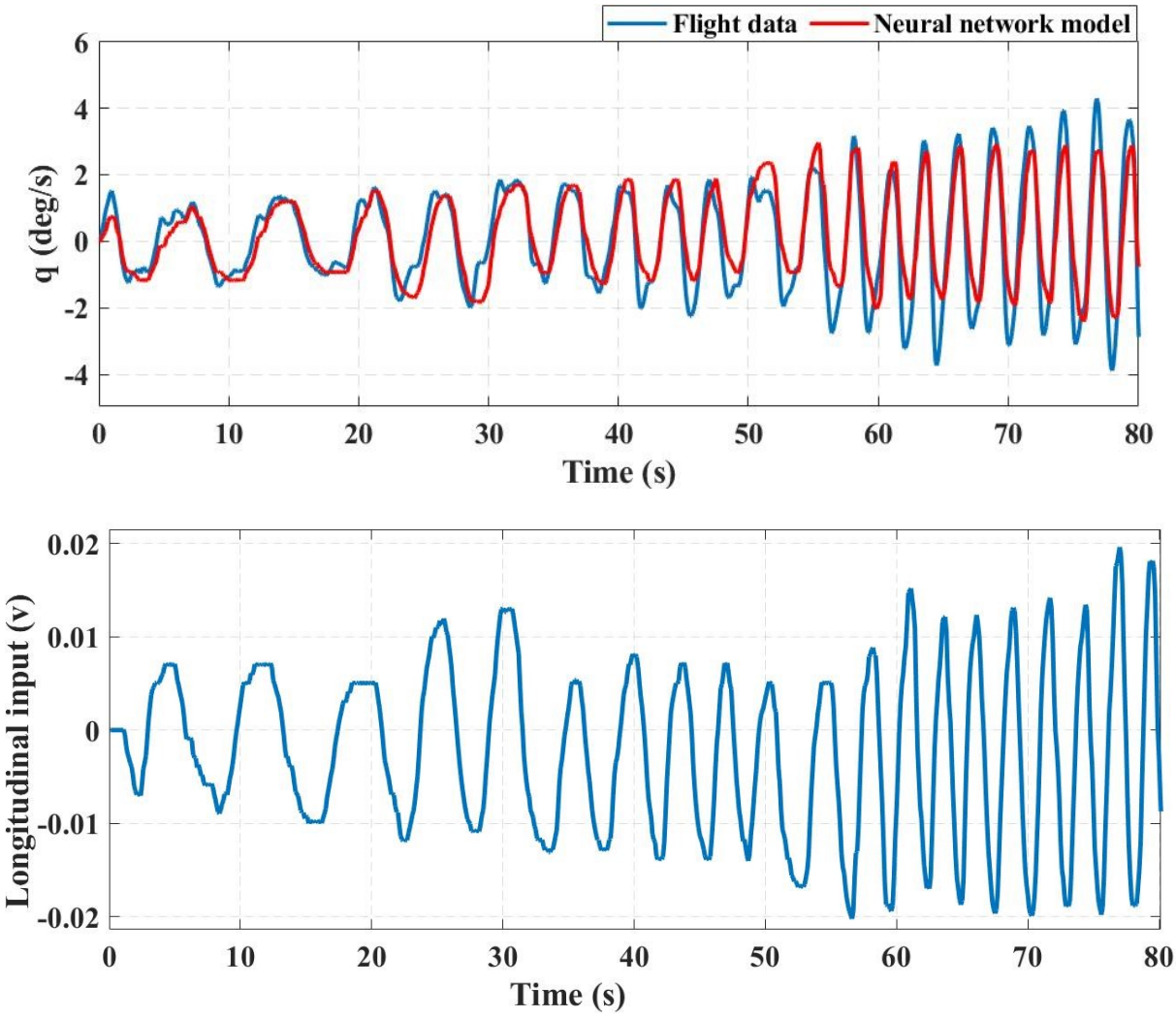

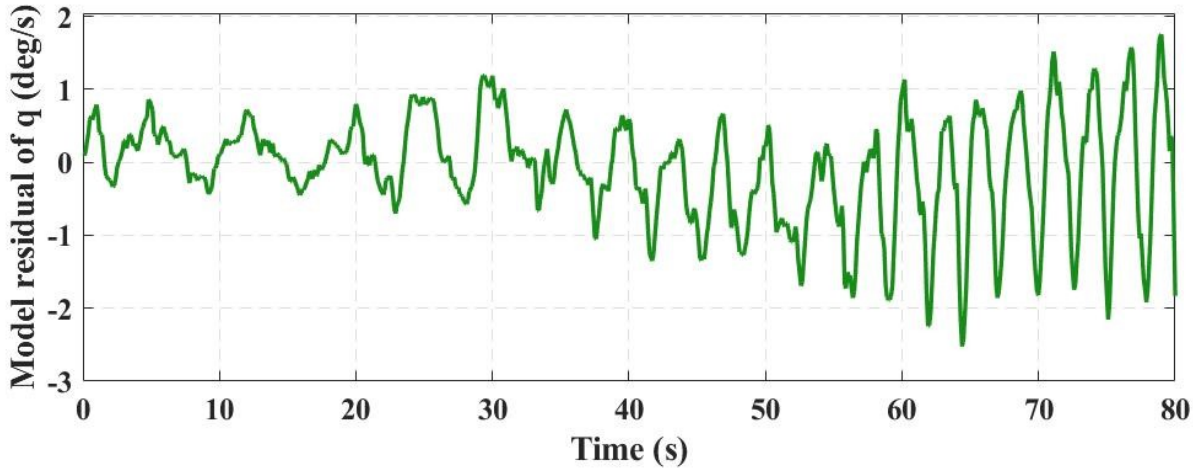

Figure 5.7: Longitudinal MLP output compared to flight data, frequency sweep

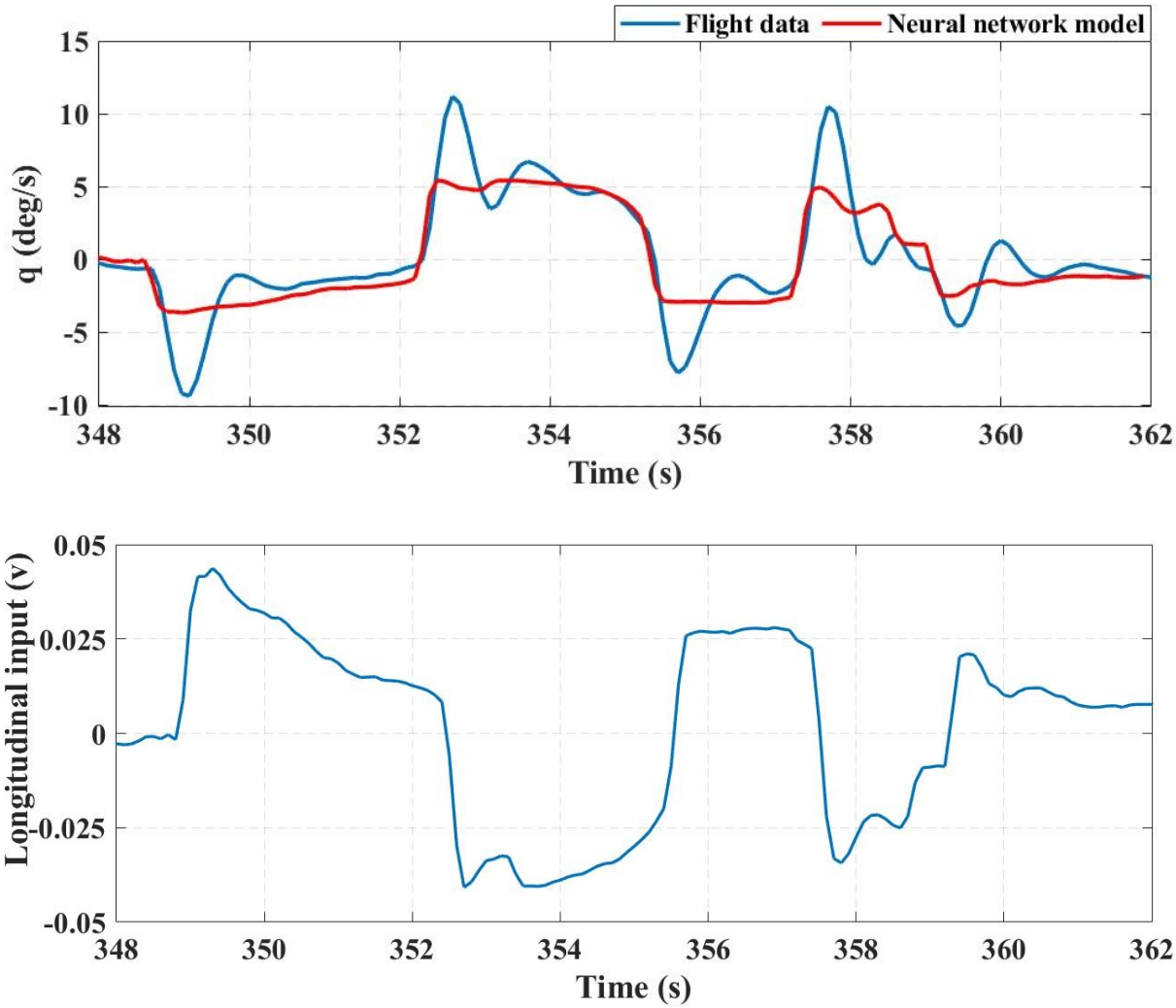

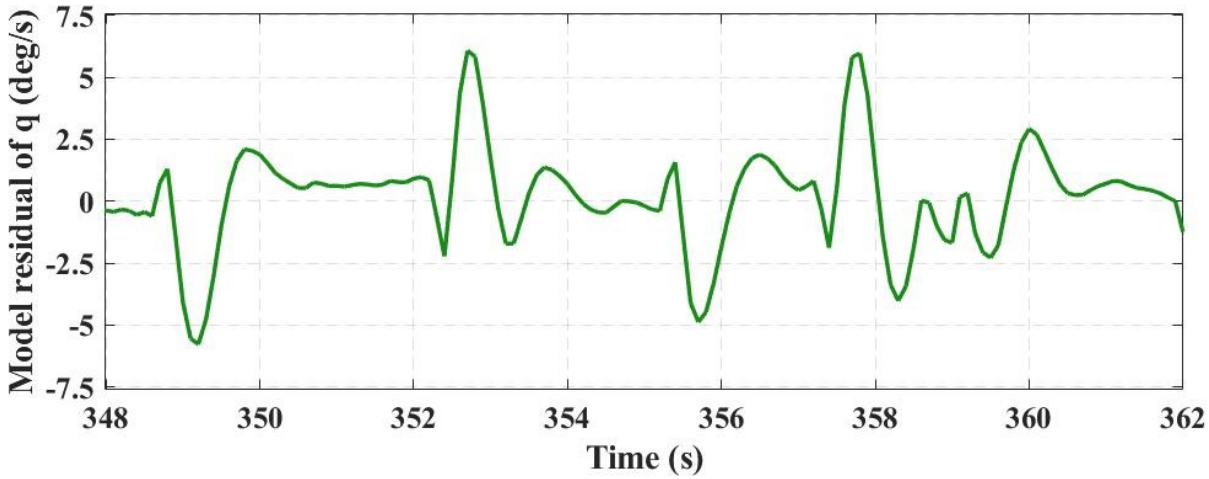

Figure 5.8: Longitudinal MLP output compared to flight data, 3-2-1-1 input

5.2.2 Lateral model

The lateral neural network model has been trained with the same MLP structure. Model output has been presented against flight data in Figure 5.9 and Figure 5.10. Figure 5.9 shows good predictability of the neural network model. The model residuals are in a very reasonable range. Figure 5.10 shows that, the model output is still very dependent on the input signal shape.

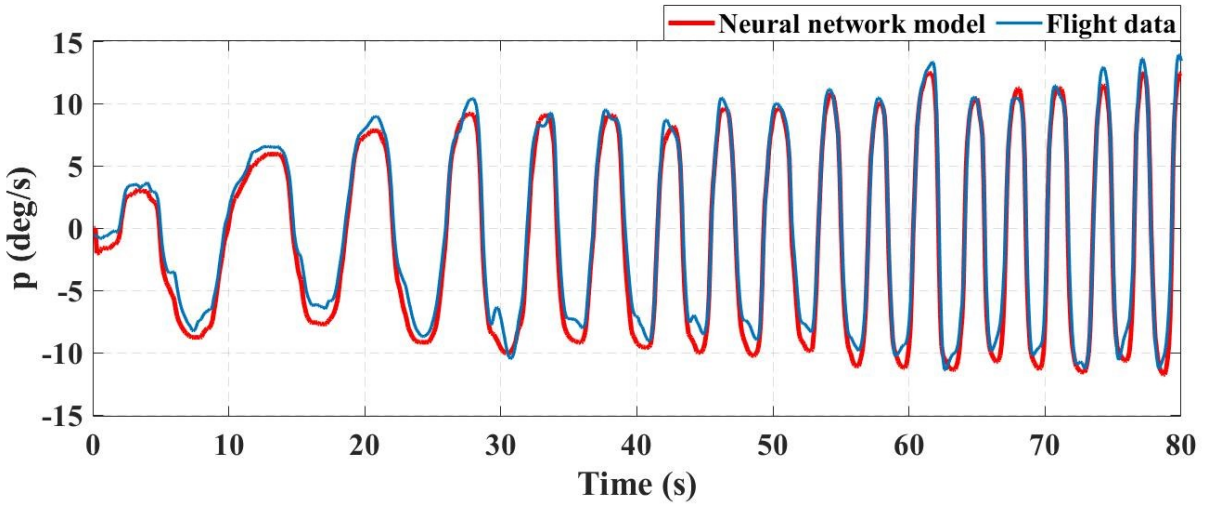

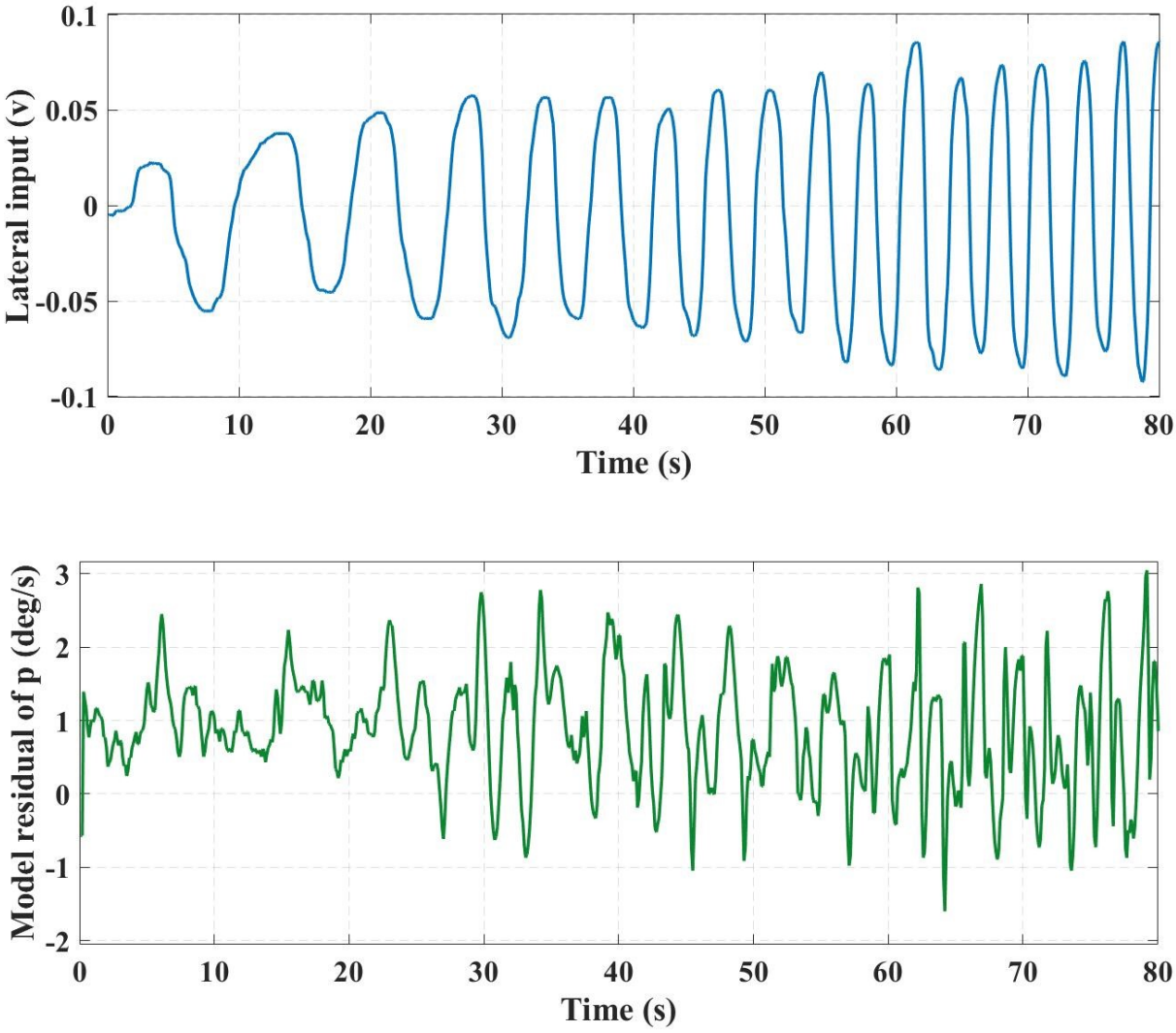

Figure 5.9: Lateral neural network model output compared to flight data, frequency sweep

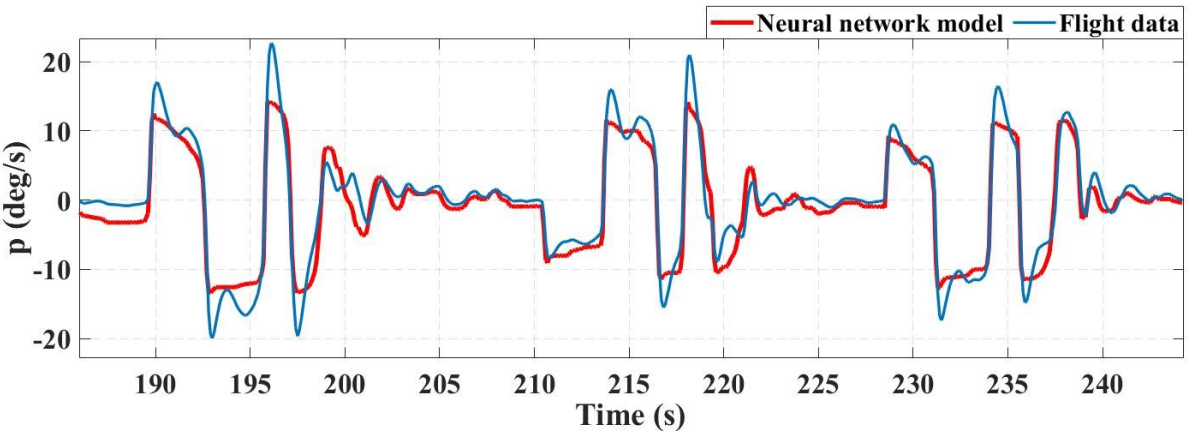

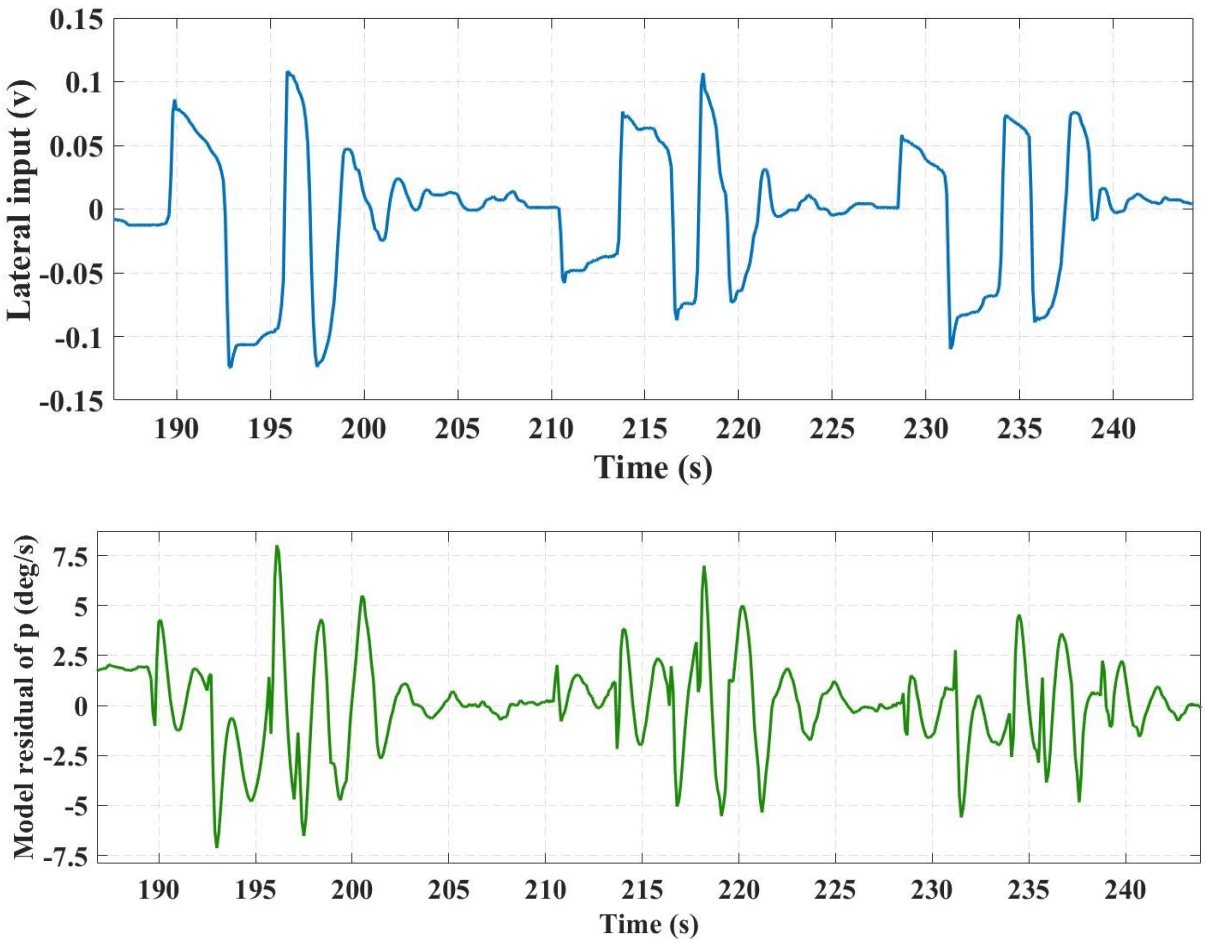

Figure 5.10: Lateral neural network model output compared to flight data, 3-2-1-1 input

5.3 Neural Network Wiener Model Identification

In Chapter 4, the transfer function model in general has very good predictability. But the accuracy of transfer function model is susceptible to the frequency and trimmed condition. On the other hand, the MLP neural network model being trained is very dependent on the input shape. A combined structure of transfer function followed by MLP is therefore being studied. This method is also known as a block-oriented approach. The most widely used block-oriented models are Wiener and Hammerstein models. In Wiener model, the linear element precedes the nonlinear one. In Hammerstein model, the nonlinear element precedes the linear one [26]. The

transfer function can already predict the system dynamics very well around trimmed condition. Therefore, the identified transfer function will form the linear element of the block-oriented model, with the nonlinear element being addressed by a MLP.

The SISO Wiener system presented as follows [28]:

$$y(n) = f\left(\frac{B(q^{-1})}{A(q^{-1})}u(n)\right) + \varepsilon(n) \tag{5.19}$$

where

$$A(q^{-1}) = 1 + a_1 q^{-1} + \cdots + a_{na} q^{-na}$$

$$B(q^{-1}) = b_1 q^{-1} + \cdots + b_{na} q^{-nb}$$

and q^{-1} is the backward shift operator, $q^{-m}y(n) = y(n-m)$, $f(\cdot)$ is the nonlinear element, $a_1, \ldots, a_{na}$, $b_1, \ldots, b_{nb}$ are unknown parameters of the linear dynamic system, and $\varepsilon(n)$ is the system output disturbance.

There are three assumptions about this model: 1) the function $f(\cdot)$ is continuous; 2) the linear dynamic system is casual and asymptotically stable; 3) the polynomial orders na and nb are known.

Given the measured input and output of the aircraft system $\{u(n), y(n)\}, n = 1, \ldots, N$, by minimizing the global cost function:

$$J = \frac{1}{2}\sum_{n=1}^{N}(y(n) - \hat{y}(n))^2 \tag{5.20}$$

$\hat{y}(n)$ is the output of the neural network Wiener model.

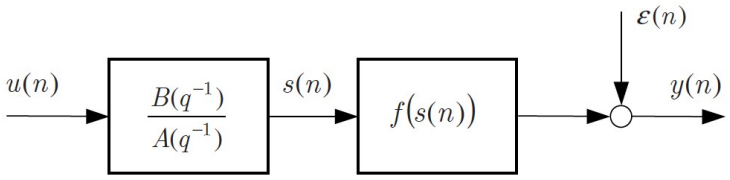

Figure 5.11: Wiener system

There are two basic approaches to find the minimum of the global cost function: the sequential mode (pattern learning) and batch learning. The sequential mode or pattern learning uses pattern-by-pattern updating of model parameters, changing their values by an amount proportional to the negative gradient of the local cost function:

$$w(n) = w(n-1) - \eta \frac{\partial J(n)}{\partial w(n-1)} \tag{5.21}$$

$$\frac{\partial J(n)}{\partial w(n-1)} = -(y(n) - \hat{y}(n)) \frac{\partial \hat{y}(n)}{\partial w(n-1)} \tag{5.22}$$

where $w(n)$ is the weight vector containing all model parameters at the time n, and $\eta > 0$ is the learning rate. This procedure will minimize the global cost function J as long as the learning rate η is sufficiently small [30].

The batch learning approach uses the whole set of input-output data $\{u(n), y(n)\}, n = 1, \dots, N,$ to update model parameters. In this technique, the global cost function J is minimized iteratively. The parameters change over all training patterns are accumulated before the parameters are actually changed [29]. The basic version gradient learning algorithm has its drawbacks: the fixed learning rate η may be chosen too large leading to unnecessary oscillations or too small to cause very slow learning process.

Series-parallel neural network Wiener model is shown in Figure 5.12, it is a feedforward type multilayer perceptron model composed of the inverse nonlinear element, a liner node with two tapped delay lines, used as a model of the linear dynamic system, and another multilayer perceptron used as a model of the nonlinear element. The assumption is that the nonlinear function $f(\cdot)$ is invertible. Model inputs are the system input $u(n)$ and system output $y(n)$. Model output $\hat{y}(n)$ is defined as:

$$\hat{y}(n) = \hat{f}(\hat{s}(n), w) \tag{5.23}$$

with

$$\hat{s}(n) = -\sum_{m=1}^{na} \hat{a}_m \hat{g}(y(n-m), v) + \sum_{m=1}^{nb} \hat{b}_m u(u-m)$$

$$\hat{f}(\hat{s}(n), w) = \sum_{j=1}^{M} w_{1j}^{(2)} \varphi\left(x_j(n)\right) + w_{10}^{(2)}$$

$$x_j(n) = w_{j1}^{(1)} \hat{s}(n) + w_{j0}^{(1)}$$

$$\hat{g}(y(n), v) = \sum_{j=1}^{M} v_{1j}^{(2)} \varphi\left(z_j(n)\right) + v_{10}^{(2)}$$

$$z_j(n) = v_{j1}^{(1)} y(n) + v_{10}^{(1)}$$

where the function $\hat{f}(\cdot)$ describes the nonlinear element model, the function $\hat{g}(\cdot)$ describes the inverse nonlinear element model, $\varphi(\cdot)$ is the activation function, $\hat{a}_1, \ldots, \hat{a}_{na}, \hat{b}_1, \ldots, \hat{b}_{nb}$ are the parameters of the linear dynamic model, $w = [w_{10}^{(1)} \ldots w_{M1}^{(1)}\ w_{10}^{(2)} \ldots\ w_{1M}^{(2)}]^T$ is the weight vector of the nonlinear element model, and $v = [v_{10}^{(1)} \ldots v_{M1}^{(1)}\ v_{10}^{(2)} \ldots v_{1M}^{(2)}]^T$ is the parameter vector of the inverse nonlinear element model.

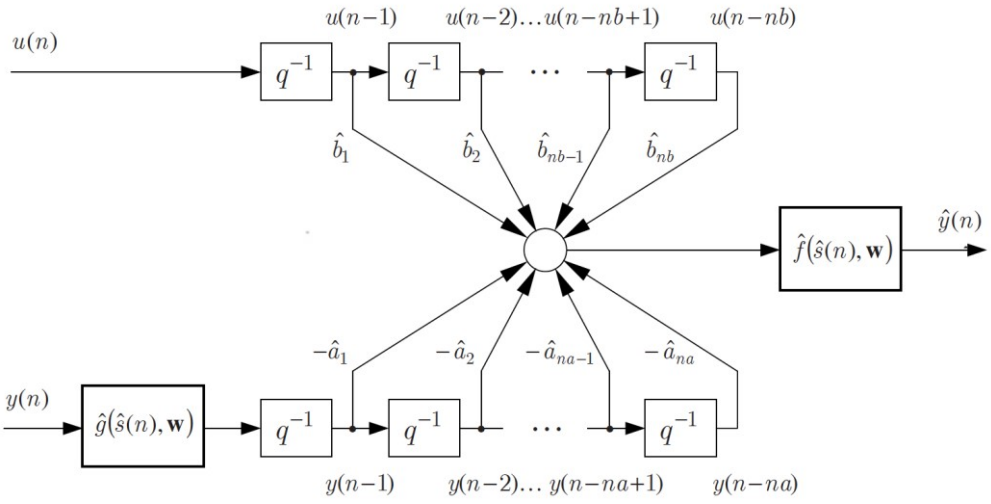

Figure 5.12: Series parallel SISO neural network Wiener model

5.3.1 Longitudinal model

The linear longitudinal transfer function model identified in Chapter 4 has been utilized as the linear part of the Wiener model. The input value to the transfer function u_{lon} remain unchanged, output value from transfer function model has been denoted by $\hat{s}(n)$, which is the input to the MLP structure in Figure 5.6. The Wiener model structure is presented in Figure 5.13. The flight data of test point one has been utilized to train the Wiener model. Wiener model response has been compared to flight data, and model residual has also been presented from Figure 5.14 (frequency sweep input) to Figure 5.15 (3-2-1-1 input).

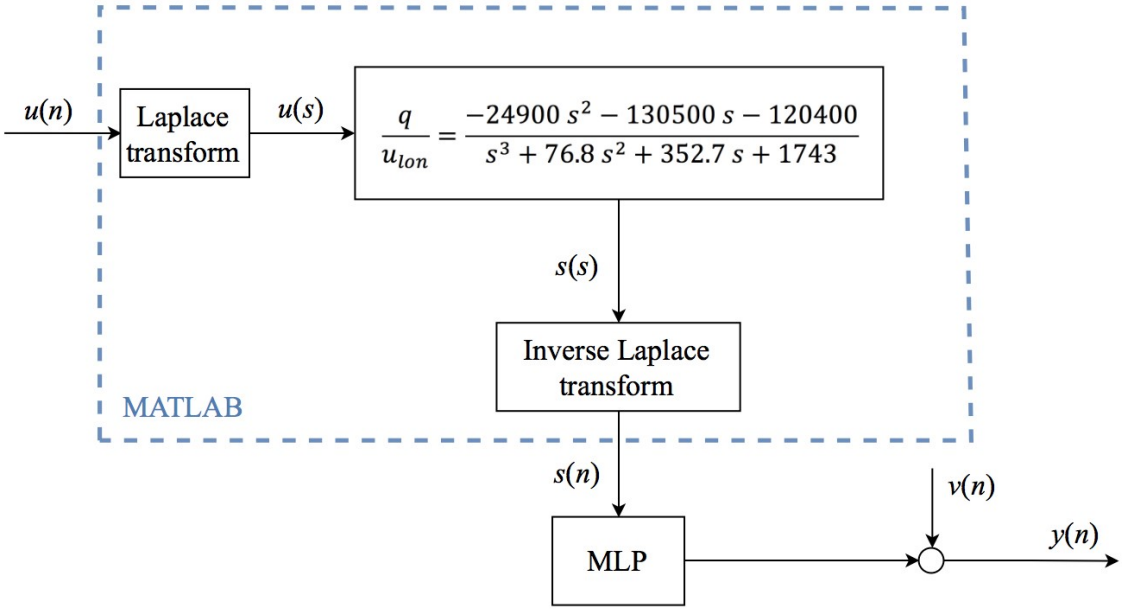

Figure 5.13: Wiener model structure for longitudinal model

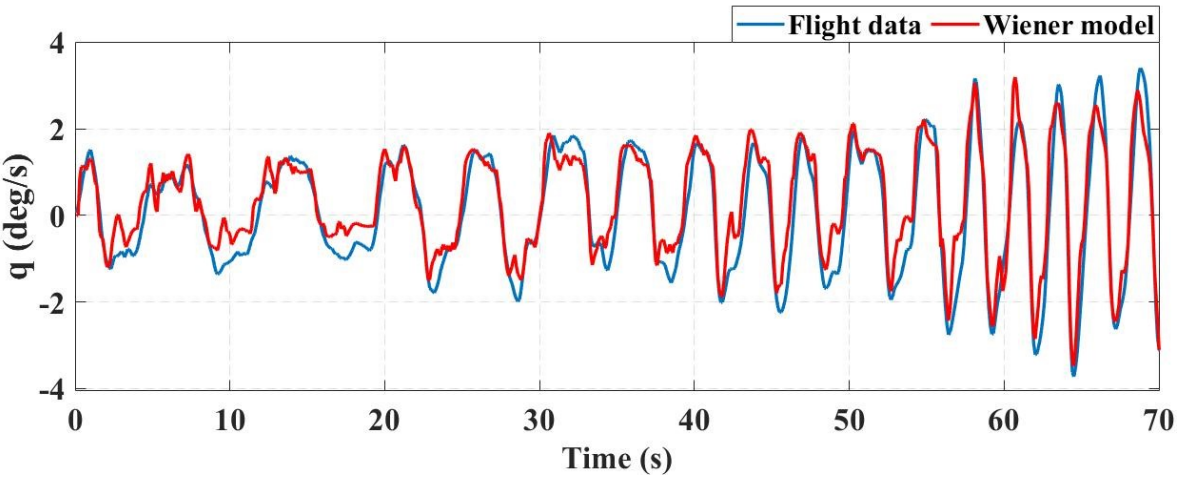
Flight data
Wiener model
q (deg/s)
Time (s)

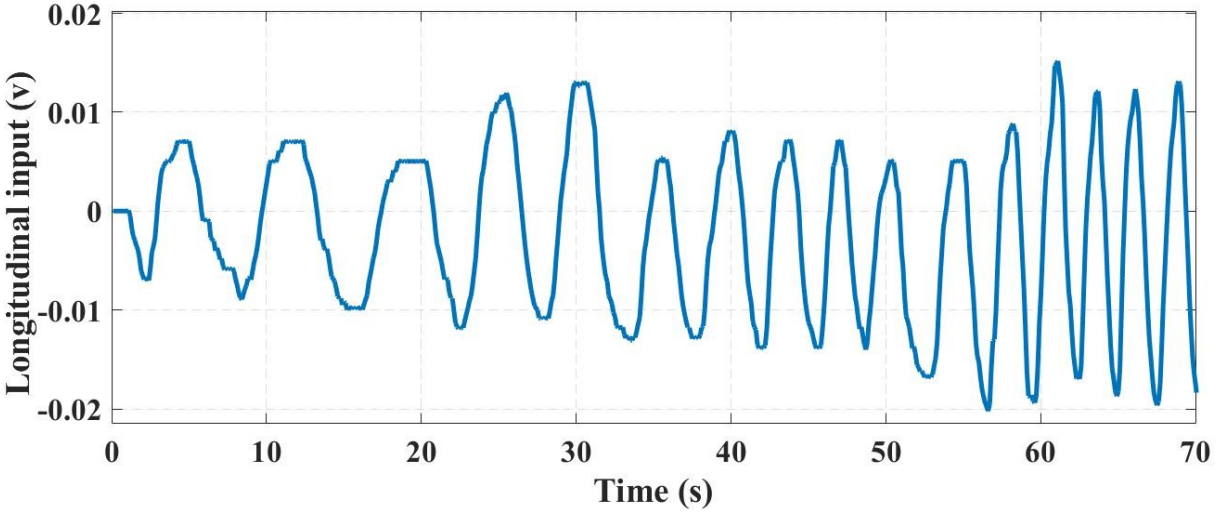
Longitudinal input (v)
Time (s)

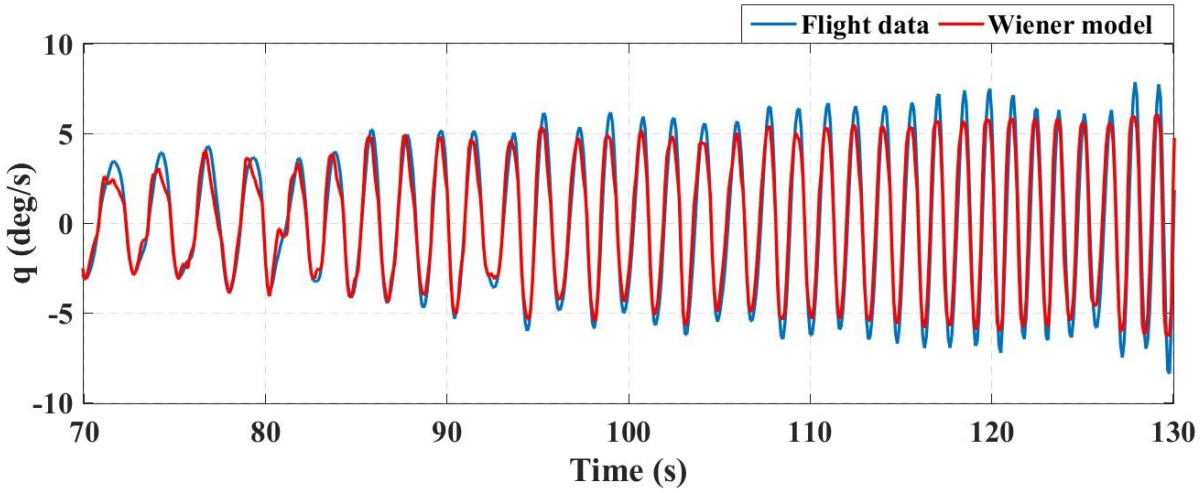
Flight data
Wiener model
q (deg/s)
Time (s)

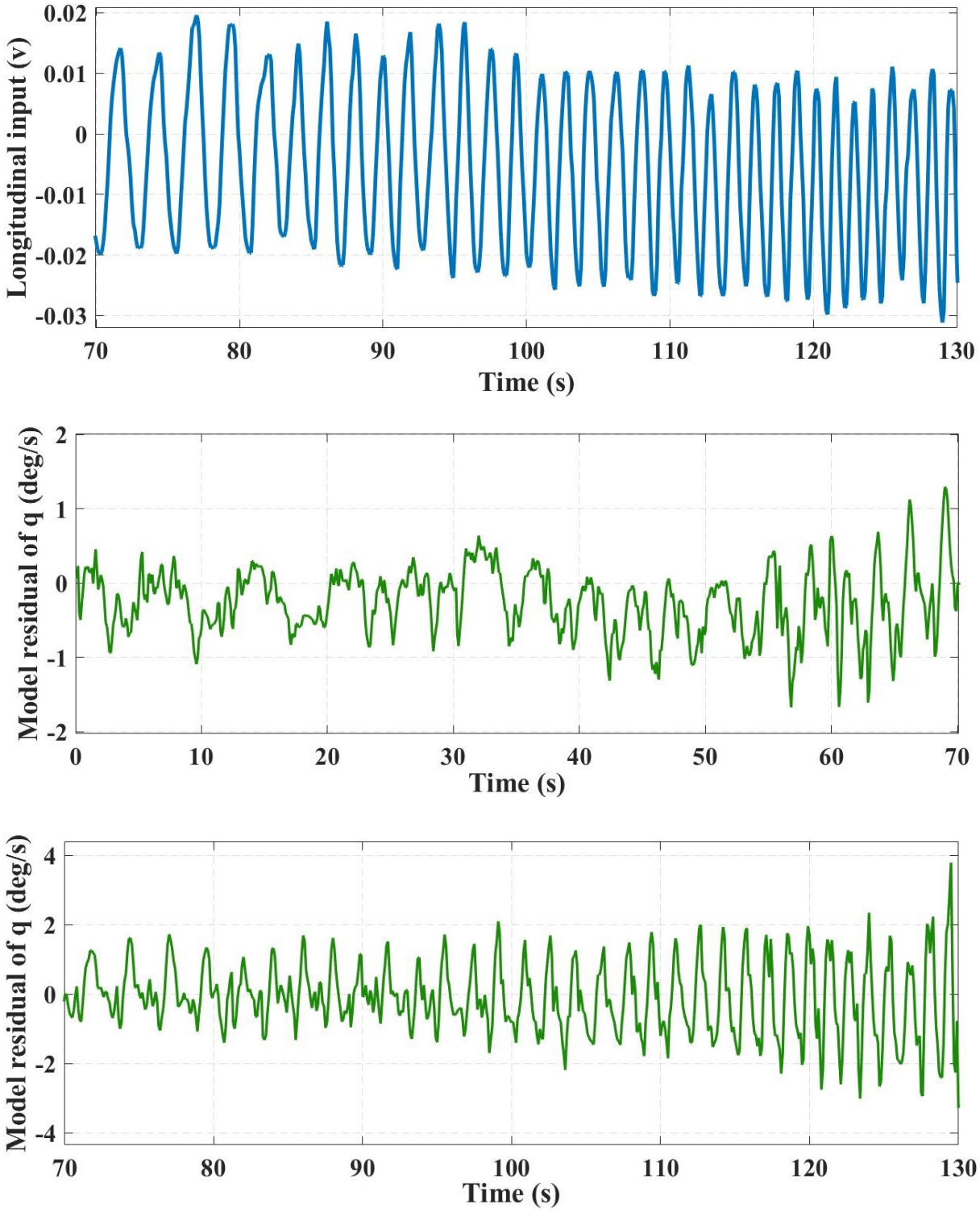

Figure 5.14: Identified Wiener model compared to flight data, longitudinal frequency sweep

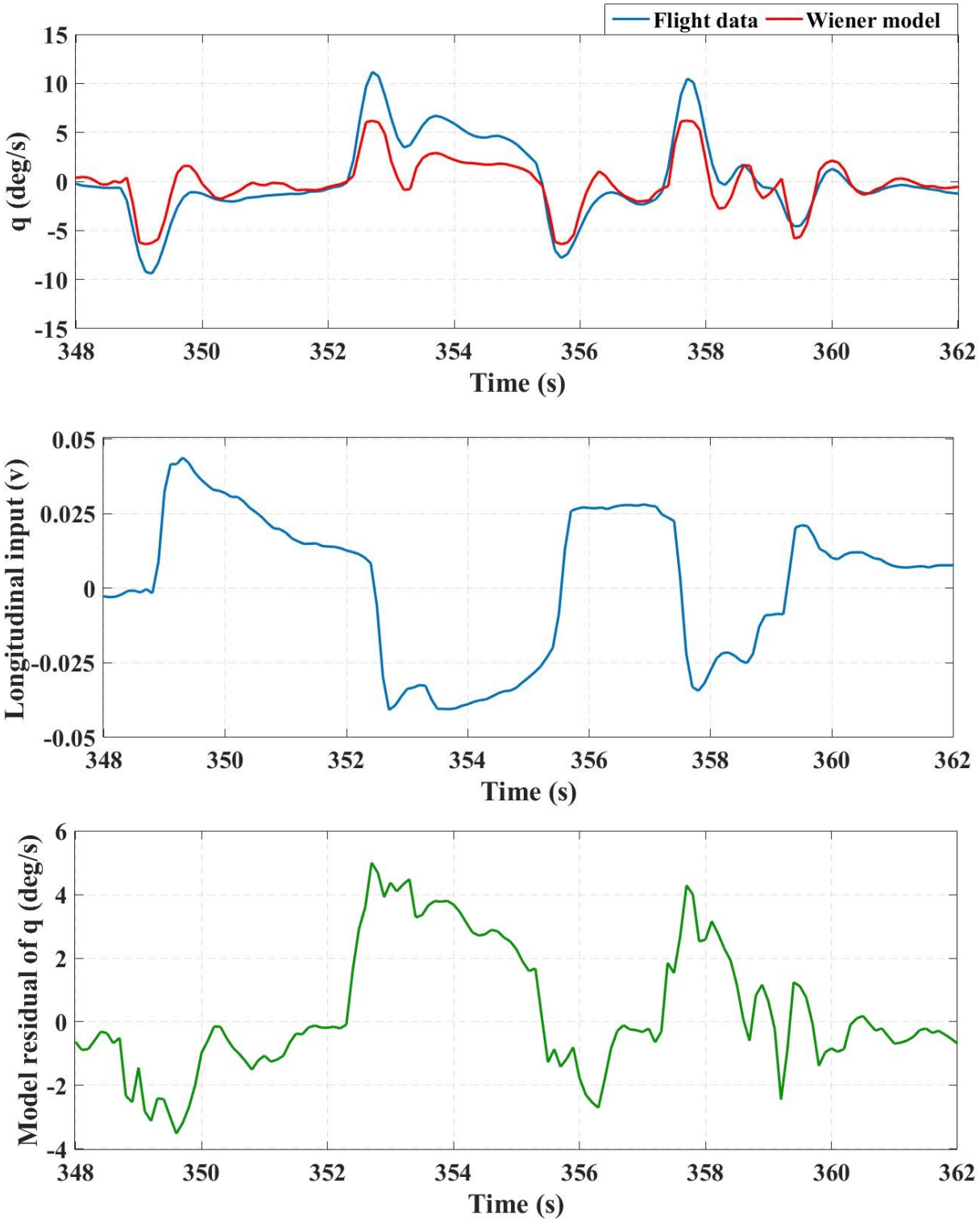

Figure 5.15: Identified Wiener model output compared to flight data, 3-2-1-1 input

5.3.2 Lateral model

Similar to the longitudinal model, the linear lateral transfer function model identified in Chapter 4 has been utilized as the linear part of the Wiener model. The input value to the transfer function u_{lat} remains unchanged, output value from the lateral transfer function model is denoted as $\hat{s}(n)$, which is the input to the MLP structure in Figure 5.6. The Wiener model structure for lateral dynamics is similar to the longitudinal one, with only the transfer function being changed. The flight data of test point two has also been utilized to train the Wiener model. Wiener model response has been compared to the flight data, and model residual has also been presented from Figure 5.17 (frequency sweep input) to Figure 5.18 (3-2-1-1 input).

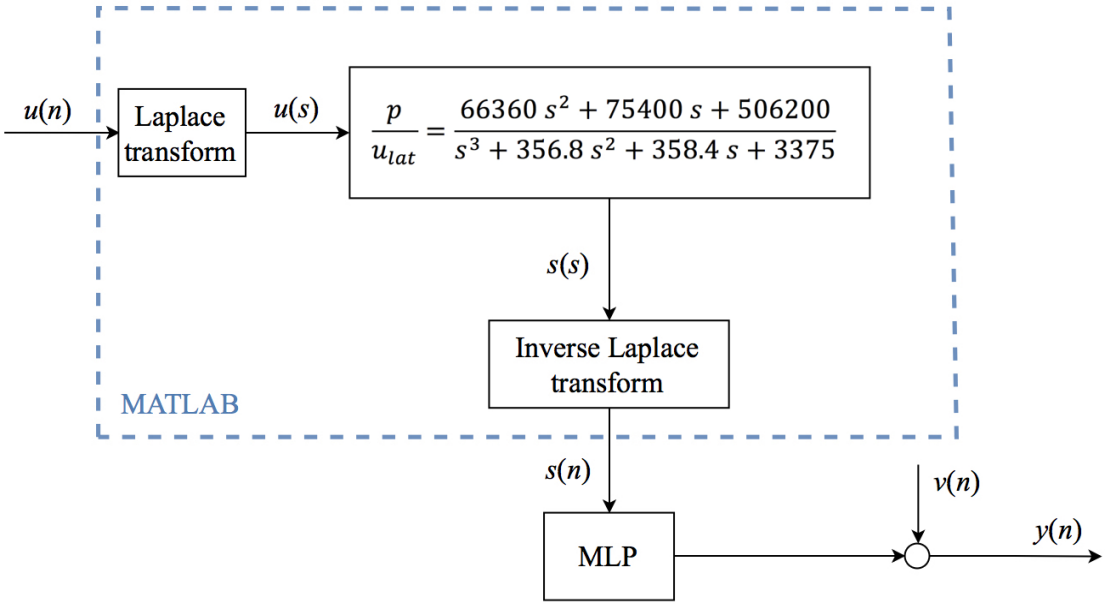

Figure 5.16: Wiener model structure for lateral model

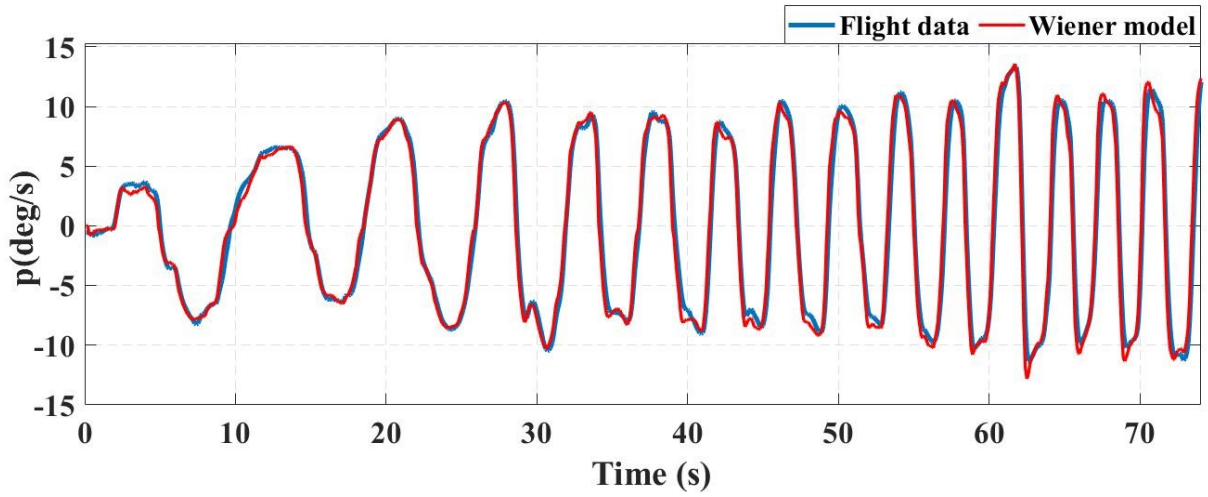
Flight data
Wiener model
p(deg/s)
Time (s)

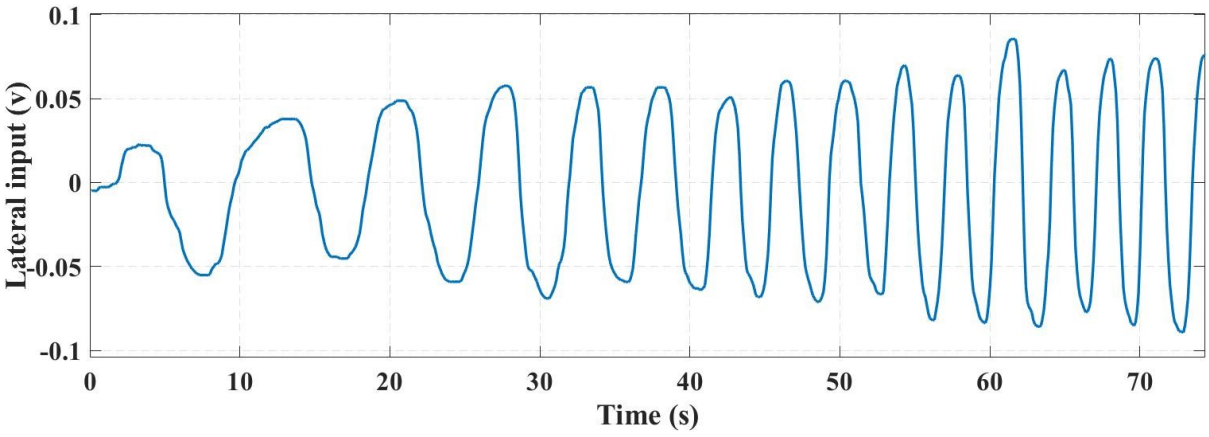
Lateral input (v)
Time (s)

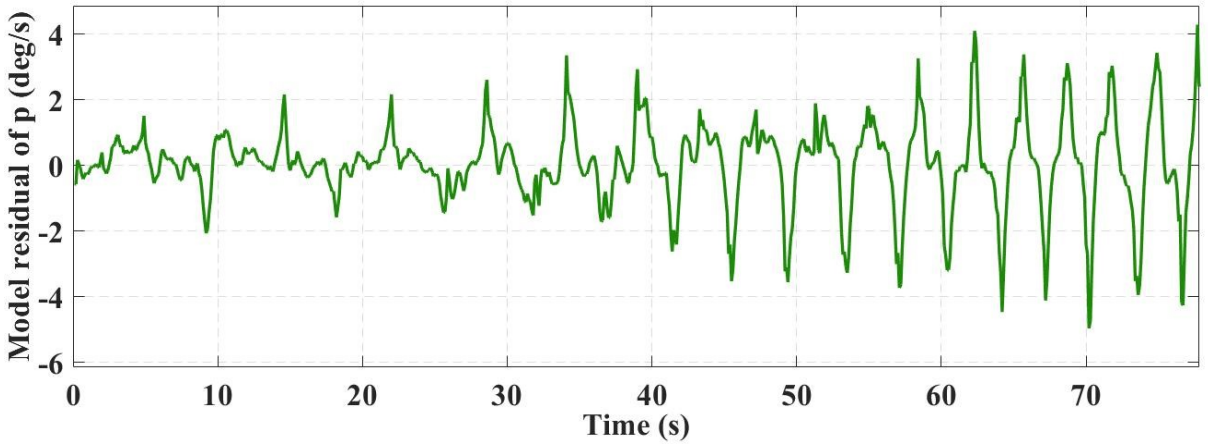
Model residual of p (deg/s)
Time (s)

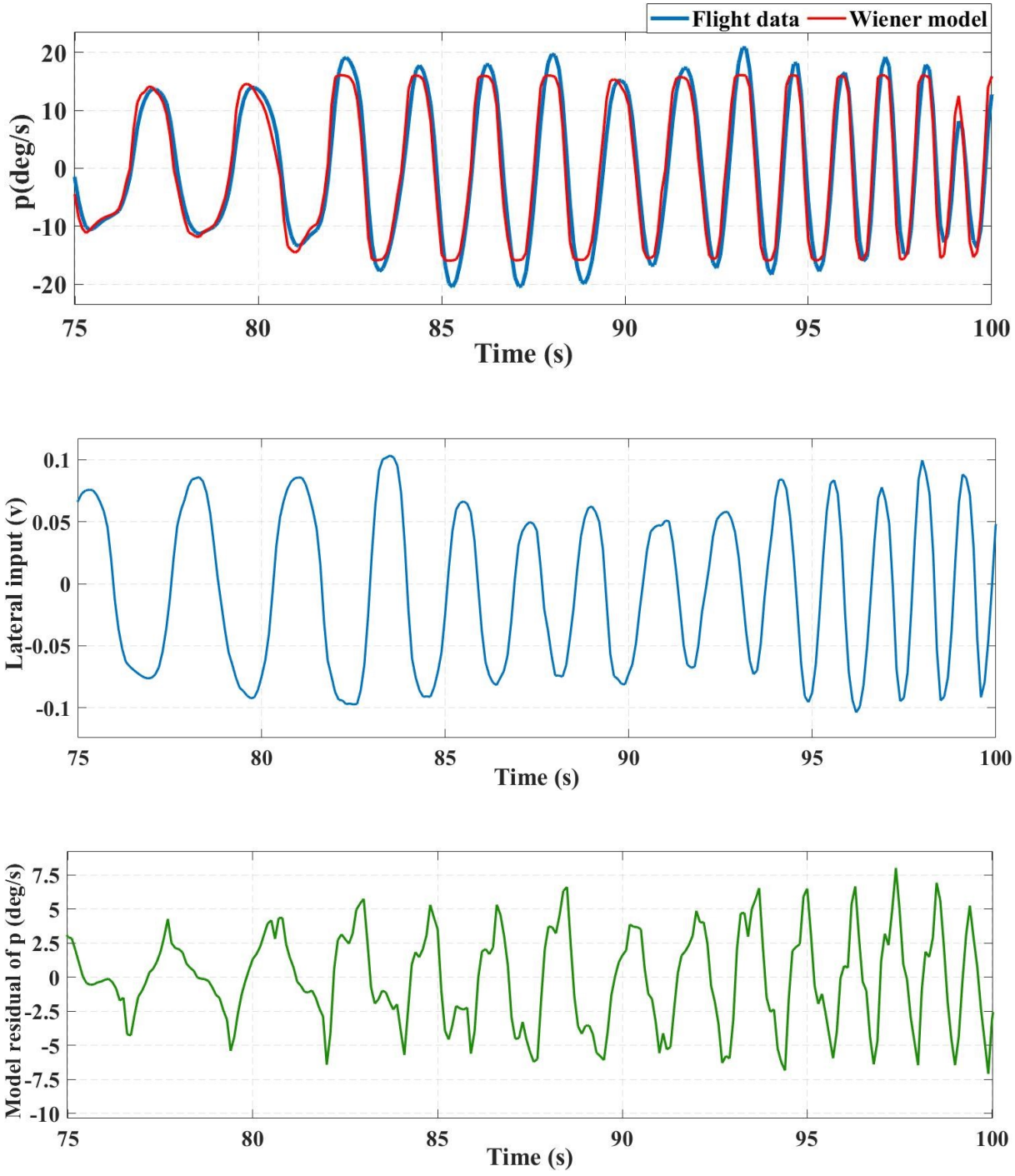

Figure 5.17: Identified Wiener model output compared to flight data, lateral frequency sweep

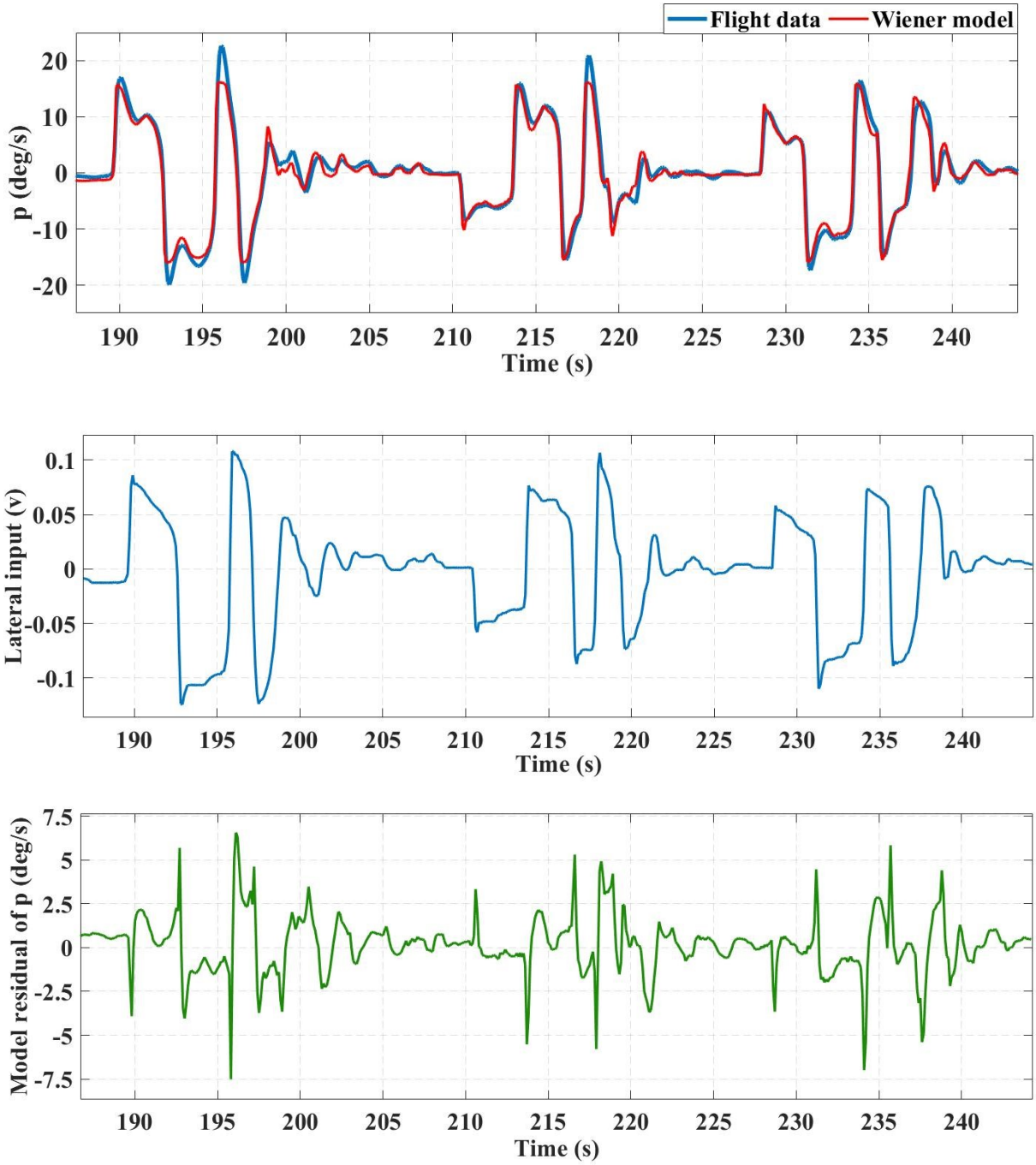

Figure 5.18: Identified Wiener model output compared to flight data, 3-2-1-1 input

In addition, the MLP black-box model in Section 5.2 has been compared with the Wiener model in Figure 5.19.

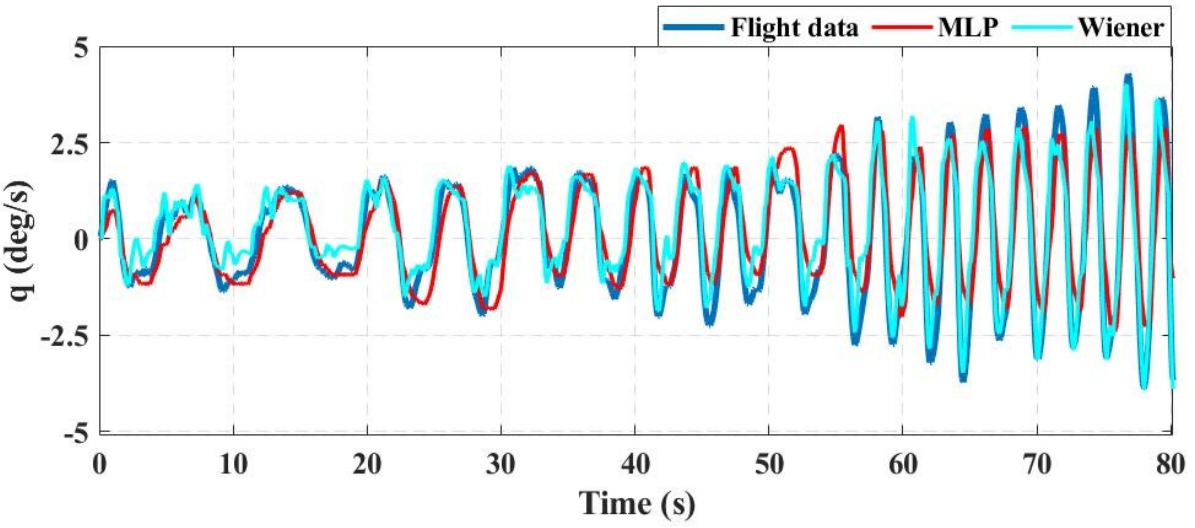
Flight data
MLP
Wiener
q (deg/s)
Time (s)

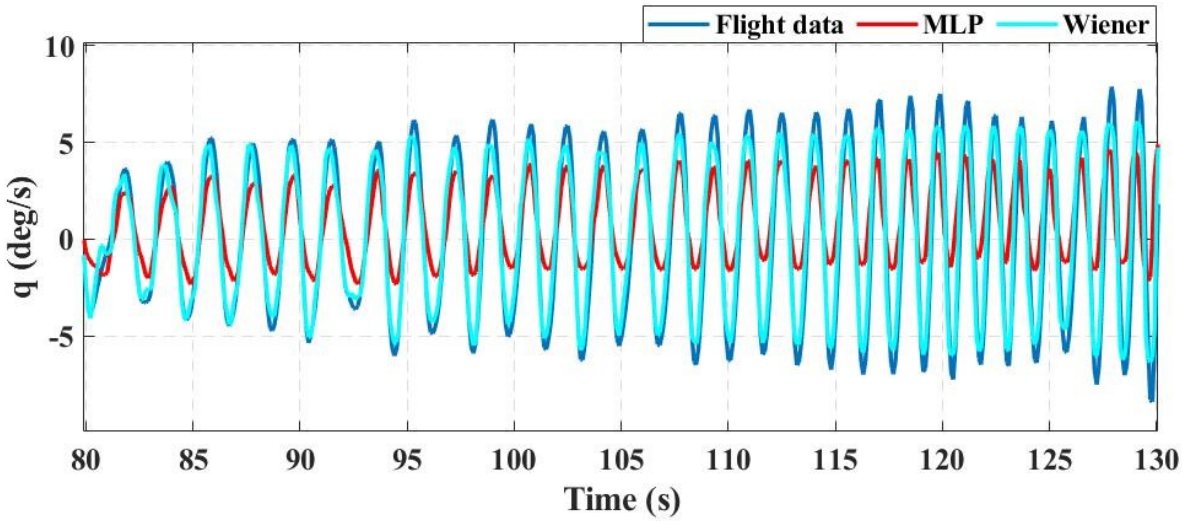
Flight data
MLP
Wiener
q (deg/s)
Time (s)

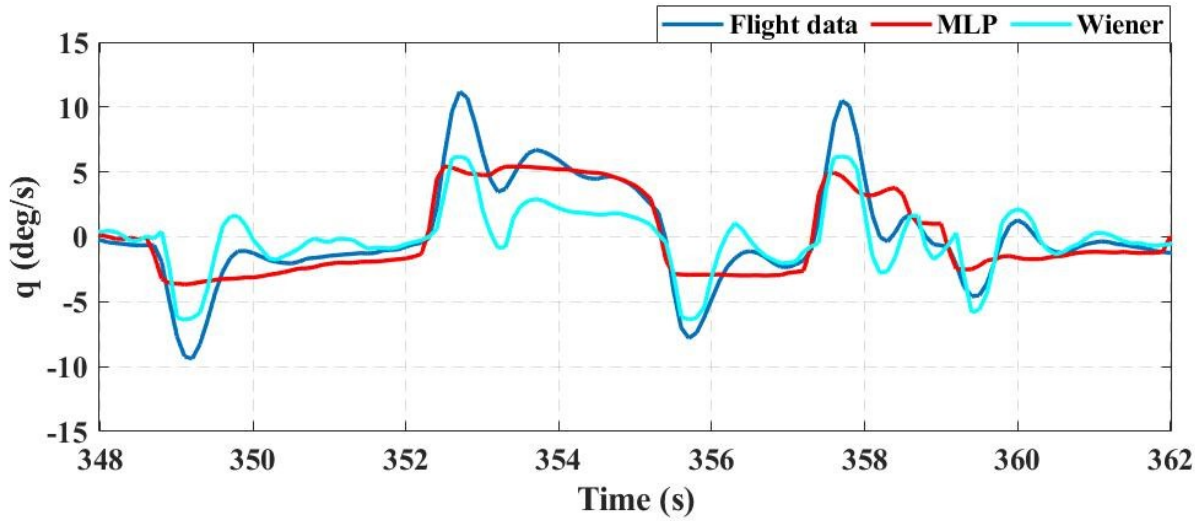
Flight data
MLP
Wiener
q (deg/s)
Time (s)

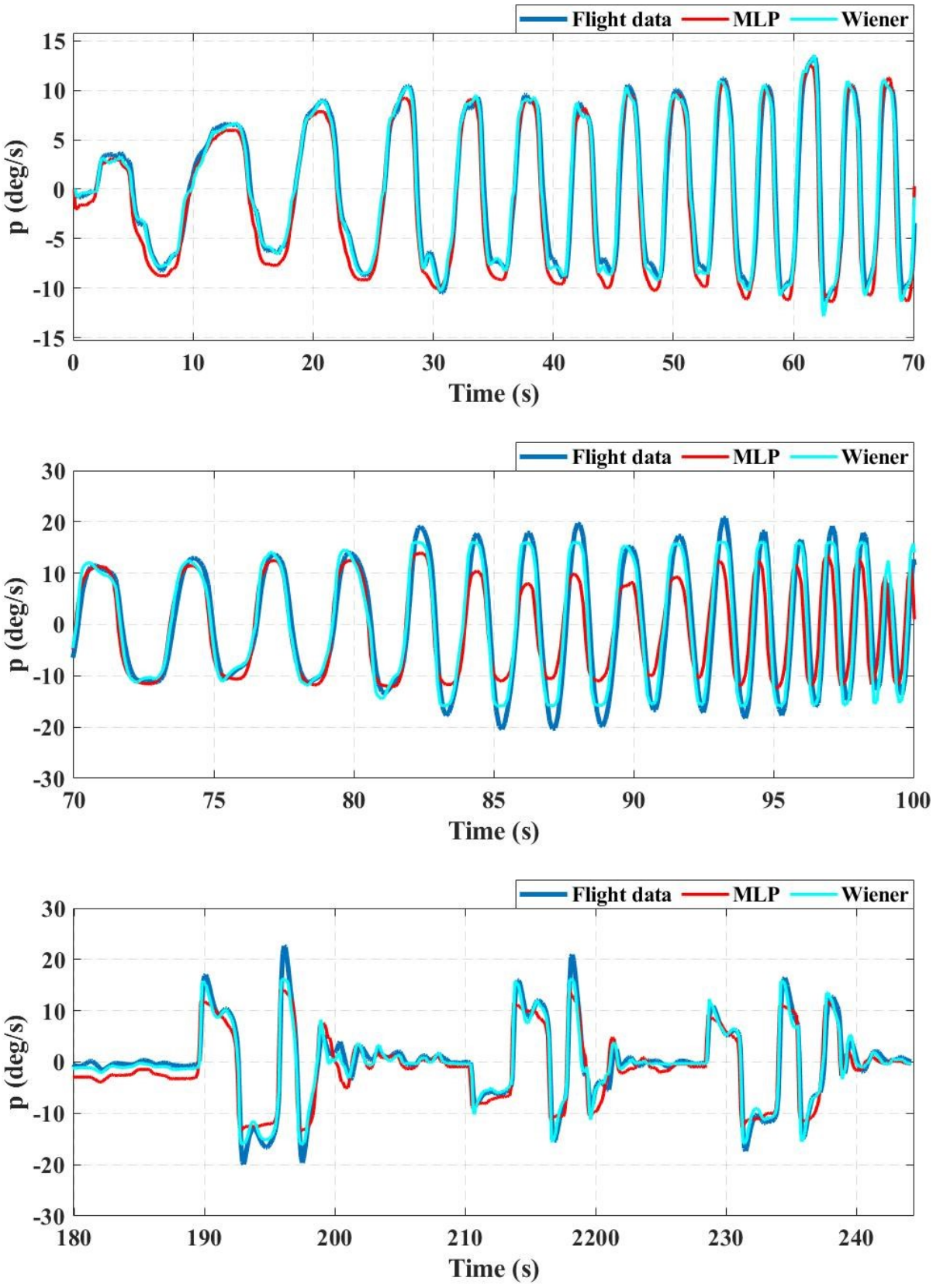

Figure 5.19: Long-EZ MLP model and Wiener model compared with flight data

5.4 Analysis and Discussion

Similar to Section 4.3, coefficient of determination R^2 and RMSE have been calculated and listed in Figure 5.20 and Table 5.1. By comparison, the table shows that the Wiener model has lowest RMSE and highest R^2 (closest to 1) on both longitudinal and lateral axes.

By combining the linear transfer function model and the MLP structure, the Wiener model output accuracy has been improved greatly, as is presented visually in Figure 5.19 and numerically in Table 5.1. Therefore, the developed block-oriented neural network Wiener model approach is an excellent tool of predicting the aircraft dynamics on both longitudinal and lateral axes.

However, both the MLP and Wiener model are only trained at one flight test condition (116 kts, 8000ft) due to the limited real flight data available currently. When there is more data available from different flight conditions in the future, both the Wiener model and MLP model structure can be improved by taking the different input conditions into account and forming a more complex neural network structure.

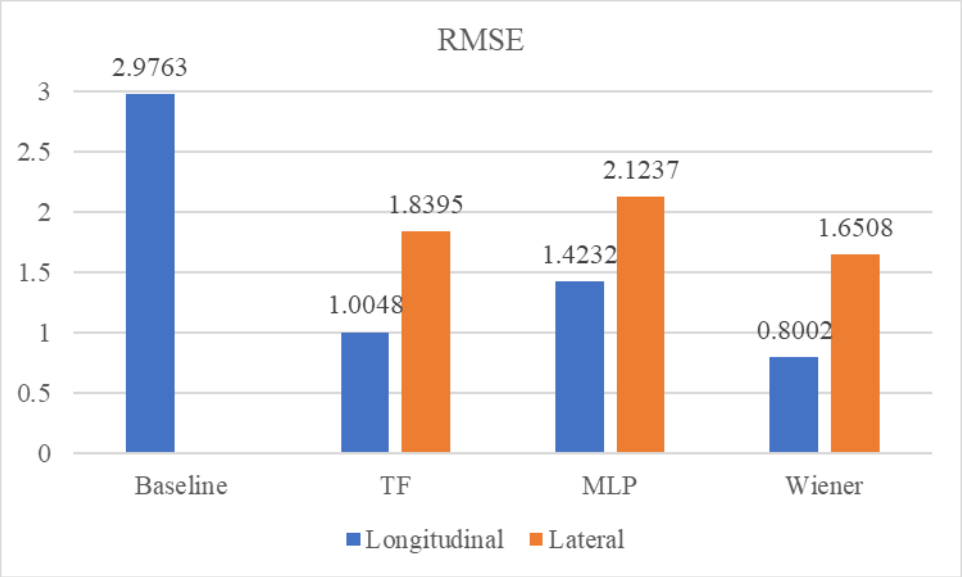

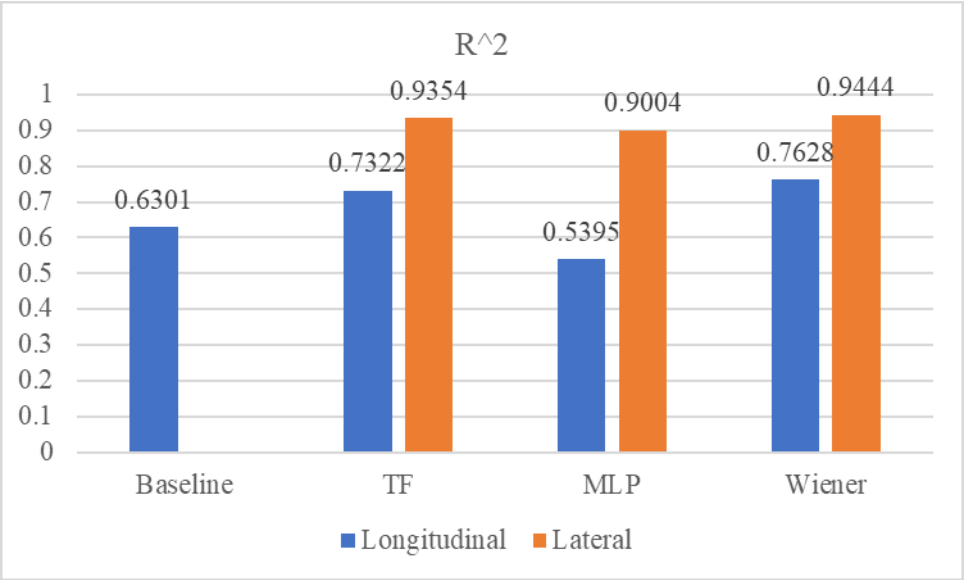

Figure 5.20: RMSE and R^2 of identified transfer function model, MLP, and Wiener model

Table 5.1: RMSE and R^2 of identified transfer function model, MLP, and Wiener model

	RMSE		R^2	
	Longitudinal	Lateral	Longitudinal	Lateral
Baseline	2.9763	--	0.6301	--
TF	1.0048	1.8395	0.7322	0.9354
MLP	1.4232	2.1237	0.5395	0.9004
Wiener	0.8002	1.6508	0.7628	0.9444

Chapter 6 Conclusions and Future Works

It is a challenging task to find an accurate mathematical model to represent the aerodynamic behavior of a fixed-wing aircraft, which is especially the case when dealing with very limited real flight data available. System identification using time-domain method is a very reliable way of modeling aircraft dynamics. The primary purpose of this study is to provide an identification tool for the aircraft Long-EZ, which provides some information about the aircraft aerodynamic characteristics that can be used in the simulation environment at a later stage. The identified model also provides some insight for autopilot design, which can also extend to the fault-tolerant control in the future.

This thesis has provided an overview of the time-domain system identification approaches, estimation and optimization methods. Fixed-wing aircraft dynamics and flight test plan have been intensively introduced. Among the various system identification approaches, baseline mode, equation error method, MLP neural network, and block-oriented Wiener model structure have been developed and trained based on the real flight data.

Firstly, baseline aircraft model structure has been determined. Stability and control derivatives from this baseline model have been calculated with Roskam's [39] method. This baseline model is essential for software-in-the-loop simulations, which identifies potential risks in the flight dynamics of the modified aircraft system in a low-cost and timely way.

Secondly, based on the flight test instrumentations available at ITPS, system identification flight test has been planned and carried out to get sufficient data for modeling. Based on this experience, improved flight tests can be planned in the future to improve the baseline model.

Thirdly, linear transfer function model structures have been determined with the physics of the aircraft. Model parameters have been identified on both longitudinal and lateral axes using time-domain method, and have been compared with baseline model and flight data. This linearized transfer function model can be utilized for flight controller design of the Long-EZ aircraft in the future.

At last, a set of Python-based code has been developed to deal with the nonlinearities in the model, which is also known as the MLP neural network. Real flight data has been used to train this neural network, the training result has been plotted against the flight data. Moreover, the identified linear model has been combined with the MLP structure to form a block-oriented model, which is called neural network wiener model. By comparing the four different models, the block-oriented model has overall the best accuracy for predicting the aircraft dynamics on longitudinal and lateral axes respectively.

The future direction of the research is to get more comprehensive flight test instrumentation (flight test boom) installed on the testbed Long-EZ, so that air data will be available for modelling. New flight test plan with different maneuvers can be designed with this air data probe being installed. More comprehensive aircraft models, such as MIMO state-space model, can be identified with flight test data. Long-EZ aircraft's aerodynamic and control derivatives can also be calculated with the equation error method, making the model more accurate and complete for software-in-the-loop simulation. Moreover, the SISO structure Wiener model can also be extended to a MIMO structure model, with different flight test condition (such as speed, altitude) being considered as input variables. The MLP structure can also be upgraded to a recursive type neural network structure, which takes the current state of the aircraft in the

feedback loop, making the model more accurate and flexible in dealing with the nonlinearities with the change of flight conditions in the future.

Bibliography

[1] L. Zadeh, "From Circuit Theory to System Theory," *Proceedings of the IRE,* vol. 50, no. 5, pp. 856-865, May 1962.

[2] V. Klein and E. A. Morelli, Aircraft System Identification: Theory and Practice, Reston: AIAA, 2006.

[3] R. V. Jategaonkar, Flight Vehicle System Identification: A Time-Domain Methodology, Reston: AIAA, 2006.

[4] M. B. Tischler and R. K. Remple, Aircraft and Rotorcraft System Identification, Virginia: AIAA, 2006.

[5] P. Hamel and R. Jategaonkar, "Evaluation of Flight Vehicle System Identification," *Journal of Aircraft,* vol. 33, pp. 9-28, Jan.-Feb., 1996.

[6] W. Milliken and Jr., "Progress in Stability and Control Research," *Journal of the Aeronautic Science,* vol. 14, pp. 494-519, 1947.

[7] L. Ljung, System Identification, Theory for the User, 2nd ed, Upper Saddle River, NJ: Prentice-Hall, 1999.

[8] V. Klein, "Application of System Identification to High Performance Aircraft," in *Proceedings of the 32nd IEEE Conference on Decision and Control*, San Antonio, TX, 1993.

[9] V. Klein and P. Murphy, "Aerodynamic Parameters of High Performance Aircraft Estimated from Wind Tunnel and Flight Test Data," in *System Identification for Integrated Aircraft Development and Flight Testing*, May 1999.

[10] J. Shen, Y. Su, Q. Liang and X. Zhu, "Calculation and Identification of the Aerodynamic Parameters for Small-Scaled Fixed-Wing UAVs," *Sensors,* vol. 18, no. 1, p. 206, Jan 2018.

[11] W. Wei, M. B. Tischler, N. Schwartz and K. Cohen, "System Identification and Flight Control of an Unmanned Quadrotor," in *Advanced UAV Aerodynamics, Flight Stability and Control: Novel Concepts, Theory and Applications*, New York, John Wiley & Sons Ltd., 2017, p. 695.

[12] M. H. Mohajerani, H. Bolandhemmat, Y. M. Zhang and H. W. Loewen, "Identification of

Low Order Equivalent Transfer Function Model of Trex-700E Helicopter from Flight Test Data," in *AIAA Science and Technology Forum and Exposition*, National Harbor, MD, 2014.

[13] Z. Liu, Y. R. Zhou and G. D. Wang, "Online Parameter Identification Study on a Small Fixed-Wing UAV," in *International Conference on Unmanned Aircraft Systems*, Arlington, VA, 2016.

[14] R. Abdulhamid, M. H. Santos, N. Oliveira and B. Maciel, "Initial Experimental Procedures for Modeling and Identification of a Fixed Wing Aerial Vehicle," in *International Conference on Unmanned Aircraft Systems*, Arlington, VA, 2016.

[15] V. Klein, "Estimation of Aircraft Aerodynamic Parameters from Flight Data," in *Progress in Aerospace Sciences*, 1989.

[16] D. Stepner and R. Mehra, "Maximum Likelihood Identification and Optimal Input Design for Identifying Aircraft Staiblity and Control Derivatives," NASA CR-2200, 1973.

[17] R. Mehra, "Maximum Likelihood Identification of Aircraft Parameters," in *Proceedings of the Joint Automatic Control Conference*, Atlanta, GA, June 1970.

[18] N. Kumar and N. Rao, "Estimation of Stability and Control Derivatives of Light Canard Research Aircraft from Flight Data," *Defense Science Journal,* vol. 54, no. 3, pp. 277-292, 2014.

[19] R. Jategaonkar, D. Fischenberg and W. Von Gruenhagen, "Aerodynamic Modeling and System Identification from Flight Data -- Recent Applications at DLR," *Journal of Aircraft,* vol. 41, no. 4, pp. 681-691, 2004.

[20] F. Nicolosi, A. De Marco and P. Della Vecchia, "Stability, Flying Qualities and Longitudinal Parameter Estimation of a Twin-Engine CS-23 Certified Light Aircraft," *Aerospace Science and Technology,* pp. 226-240, 2013.

[21] G. Chowdhary and R. Jategaonkar, "Aerodynamic Parameter Estimation from Flight Data Applying Extended and Unscented Kalman Filter," *Aerospace Science and Technology,* vol. 14, pp. 106-117, 2010.

[22] J. Garcia-Velo and B. Walker, "Aerodynamic Parameter Estimation for High-Performance Aircraft Using Extended Kalman Filtering," *Journal of Guidance, Control and Dynamics,* vol. 20, no. 6, pp. 1257-1259, November-December 1997.

[23] A. Kokolios, "Use of a Kalman Filter for the Determination of Aircraft Aerodynamic

Characteristics from Flight Test Data," in *AIAA Aerospace Sciences Meeting & Exhibit*, Reno, NV, 1994.

[24] J. Bauer and D. Andrisani, "Estimating Short-Period Dynamics Using an Extended Kalman Filter," in *Fifth Biannual Flight Test Conference*, Ontario, CA, May 1990.

[25] M. Shinbrot, "A Least Squares Curve Fitting Method with Application of the Calculation of Stability Coefficients from Transient-Response Data," NACA TN 2341, 1951.

[26] A. Janczak, Identification of Nonlinear Systems Using Neural Networks and Polynomial Models, Switzerland: Springer, 2005.

[27] S. Shanmuganathan and S. Samarasinghe, Artificial Neural Network Modelling, Springer International Publishinig, 2016.

[28] M. Gupta, L. Jin and N. Homma, Neural Networks: From Fundamentals to Advanced Theory, Hoboken: John Wiley and Sons, 2003.

[29] O. Nelles, Nonlinear System Identification. From Classical Approaches to Neural Networks and Fuzzy Models, New York, Berlin, Heidelberg: Springer, 2001.

[30] R. J. Williams and D. Zipser, "A Learning Algorithm for Continually Running Fully Recurrent Neural Networks," *Neural Computations,* vol. 1, pp. 270-280, 1989.

[31] T. Kohonene and G. Deboeck, Visual Explorations in Finance with Self-organizing Maps, London: Springer, 1998.

[32] W. McCulloch and W. Pitts, "A Logical Calculus of the Ideas Immanent in Nervous Activity," *Bulletin of Mathematical Biophysics,* vol. 5, pp. 115-133, 1943.

[33] D. Hebb, The Organization of Behavior: A Neuropsychological Theory, New York: Wiley, 1949.

[34] F. Rosenblatt, "The Perceptron: A Probabilistic Model for Information Storage and Organization in the Brain," *Psychological Review,* vol. 65, no. 6, pp. 386-408, 1958.

[35] M. Minsky and S. Papert, Perceptrons: An Introduction to Computational Geometry, Cambridge: MIT Press, 1969.

[36] P. Werbos, The Roots of Backpropagation: From Ordered Derivatives to Neural Networks and Political Forecasting, New York: Wiley, 1994.

[37] J. Hopfield, "Neural Networks and Physical Systems with Emergent Collective Computational Abilities," *Proceedings of the National Academy of Science,* vol. 79, pp.

2554-2558, 1982.

[38] J. Wang and Y. Chen, "A Hammerstein-Wiener Recurrent Neural Network with Universal Approximation Capability," in *IEEE International Conference on Systems, Man and Cybernetics, Systems, Man and Cybernetics*, 2008.

[39] J. Raskam, Methods for Estimating Stability and Control Derivatives of Conventional Subsonic Airplanes, USA: Roskam Aviation and Engineering Corporation, 1971.

[40] B. L. Stevens, F. L. Lewis and E. N. Johnson, Aircraft Control and Simulation: Dynamics, Controls Design, and Autonomous Systems, Hoboken, New Jersey: John Wiley & Sons, 2016.

[41] "JSBSim," [Online]. Available: http://www.openvsp.org.

[42] D. Y. Xu, Z. X. Liu and Y. M. Zhang, "System Identification of Long-EZ Fixed-Wing Aircraft Using Time-Domain Method," in *The 14th International Conference on Intelligent Unmanned System*, Jeju, South Korea, 2018.

[43] "OpenVsp," [Online]. Available: http://www.openvsp.org.

[44] D. T. Ward and T. W. Strganac, Introduction to Flight Test Engineering, Dubuque, Iowa: Kendall/Hunt Publising Company, 1998.

[45] Rutan Aircraft Factory Inc., "http://www.ez.org/downloads/longez_poh.pdf," 1980. [Online].

[46] M. Mohajerani, Frequency-Domain System Identification for Unmanned Helicopters from Flight Data, Master's Thesis, Concordia University, 2014.

[47] E. A. Morelli, "Flight Test Validation of Optimal Input Design and Comparison to Conventional Input," NASA Langley Research Center, Hampton, Virginia, USA.

[48] J. M. Ortega, Iterative Solution of Nonlinear Equations in Several Variables, New York: Academic Press, 1970.

[49] A. V. Balakrishnan, Communication Theory, New York: McGraw-Hill, 1968.

[50] K. S. P. Kumar and R. Sridhar, "On the Identification of Control Systems by the Quasi-Linearization Method," *IEEE Transactions on Automatic Control,* vol. AC-9, pp. 151-154, 1964.

[51] R. L. Kashyap, "A Bayesian Comparison of Different Classes of Dynamic Models Using Empirical Data," *IEEE Transaction on Automatic Control,* vol. AC-22, no. 5, pp. 715-

727, 1977.

[52] Y. M. Zhang and X. R. Li, "A Fast U-D Factorization-Based Learning Algorithm with Applications to Nonlinear System Modeling and Identification," *IEEE Transactions on Neural Networks,* vol. 10, no. 4, pp. 930-938, 1999.

[53] L. Rutkowski, New Soft Computing Techniques for System Modelling, Pattern Classification and Image Processing, Berlin, Heidelberg: Springer, 2004.

[54] "Keras," [Online]. Available: https://keras.io.

[55] A. P. Sage and J. L. Melsa, System Identification, New York: Academic International Press, 1971.

[56] P. Eykhoff, System Identification, Parameter and State Estimation, New York: Wiley, 1974.

[57] G. Goodwin and R. Payne, Dynamic System Identification: Experiment Design and Data Analysis, New York: Academic International Press, 1977.

[58] H. Greenberg, "A Survey of Methods for Determining Stability Parameters of an Airplane from Dynamic Flight Measurements," 1951.

[59] T. Hsia, System Identification, Lexington, MA: Lexington Books, 1977.

[60] E. A. Morelli, Flight Test Maneuvers for Efficient Aerodynamic Modelling, Hampton: NASA Langley Research Center.

[61] J. P. Norton, An Introduction to Identification, London: Academic International Press, 1986.

[62] F. Schweppe, Uncertain Dynamic Systems, Upper Saddle River, NJ: Prentice-Hall, 1973.

[63] T. Söderström and P. Stoica, System Identification, Upper Saddle River, NJ, Prentice-Hall, 1989.

[64] L. Taylor, K. Iliff and B. Powers, "A Comparison of Newton-Raphson and Other Methods for Determining Stability Derivatives from Flight Data," *3rd Flight Test, Simulation, and Support Conference,* pp. 69-315, 1969.

[65] O. Gerlach, "The Determination of Stability Derivatives and Performance Characteristics from Dynamic Maneuvers," in *Society of Automotive Engineers,* Paper 700236, 1970.